2022

Characterizing the Role of Tissue-Specific Retinol Dehydrogenases

Kelli Rae Goggans
University Of Alabama At Birmingham

CHARACTERIZING THE ROLE OF TISSUE-SPECIFIC RETINOL DEHYDROGENASES

by

KELLI RAE GOGGANS

NATALIA KEDISHVILI, COMMITTEE CHAIR
SHANNON BAILEY
KAREN GAMBLE
KELLY NICHOLS
NABIHA YUSUF
RUI ZHAO

A DISSERTATION

Submitted to the graduate faculty of The University of Alabama at Birmingham,
in partial fulfillment of the requirements for the degree of
Doctor of Philosophy

BIRMINGHAM, ALABAMA

2022

CHARACTERIZING THE ROLE OF TISSUE-SPECIFIC RETINOL DEHYDROGENASES

KELLI RAE GOGGANS

GENETICS, GENOMICS, AND BIOINFORMATICS

ABSTRACT

The bioactive form of vitamin A, retinoic acid is essential for development, cellular differentiation, epigenetic modifications, the immune system, and a variety of other processes due to its ability to regulate over 500 genes through activation of nuclear receptors. While many studies have focused on characterizing the biosynthesis and signaling of retinoic acid in embryogenesis, few have focused on adult tissues. Recent research has identified a novel retinol dehydrogenase, retinol dehydrogenase epidermal 2 (RDHE2), and shown RDHE2 is a potent, physiologically relevant retinol dehydrogenase in *Xenopus*. The work in this dissertation characterizes RDHE2 in mammalian models. We identify a paralog of RDHE2, RDHE2-similar (RDHE2S; collectively, RDHEs), and demonstrate both enzymes are physiologically relevant in mice. Furthermore, we demonstrate that RDHEs are tissue-specific retinol dehydrogenases that contribute to both developmental processes and maintenance of adult tissues. RDHEs are most highly expressed in skin, and the absence of RDHEs affects hair follicle development and alters the progression of the hair cycle in adult mice. However, transcripts of RDHEs are expressed in a variety of other tissues, and their absence alters whole body composition with aging. Interestingly, absence of RDHEs does not phenocopy systemic vitamin A deficiency, despite lowering retinoic acid levels in skin. Overall, this dissertation characterizes RDHEs in mammals and demonstrates their capacity to regulate retinoic

acid biosynthesis in a tissue-specific manner, the disruption of which causes novel and diverse effects.

Keywords: retinoid acid biosynthesis, vitamin A deficiency, hair cycle, hair follicle, body composition, whole body metabolism

DEDICATION

I would like to dedicate this dissertation to my husband, Charlie Goggans, and my grandmother, Linda Seales, without whom this dissertation might not exist. Both Charlie and my grandmother have listened and contributed to numerous discussions of the science within these pages, offering opportunities to explore my own thoughts and gain insight from others. Additionally, thank you both for your sacrifices as I have pursued my PhD, it means the world to me.

ACKNOWLEDGMENTS

First, thank you to my lab, specifically my mentor, Natalia Kedishvili, and Olga Belyaeva and Alla Klyuyeva. You have all contributed significantly to my training and education as a scientist, and I greatly appreciate all the time you have invested. I have also enjoyed getting to know all of you individually and building relationships that I hope we will carry on. Secondly, thank you to Karen Gamble and Shannon Bailey, as well as your labs; you have adopted me into the field of biological rhythms and fostered my growth beyond anything that was asked or expected. Also, thank you to Helen Everts, my collaborator at Texas Woman's University; as an expert in the retinoid field and hair follicles, you have been an invaluable mentor. To my other committee members, thank you for all your guidance, questions, and critiques as I have developed my project and skills. Furthermore, thank you to my parents, who have been supportive of my decisions every step of my graduate career. Everyone listed here was integral to my success.

TABLE OF CONTENTS

Page

LIST OF TABLES

Table *Page*

MICE LACKING THE EPIDERMAL RETINOL DEHYDROGENASES SDR16C5 AND SDR16C6 DISPLAY ACCELERATED HAIR GROWTH AND ENLARGED MEIBOMIAN GLANDS

LIST OF FIGURES

Figure *Page*

INTRODUCTION

MICE LACKING THE EPIDERMAL RETINOL DEHYDROGENASES SDR16C5 AND SDR16C6 DISPLAY ACCELERATED HAIR GROWTH AND ENLARGED MEIBOMIAN GLANDS

EPIDERMAL RETINOL DEHYDROGENASES FLUCTUATE ACROSS THE HAIR CYCLE AND INFLUENCE STEM CELLS

ABSENCE OF EPIDERMAL RETINOL DEHYDROGENASES ALTERS BODY COMPOSITION AND METABOLISM

LIST OF ABBREVIATIONS

ALDH	aldehyde dehydrogenase
ALDH1A1	aldehyde dehydrogenase family 1 member A1
ALDH1A2	aldehyde dehydrogenase family 1 member A2
ALDH1A3	aldehyde dehydrogenase family 1 member A3
AR	androgen receptor
ARE	androgen response elements
bp	base pair
BCO1	β-carotene oxygenase type 1
BMC	bone mineral content
BMD	bone mineral density
BSA	bovine serum ablumin
CRABP	cellular retinoic acid binding protein
CYP26A1	cytochrome P450 family 26 subfamily A member 1
CYP26B1	cytochrome P450 family 26 subfamily B member 1
CYP26C1	cytochrome P450 family 26 subfamily C member 1
DGAT1	diacylglycerol O-acyltransferase 1
DGAT2	diacylglycerol O-acyltransferase 2
DHRS3	dehydrogenase/reductase 3 (also SDR16C1)
DHRS9	dehydrogenase/reductase 9

DKO	*Rdhe2*$^{-/-}$/*Rdhe2s*$^{-/-}$ double knockout
DXA	dual energy x-ray absorptiometry
ER	estrogen receptor
ERK	extracellular kinase
ESC	embryonic stem cells
ESR1	estrogen receptor α
ESR2	estrogen receptor β
FABP5	fatty acid binding protein 5
GT	genotype
H&E	hematoxylin and eosin
HFD	high-fat diet
HFSC	hair follicle stem cell
IHC	immunohistochemistry
IR	immunoreactivity
LGR5	leucine-rich repeat containing G-protein coupled receptor
LRAT	lecithin retinol acyltransferase
MC5R	melanocortin-5 receptor
ORF	open reading frame
PD	postnatal day
PLIN2	perilipin 2
POR	cytochrome P450
PPARδ	peroxisome proliferator activated receptor δ
PPARγ	peroxisome proliferator activated receptor γ

RA	retinoic acid
RAL	retinaldehyde
RAR	retinoic acid receptor
RARE	retinoic acid response element
RALDH	retinaldehyde dehydrogenase
RBP1	retinol binding protein 1
RBP4	retinol binding protein 4
RD	regular chow diet
RDH	retinol dehydrogenase
RDH10	retinol dehydrogenase 10 (also SDR16C4)
RDHEs	collectively RDHE2 and RDHE2S
RDHE2	retinol dehydrogenase epidermal 2 (also SDR16C5)
RDHE2S	retinol dehydrogenase epidermal 2-similar (also SDR16C6)
RE	retinyl esters
REE	resting energy expenditure
RER	respiratory exchange ratio
retSDR2	retinal short-chain dehydrogenase/reductase 2
ROL	retinol
RXR	retinoid X receptor
SCD1	stearyl CoA desaturase
SDR	short-chain dehydrogenase/reductase
SDR16C1	short-chain dehydrogenase/reductase family 16C member 1
SDR16C4	short-chain dehydrogenase/reductase family 16C member 4

SDR16C5	short-chain dehydrogenase/reductase family 16C member 5
SDR16C6	short-chain dehydrogenase/reductase family 16C member 6
SHH	sonic hedgehog
STRA6	simulated by retinoid acid gene 6
SOX9	SRY (sex determining regionY)-box9
TBST	tris-buffered saline with Tween 20
TBX1	T-box 1
TEE	total energy expenditure
VAD	vitamin A deficient
WT	wild-type

INTRODUCTION

Vitamin A Uptake

Vitamin A is a fat-soluble vitamin, and the bioactive form, all-*trans*-retinoic acid (RA), is capable of activating gene transcription to alter cellular proliferation, differentiation, and metabolism. RA is required during embryogenesis to ensure proper development and on through adulthood for proper maintenance of skeletal structure, skin health, and the immune system. Though RA and its retinoid analogues, have been utilized in medical therapies since the 1960s due to their efficacy, the molecular pathways of synthesizing RA from vitamin A are still being characterized.

All-*trans*-retinol, the biologically available form of vitamin A, is obtained in the diet from either animal products as retinyl esters or plants as β-carotene. In the small intestine, retinyl esters are hydrolyzed to retinol for absorption; β-carotene itself can be absorbed and is then cleaved into two molecules of retinaldehyde, which are reduced to retinol. Retinol is esterified by lecithin retinol acyltransferase (LRAT) before being incorporated into chylomicrons, which are transported through the lymphatic system to the liver. In the liver, retinyl esters can be taken up by hepatocytes to be stored in stellate cells, the primary site of vitamin A storage for the body. Stored retinol is released from the liver into the blood, bound by retinol-binding protein 4 (RBP4), for transport to peripheral tissues [1,2].

Retinol is taken up for tissues by STRA6, stimulated by retinoic acid gene 6 protein homolog, a plasma membrane receptor for retinol bound to RBP4. Inside the cell retinol is bound to retinol binding protein 1 (RBP1) or localized to the cell's phospholipid membranes, due to retinol's hydrophobicity. LRAT is required in almost all tissues to esterify retinol for storage as retinyl esters, as the tissues of LRAT-deficient mice lack detectable retinyl esters. However, the adipose tissue of LRAT-deficient mice actually exhibits increased retinyl esters levels, indicating there are other tissue-specific enzymes involved in retinol esterification [1]. For instance, in skin, diacylglycerol O-acyltransferase 1 (DGAT1) can esterify retinol, but DGAT1 is shown to primarily deal with excessive levels of retinol [3]. DGAT1 and DGAT2 are expressed in white adipose tissue and considered potential therapeutic targets for altering lipid metabolism [4]. β-carotene oxygenase type 1 (BCO1), which is capable of metabolizing β-carotene to retinaldehyde, exhibits a wide tissue distribution pattern indicating the absorption of plasma β-carotene is also a possible mechanism for obtaining retinol. For example, following UV exposure, which causes localized vitamin A deficiency in skin [5], BCO1 exhibits increased activity. This demonstrates BCO1 can provide tissue-specific retinaldehyde, an intermediate of RA biosynthesis, in depleted conditions [6]

Retinoic Acid Biosynthesis and Degradation

There are two oxidative steps to convert retinol to RA. The oxidation of retinol to retinaldehyde is performed by enzymes of the short-chain dehydrogenase/reductase (SDR) 16C family [7]. The first physiologically relevant retinol dehydrogenase characterized was retinol dehydrogenase 10 (RDH10), a ubiquitously expressed RDH

that is essential to embryonic development, given its initial discovery via a random mutagenesis screen [8]. Further characterization of RDH10 revealed only suboptimal RA signaling in *Rdh10*$^{-/-}$ mutants, with low levels of RA activity detected during embryogenesis [9]. Additionally, retinaldehyde supplementation to mothers is sufficient to rescue *Rdh10*$^{-/-}$ mutant pups, indicating it is not an essential retinol dehydrogenase for adult mice. RDH10 interacts with and mutually stabilizes and activates dehydrogenase/ reductase 3 (DHRS3), another member of the SDR16C family which can convert the retinaldehyde produced by RDH10 back to retinol [10]. *Dhrs3* knockout is also lethal in either late gestation or early postnatal life [11]. DHRS3 expression is induced by RA, and together, RDH10 and DHRS3 contribute to a robust regulatory mechanism that allows for tight control over RA biosynthesis and homeostasis [10].

Due to the incomplete ablation of RA signaling in *Rdh10*$^{-/-}$ mouse mutants, it was assumed there was another retinol dehydrogenase yet to be identified. *SDR16C5*, or retinol dehydrogenase epidermal 2 (*RDHE2*), was first identified due to its upregulation in psoriatic skin compared to healthy skin of patients and named so due to its high sequence homology with another SDR16C family member, human retinal short-chain dehydrogenase/reductase 2 (retSDR2) [12]. RDHE2 was characterized as transmembrane protein that localized to the endoplasmic reticulum [13] and was first demonstrated to be a potent retinol dehydrogenase in *Xenopus* embryos [14]. In mice, *Rdhe2* is encoded by a gene located 20 Mb downstream of *Rdh10* on chromosome 8, and even further downstream there is a paralog, RDHE2-similar (*Rdhe2s*), sharing ~60% sequence homology with *Rdhe2* [13]. In humans, *RDHE2* and *RDHE2S* share 59% and 56% sequence similarity with *RDH10*, respectively, and human RDHE2 was characterized *in*

vitro as a retinol dehydrogenase [7]. Transcripts of human RDHE2 were present in brain, heart, digestive tract tissues, lymph nodes, lungs, mammary gland, and pancreas in addition to its expression in human skin, showing a widespread but not ubiquitous expression pattern, especially due to its apparent absence in the liver, where vitamin A storage and metabolism is an essential function. Additionally, recombinant human RDHE2S protein is unstable when expressed in HEK293 cells and does not contribute to RA biosynthesis in human cells [7]. Further investigation of tissue-specific retinol dehydrogenases is required to determine their contribution to RA biosynthesis in different tissues in physiology and disease.

The second step of RA biosynthesis, the oxidation of retinaldehyde to RA, is performed by aldehyde dehydrogenase family 1 member A1 – 3 (ALDH1A1 – 3) and is irreversible. ALDH1A1 – 3 are well characterized enzymes in embryogenesis, but their expression patterns and functions in adult tissues are not well studied, partially due to the embryonic lethality of genetic knockouts (ALDH1A2, ALDH1A3) and lack of apparent phenotypes (ALDH1A1). Additionally, ALDH1A1 recognize other substrates and can contribute to non-retinoid related phenotypes [2].

RA in cells is bound to cellular RA binding proteins (CRABPs). RA bound to CRABP1 (holoCRABP1) is thought to be bound for degradation; additionally, recent studies have shown holoCRABP1 can rapidly activate the extracellular kinase (ERK) pathway [15]. This and other non-genomic mechanisms of action for RA are still being characterized and studied in the field. The other CRABP, CRABP2, binds RA to be transported into the nucleus and activate retinoic acid receptors (RARs). However,

CRABPs are not necessary for RA signaling, as knockout mice are viable and appear normal, aside from a minor limb malformation [reviewed in 2].

RA is degraded by 3 members of the cytochrome P450 superfamily, CYP26A1, CYP26B1, and CYP26C1. CYP26A1 and CYP26B1 are required for development where they exhibit unique expression patterns; however, their expression patterns generally overlap in adult tissues, where CYP26B1 is the predominant enzyme in all tissues except liver and lung. CYP26C1 is not required for development, though that is primarily when it is expressed, and is more promiscuous than the other CYP26s [2]. RA can also upregulate the expression of CYP26 enzymes to promote RA degradation via a negative feedback loop.

Retinoic Acid Signaling

RA receptors (RARs) are nuclear receptors, a superfamily of transcription factors with conserved domains for DNA binding, ligand binding, and transactivation. Hormones activate nuclear receptors to alter transcription in a highly variable and reversible manner, as the ligands are dynamically produced and degraded. [16]. RA is a ligand for RARs and binding of RA causes the dissociation of corepressors and the recruitment of coactivators to activate transcription. There are three RARs (α, β, and γ), and they all heterodimerize with retinoid X receptors (RXRs), which are also nuclear receptors and have three types (α, β, and γ). RARs heterodimerized with RXRs bind RA Response Elements (RAREs) in DNA to regulate the expression of over 500 genes [17]. In the absence of RA, RAR/RXR heterodimers are associated with co-repressors that inhibit transcription. However, upon RA binding, these co-repressors are released, and co-activators are recruited to initiate

transcription through chromatin remodeling. Additionally, numerous transcription factors are regulated by RA and generate secondary, indirect responses for RA-associated regulation [18]. The removal of RA from RARs and the nucleus is still undefined in the field. RARs can be degraded through the ubiquitin-proteasome system, and this process has been proposed to limit RA activity [19].

RA-activated RARs are capable of exerting profound but fine-tuned effects on epigenetic remodeling. Active and repressive histone marks can be increased initially upon RA-induction, but ultimately giving way to activating marks. This allows for delayed effects and ascribes a temporal component of RA-regulated transcription [20]. Depending upon cell type, RARα is also found outside the nucleus and associates with cellular membranes by interacting with G proteins [19,21]. RA's non-genomic mechanisms have demonstrated temporal advantages of this multi-step mechanism. For example, in their characterization of CRABP1, Lin *et al.* [15] demonstrated that CRABP1 is responsible for an immediate RA response (within 1 hour) via activation of the ERK pathway. However, there was another activation of the ERK pathway 12 hours after RA administration, due to RA signaling through RARs. In the case of the embryonic stem cells Lin *et al.* was working with, the first RA response slowed cell cycle progression, priming the stem cells for the second RA wave which is required to initiate differentiation [15]. These RA-induced kinase activation cascades can also regulate genomic signaling through phosphorylation of RARs and RXRs [19].

The transcriptional activation initiated by RA binding to RARs is strongly associated with epigenetic changes that are essential for promoting differentiation and inhibiting proliferation [18]. In particular, RA signaling is mutually antagonistic to

Wnt/β-catenin signaling. β-catenin upregulates enzymes involved in RA degradation, while RA-activated RARs can bind β-catenin to competitively inhibit the binding of other transcription factors essential for proper β-catenin signaling [22,23]. Androgens and estrogens are sex-specific hormones that also activate nuclear receptors, androgen receptor (AR) and estrogen receptor (ER), respectively. Retinoids are capable of inhibiting androgen-stimulated cell proliferation [24] through transcriptional regulation of AR and undefined post-translational mechanism [25]. AR can also antagonize the activity of RARs, possibly through sterically inhibiting recruitment of corepressors and coactivators at genes where RAREs and androgen response elements (AREs) allow for adjacent binding of the receptors [26]. Additionally, RARα (RARα) has been shown to be part of the ER transcription complex and capable of facilitating ER-associated proliferation; however, RA can also drive RARα associated RA-signaling, removing RARα from the ER complex and inhibiting ER-associated proliferation [27]. This mechanism demonstrates how RARα agonists and antagonists are capable of inhibiting cancer growth and emphasizes the need for a highly-regulated homeostatic level of RA.

RA has also been shown to activate another nuclear receptor peroxisome proliferator activated receptor δ (PPARδ), specifically in keratinocytes and adipocytes, which express higher levels of fatty acid binding protein 5 (FABP5) than CRABP2. FABP5 also binds RA and specifically in skin has been shown to regulate RA signaling alongside CRABP1 and CRABP2 [23]. RA-activation of PPARδ explains how RA exhibits a proliferative effect in keratinocytes and contributes to whole body energy expenditure [19,28].

Regulation of Retinoic Acid Biosynthesis

RA levels are self-regulated by negative feedback loops. RA activates RARs that allow for transcription initiation of genes involved in the uptake of retinol and its biosynthesis (*Stra6, Rbp1, Lrat*) and its degradation (*Cyp26a1, Cyp26b1,* and *Cyp26c1*) [2]. Upregulation of STRA6 allows more retinol into the cell, and an increase in the cellular-retinol pool requires upregulation of RBP1. LRAT assists with storing the excessive levels of retinol, though in the skin LRAT has been shown to have limits to its ability to store excess retinol and DGAT1 is essential for retinol esterification to retinyl esters in these conditions [3]. In organotypic epithelial cultures , which are derived from primary human keratinocytes and differentiated on mesh at a liquid-air interface to replicate the stratification of human epidermis, RDHE2 is down-regulated by RA [7], but this has yet to be shown in *vivo*. The regulation of RDHEs by RA would allow for another level of regulation, especially in tissues that are sensitive to RA levels, such as skin. CYP26A1, CYP26B1, and CYP26C1 are responsible for RA degradation, and thus their upregulation by RA allows for excessive RA to be degraded more rapidly.

Retinoic Acid Biosynthesis and Signaling in the Skin and the Hair Follicle

Most of the research on RA biosynthesis and signaling pertains to its role in embryogenesis due to how essential RA is for embryogenesis. Also, defects in development from either RA deficiency or toxicity are well-characterized and easily recognized. However, due to accessibility and therapeutic capabilities, retinoids have been studied in the context of human skin and the hair cycle since the 1960s, when they were determined to alter epidermal differentiation and keratinization [29]. Today

retinoids are potent and efficient dermatotherapy options for a variety of diseases including acne vulgaris, psoriasis, and skin cancer [30]. Additionally, dysregulation of retinoid metabolism is implicated in these diseases and various types of alopecia (hair loss) [3,12,31]. Biopsies from patients with alopecia exhibit an increased expression of RA biosynthesis enzymes, and mouse models fed either excessive levels of vitamin A or no vitamin A exhibited altered and worse alopecia [32]. Despite its known effects on skin and dysregulation in disease, the enzymes facilitating homeostatic RA biosynthesis in skin are still not well characterized.

RA is necessary for proper skin development, as dominant-negative RARα, RARβ, and RARγ mouse models produced immature and thin skin lacking hair follicles [33]. The identification and *in vitro* characterization of RDHE2 and RDHE2S are a step towards further defining RA biosynthesis in the skin [7,12]. Additionally, immunohistochemistry (IHC) analysis of enzymes involved in RA biosynthesis highlights a potential role of RA in the hair follicle specifically. The hair follicle is a skin appendage, sometimes referred to as a miniorgan, constantly undergoing organogenesis to produce new hair fibers. Classically, the hair cycle is defined as beginning with anagen, a period characterized by cellular proliferation and the production of the hair fiber. Melanogenesis, which provides pigmentation for the hair fiber, is also temporally tied to anagen. Once the proliferation and differentiation processes of anagen are complete, the structures of the hair follicle that supported the production of the hair fiber (termed the cycling hair follicle) undergo rapid apoptosis. This phase of the hair cycle is termed catagen, and the follicle rapidly regresses back to the smaller, permanent structures (the isthmus and infundibulum) of the hair follicle. The third and last phase of

the hair cycle, telogen, is described as a period of rest due to its lack of morphological changes, as seen in anagen and catagen [34]. However, some studies highlight the enrichment of genes involved in metabolite generation, suggesting that molecularly the hair follicle is quite active and preparing for the next cycle [35].

IHC in female mice followed the proteins involved in the RA biosynthesis pathway across the hair cycle, identifying temporal and spatial changes [36]. However, this study included dehydrogenase/reductase 9 (DHRS9) that has since been proven to not be a retinol dehydrogenase [37], so the previous study does not account for differences at the level of retinol dehydrogenases. IHC for RA biosynthesis enzymes (ALDH1A1-3), RA-binding proteins (CRABP1/2), and RA-signaling proteins (RARα/β/γ) revealed these proteins localized to the lower cycling follicle and to regions of the permanent hair follicle, such as the hair follicle bulge, specifically during anagen. ALDH1A2, CRABP2, RARα, and RARγ remain localized to the hair follicle bulge throughout the rest of the hair cycle, though the other proteins (ALDH1A1, ALDH1A3, RARβ) are specifically localized to the hair follicle bulge only during anagen [36]. This pattern was confirmed for mid-anagen through analysis of RA reporter mice and emphasized RA signaling localizing to the hair follicle bulge [31]. The hair follicle bulge is a stem cell niche, residing directly below the sebaceous gland and responsible for providing progenitors for the hair cycle [31].

Changes in RA levels are known to alter the hair cycle. Elevated endogenous levels of RA in skin can cause cyclical hair loss due to excessive hair shedding and early anagen initiation [3], and early anagen initiation can also be induced through exogenous application of retinoids [38]. Delays in anagen initiation due to reductions in RA

signaling [39,40] support the conclusion that RA is required for anagen initiation. This conflicts with the current understanding of anagen initiation, where Wnt/β-catenin signaling and Shh signaling are required signaling mechanisms for anagen initiation [34]. As described previously, RA is antagonistic to Wnt/ β-catenin signaling, suggesting that RA levels must be low at anagen initiation to allow for Wnt/ β-catenin and Shh signaling. Exogenous RA has also been shown to induce catagen in cultured hair follicles [38], which conflicts with increased endogenous levels of RA delaying catagen [3]. With these seemingly conflicting results, RA's role in hair cycle progression is unclear. However, if RA levels cycle rhythmically across the hair cycle phases, as is suggested by the IHC of RA biosynthesis and signaling enzymes, then it may be the alteration of rhythmic timing or signaling intensity that allows RA to have diverse and opposing roles in the hair cycle.

Effects of Vitamin A on General Metabolism

Several studies document treatment with RA decreases adipose tissue mass and improves weight loss of mice fed a high-fat diet (HFD). In these studies, RA treatment also increases dark phase energy expenditure [41], improves insulin resistance [28,42] and glucose tolerance [43], and reverses liver hepatosteatosis [41,43]. This is due to RA's ability to globally stimulate fatty acid oxidation [44] and alter adipocyte differentiation [41]. The effects of vitamin A deficiency (VAD) on body composition and metabolism are less well studied, and experimental standards for achieving VAD models are not well-defined. Many studies begin feeding rodents VAD diet at weaning, despite research showing the animals have already developed liver stores of vitamin A. In general, these studies also report decreases in body mass and fat [45], impaired motor function [46,47],

and decreased locomotor activity levels [48–50], indicating that even acute VAD can alter body composition and locomotor activity. These effects are regulated by complex molecular pathways, activated by RA binding to RARs, and are still being investigated and described in tissue-specific studies.

Skeletal structure and integrity are also affected by RA levels. There is growing concern in the field that fortification of food, such as milk, with vitamin A has led to increased rates of osteoporosis in some countries [51]. Indeed, animals fed excessive levels of vitamin A have increased bone fragility, and in humans high vitamin A intake indicates an increased risk of bone fractures [52]. VAD increases bone thickness, possibly through the dysregulation of matrix molecule degradation [53]. The molecular mechanisms through which RA alters bone composition are still undefined *in vivo*, though *in vitro* studies highlight RA's ability to promote osteoblast differentiation and bone formation [52].

Research Overview

The research presented in this dissertation focuses on characterizing the role of RDHE2 and RDHE2S (collectively referred to as RDHEs) in skin and whole-body physiology. We demonstrated murine RDHEs are retinol dehydrogenases *in vivo* and are expressed highly in skin, with transcripts also detected in esophagus, stomach, tongue, adipose tissue, intestine, and colon. We generated a mouse model lacking *Rdhe2* and *Rdhe2s* to determine the role of these tissue-specific retinol dehydrogenases. Mice lacking RDHEs exhibit an accelerated hair cycle and enlarged meibomian glands; additionally, with age, demonstrate decreased weight and adiposity and increased

locomotor activity and energy expenditure than age-matched wild-type mice. We show that RDHEs are the primary retinol dehydrogenases for skin, contributing to development and regulation of hair follicles and the hair cycle. Additionally, we critically examine vitamin A deficiency and its effect on mice lacking RDHEs in whole body composition, locomotor activity, and energy metabolism. Vitamin A deficiency significantly increases fat percentage, bone mineral density, and energy expenditure, while decreasing locomotor activity. Absence of RDHEs does not phenocopy vitamin A deficiency, decreasing bone mineral density and energy expenditure, and vitamin A deficiency in the absence of RDHEs induces anaerobic respiration during the dark phase. Collectively, these findings characterize RDHEs as potent retinol dehydrogenases that contribute to development and maintenance of a variety of tissues. Our studies also highlight how the absence of RDHEs results in a dysregulation of whole body RA biosynthesis that is not in complete agreement with VAD or excessive RA levels, implying RDHEs contribute to the regulation of RA biosynthesis in a tissue-specific manner.

MICE LACKING THE EPIDERMAL RETINOL DEHYDROGENASES SDR16C5 AND SDR16C6 DISPLAY ACCELERATED HAIR GROWTH AND ENLARGED MEIBOMIAN GLANDS

by

LIZHI WU, OLGA V. BELYAEVA, MARK K. ADAMS, ALLA V. KLYUYEVA, SEUNG-AH LEE, KELLI R. GOGGANS, ROBERT A. KESTERSON, KIRILL M. POPOV, NATALIA Y. KEDISHVILI

The Journal of Biological Chemistry. 294(45): 17060-17074

Abstract

Retinol dehydrogenases catalyze the rate-limiting step in the biosynthesis of retinoic acid, a bioactive lipid molecule that regulates the expression of hundreds of genes by binding to nuclear transcription factors, the retinoic acid receptors. Several enzymes exhibit retinol dehydrogenase activities *in vitro*; however, their physiological relevance for retinoic acid biosynthesis *in vivo* remains unclear. Here, we present evidence that two murine epidermal retinol dehydrogenases, short-chain dehydrogenase/reductase family 16C member 5 (SDR16C5) and SDR16C6, contribute to retinoic acid biosynthesis in living cells and are also essential for the oxidation of retinol to retinaldehyde *in vivo*. Mice with targeted knockout of the more catalytically active SDR16C6 enzyme have no obvious phenotype, possibly due to functional redundancy, because *Sdr16c5* and *Sdr16c6* exhibit an overlapping expression pattern during later developmental stages and in adulthood. Mice that lack both enzymes are viable and fertile, but display accelerated hair growth after shaving and also enlarged meibomian glands, consistent with a nearly 80% reduction in the retinol dehydrogenase activities of skin membrane fractions from the *Sdr16c5/Sdr16c6* double-knockout mice. The up-regulation of hair-follicle stem cell genes is consistent with reduced retinoic acid signaling in the skin of the double-knockout mice. These results indicate that the retinol dehydrogenase activities of murine SDR16C5 and SDR16C6 enzymes are not critical for survival, but are responsible for most of the retinol dehydrogenase activity in skin, essential for the regulation of the hair-follicle cycle, and required for the maintenance of both sebaceous and meibomian glands.

Introduction

All-*trans*-Retinoic acid (RA) is the major bioactive form of vitamin A that influences a broad spectrum of physiological processes including embryogenesis and epithelial homeostasis [1-4]. In the nucleus, RA regulates gene expression primarily through binding to nuclear transcription factors retinoic acid receptors (RAR, α, β and γ), which act as heterodimers with retinoid X receptors [5, 6]. In the cytoplasm, RA regulates the activity of ERK kinase [7] and exhibits numerous other extranuclear activities [8]. RA is synthesized from the alcohol form of vitamin A (all-*trans*-retinol) via a two-step process. In the first step, retinol dehydrogenases oxidize all-*trans*-retinol to all-*trans*-retinaldehyde, which is oxidized further by retinaldehyde dehydrogenases (RALDH) to RA [reviewed in ref. 9].

The oxidation of retinol to retinaldehyde is the rate-limiting step in RA biosynthesis [10]. Several members of the short-chain dehydrogenase/reductase (SDR) superfamily of proteins catalyze this reaction *in vitro* [9], but only one of the retinoid-active SDRs characterized to date, murine retinol dehydrogenase 10 (RDH10), is known to be indispensable for RA biosynthesis, because embryos lacking functional RDH10 do not survive past E12.5 [11]. RDH10-null embryos display numerous abnormalities including forelimb, craniofacial, neural, and heart defects [12, 13]. The severity of the phenotype indicates that RDH10 functions as the major murine retinol dehydrogenase during mid-embryogenesis. However, while the ablation of RDH10 eliminates most of the retinol dehydrogenase activity during the early stages of development, RA synthesis persists in the neural tube of RDH10-null embryos at E9.5 and E10.5 [14, 15]. Importantly, *Rdh10*$^{-/-}$ embryos can be rescued by supplementation of maternal diets with

retinaldehyde between embryonic stages E7.5 through E9.5. Thus, RDH10 appears to be dispensable during later stages of development and transition to adulthood [11]. These data point towards the existence of RDH10-independent sources of RA. However, the identities of additional retinol dehydrogenases accounting for this residual retinaldehyde synthesis remain elusive.

RDH10 belongs to the 16C family of the SDR superfamily of proteins [16, 17]. Notably, two other genes encoding members of the SDR16C family are located adjacent to the gene encoding RDH10 in the human genome on chromosome 8: retinol dehydrogenase epidermal 2 (RDHE2, SDR16C5) and retinol dehydrogenase epidermal 2-similar (RDHE2S, SDR16C6) [18, 19]. The deduced RDHE2 and RDHE2S proteins share the highest sequence homology (~43%) with RDH10 (SDR16C4). As we reported previously, the single ortholog of human genes encoding RDHE2 and RDHE2S in *Xenopus laevis* functions as a retinol dehydrogenase *in vivo* and is essential for embryonic development in frogs [20]. These findings imply that mammalian RDHE2 and RDHE2S complement RDH10 in generating retinaldehyde for RA biosynthesis. However, it remains to be established whether the *in vivo* function of amphibian rdhe2 is conserved by its mammalian orthologs. This study was undertaken in order to assess the catalytic properties of mammalian RDHE2 and RDHE2S as compared to amphibian rdhe2, to determine the expression patterns of RDHE2 and RDHE2S in mice, and to establish whether these enzymes are essential for RA biosynthesis in mammals.

Experimental Procedures

Expression constructs

All primer sequences with corresponding restriction sites used for generation of constructs are listed in Table S1. Constructs encoding FLAG-tagged murine RDHE2S and *Xenopus laevis* rdhe2 in pCMV-Tag 4A vector were described previously [18, 20]. Murine *Rdhe2* cDNA was obtained by RT-PCR of mouse skin and liver mRNA and cloned into SalI and XbaI sites of pBluescript II SK (-) vector.

To generate FLAG-tagged RDHE2 expression construct, the corresponding cDNA was cloned into pCMV-Tag 4A vector in frame with the C-terminal FLAG tag. Subsequently, the FLAG-tagged construct was amplified using primers specified in Supplemental Table I and cloned into pCS105 and pVL1393 vectors. In addition, a His-tagged RDHE2 construct was generated using a modified pVL1393 vector containing an in-frame C-terminal His6-tag [87].

Human HA-tagged RALDH1 expression construct in pcDNA3.1-neo (CMV promoter) was a generous gift of Dr. Sylvie Mader in the Department of Biochemistry, University of Montreal, Canada. All expression constructs and plasmids were verified by sequencing.

Cell culture models

For activity assays in intact cells, SDR constructs were expressed in human HEK293 cells following the previously published protocols [30, 32]. The transfected cells were incubated with all-*trans*-retinol or all-*trans*-retinaldehyde as indicated. Retinoids were extracted and analyzed by normal phase HPLC as described previously

[30]. For kinetic analysis, RDHE2, RDHE2S and frog rdhe2 were expressed in Sf9 insect cells using pVL1393 transfer vector and BaculoGold Baculovirus Expression System (BD Biosciences, San Jose, CA). The subcellular fractions were isolated by differential centrifugation as described [87]. The membrane pellets were resuspended in 90 mM KH2PO4, 40 mM KCl (pH 7.4) and 20% glycerol (w/v).

In vitro activity assays and immunoblotting

Activity assays using subcellular fractions of Sf9 cells were performed as described previously [30]. The K_m and V_{max} values for all-*trans*-retinol, 9-*cis*-retinol, 11-*cis*-retinol, or all-*trans*-retinaldehyde were obtained using seven concentrations of each substrate (0.0625-8 μM) in the presence of 1 mM NAD(H). The K_m and V_{max} values for NAD^+ and NADH were determined at fixed concentration of all-*trans*-retinol or all-*trans*-retinaldehyde (5 μM) and seven concentrations of NAD+ or NADH (1-500 μM).

Western blot analysis was performed using rabbit polyclonal antibodies against FLAG-epitope (Sigma Aldrich, St. Louis, MO) and β-actin (Abcam, Cambridge, UK); and mouse monoclonal antibodies against His-epitope (Clontech, BD Biosciences, Mountain View, CA) and HA-epitope (received as a gift from Dr. Hengbin Wang, Department of Biochemistry and Molecular Genetics, University of Alabama at Birmingham School of Medicine).

Protein samples were separated in 12% polyacrylamide gels in the presence of sodium dodecyl sulfate and transferred to Amersham Hybond P PVDF membranes (GE Healthcare, Little Chalfont, UK). Following transfer, membranes were blocked with 4% bovine serum albumin (BSA) in Tris-buffered saline with Tween 20 (TBST) and

incubated with rabbit polyclonal or mouse monoclonal antibodies diluted with 4% BSA in TBST overnight at 4°C. Dilutions of primary antibodies are indicated in figure legends. Membranes were rinsed with TBST and incubated for 1 h at room temperature in goat anti-rabbit antibody or goat anti-mouse antibody conjugated to horseradish peroxidase (Jackson ImmunoResearch Laboratories, Inc., West Grove, PA), both of which were diluted 1:10,000 with 4% BSA in TBST. Protein visualization was achieved with Pierce ECL Western Blotting Substrate (Thermo Fisher Scientific, Waltham, MA).

Generation of Rdhe2s$^{-/-}$ mouse model

Rdhe2s$^{+/-}$ mice were generated using the *Sdr16c6$^{tm1a(KOMP)Wtsi}$* 'knockout-first' allele obtained from the KOMP repository (https://www.komp.org/pdf.php?projectID=41879, SangerID design 43965). The 'knockout-first' allele contains an IRES:*lacZ* trapping cassette and a floxed promoter-driven *neo* cassette inserted into the intron of a gene, disrupting gene function. The targeting vector (KOMP design 43965) was digested with AsiSI and SalI enzymes, which resulted in a 1,431 base pair truncation of the 5' homology arm. Electroporation of the linearized vector in mouse embryonic stem cells (ESC), selection of ESC-derived clones and isolation of genomic DNA was performed by the University of Alabama at Birmingham Transgenic & Genetically Engineered Models facility. ESC-derived clones carrying a targeted insertion of the "knockout first" cassette were identified by long-range PCR spanning 5' and 3' homology arms using SequalPrep long PCR kit (Invitrogen, Life Technologies) with primers listed in Table S1. Chimeras were generated by the University of Alabama at Birmingham Transgenic & Genetically Engineered Models

facility. Male chimeras were crossed to wild-type C57Bl56/J mice, and pups were genotyped to identify heterozygote founders carrying a "knockout first" allele. Crossing of these mice to FLPeR mice carrying a gene encoding FLP recombinase resulted in conversion of the 'knockout-first' allele to a conditional allele, restoring gene activity. Subsequent crossing of FLP excised mice to EIIa-cre mice, which express Cre recombinase prior to implantations, resulted in a mouse with a deletion of exon 4 and a frameshift mutation (Fig. S1). Genotyping of mice crossed to FLPeR mice was accomplished using DNA isolated from tails and the primers listed in Table S1.

Generation of Rdhe2$^{-/-}$;Rdhe2s$^{-/-}$ mouse models

Murine *Sdr16c6* is located immediately upstream of murine *Sdr16c5* gene. For both genes, CRISPR guide RNAs were designed to target exons 2 and 5, which encode the conserved cofactor and substrate binding site motifs, respectively (Table S2, Figs. 3 A and S3). Guide RNAs were designed as described previously [88]. Six F0 pups were born following CRISPR-Cas9 microinjections. For the initial screening, the targeted exons 2 and 5 were PCR-amplified from genomic DNA isolated from tail snips and separated by electrophoresis in polyacrylamide gel. In mouse #21855, the electrophoretic mobility shift assay revealed heterogeneous bands in PCR-products corresponding to exon 2 of *Sdr16c5,* and exon 5 of *Sdr16c6*, suggesting the formation of heteroduplexes. In mouse #21853, PCR-product for exon 5 of *Sdr16c5* was completely absent, indicating that CRISPR-Cas9 injections generated a larger deletion(s) in this animal, and that both copies of *Sdr16c6-Sdr16c5* locus are mutated.

Subcloning and resequencing of the targeted exons in mouse #21855 identified a 3-base pair (bp) deletion in exon 2 of *Sdr16c5*, as well as 1- and 3-bp deletions in exon 5 of *Sdr16c6*. The loss of a single amino acid resulting from the 3-bp deletion may not lead to a complete loss of enzymatic activity of SDR16C5 (RDHE2), and the frameshift-causing 1-bp deletion in *Sdr16c6* was expected to result in a knock-out of *Sdr16c6* gene only. As we already had an established knock-out strain of *Sdr16c6*, mouse #21855 was not used as a founder.

To precisely define the alleles generated in mouse #21853, we performed a series of PCR amplifications with primer pairs as indicated in Fig. 3 A and in Table S1. We assumed that the products would only be generated if the primers' annealing sites were brought close enough as a result of deletion, because the distance between the annealing sites in the WT type allele is too large for efficient amplification. The primer pair 4 yielded a 585 bp product in mouse #21853, but not in other F0 animals. The product contained a chimeric sequence comprised of incomplete exon 5 of *Sdr16c6*, incomplete exon 5 of *Sdr16c5* gene, and a 298 bp insertion corresponding to an inverted partial sequence of exon 2 of *Sdr16c5* (Figs. 3A and S3). This result indicated that mouse #21853 contained a large 56,057 bp deletion covering the region between CRISPR targets in exon 5 of *Sdr16c6* and exon 5 of *Sdr16c5*. The open reading frame (ORF) of the chimeric transcript encodes a truncated polypeptide (Fig. S3). We have designated this double $Sdr16c6^{-/-};Sdr16c5^{-/-}$ knock-out allele as DKO1.

The existence of a full-length PCR product for exon 5 of *Sdr16c6*, which was obtained during initial F0 screening was inconsistent with DKO1 allele, which retains only part of this exon. This result suggested that mouse #21853 carries a second mutant

allele. PCR amplification of individual exons 4 and 6 of *Sdr16c5* yielded fragments of expected size, indicating that a shorter than DKO1 deletion occurred in the second allele of the same animal. This shorter deletion resulted in a loss of a single exon 5 in *Sdr16c5*. Long range PCR amplification with primers spanning exons 4 through 6 yielded a 4,912 bp product in WT mouse but a shorter product in mouse #21853. Sequencing of this product confirmed the deletion of 1,837 bp, which covers exon 5 of *Sdr16c5* and a portion of flanking intronic sequences. This allele was designated DKO2 (Figs. 3 A and S3).

Thus, mouse #21853 carried two different CRISPR-Cas9 generated alleles, DKO1 and DKO2. This animal was used as the founder, and crossed to WT females to isolate DKO1 and DKO2 strains. Re-sequencing of individual exons in DKO2 strain revealed a short 8-bp deletion in exon 2 of *Sdr16c6,* in addition to deleted exon 5 in *Sdr16c5*. Thus, the ORFs of both *Sdr16c6* and *Sdr16c5* in DKO2 allele are predicted to encode truncated proteins (Figs. 3A and S3). DKO2 represents a second double knock-out strain.

Mice were maintained on either on LabDiet NIH-31 (PMI Nutrition International) containing 22 IU vitamin A/g or on vitamin A-deficient diet Teklad TD.86143 (Envigo) in a facility approved by the Association for Assessment and Accreditation of Laboratory Animal Care. Mice were euthanized by CO_2 inhalation followed by cervical dislocation, in accordance with Institutional Animal Care and Use Committee guidelines at the University of Alabama at Birmingham.

β-Galactosidase staining and in situ hybridizations

Adult mice were arranged in mating pairs and females were checked for vaginal plugs at noon of the following day. The presence of a plug was considered to represent a developmental stage of E0.5. Genotypes were determined using DNA isolated from yolk sacs. Full length mouse *Rdhe2* cDNA in pBluescript II SK (-) vector was used for generation of antisense probes for *in situ* hybridization. Probes were synthesized using linearized template, T3 RNA Polymerase (Promega), and digoxigenin RNA labeling mix (Roche Applied Science). Skin was isolated from the backs of 4 months old male C57BL/J6 mice, fixed overnight in 4% paraformaldehyde at 4°C, and embedded in paraffin. The paraffin-embedded skin was cut into ten-micron sections, which were placed on Superfrost Plus microscope slides (Fisher Scientific). *In situ* hybridization was carried out following standard procedures. β-Galactosidase staining was performed on E14.5 *Rdhe2s*$^{+/-}$ embryos and skin isolated from 4 months old *Rdhe2s*$^{+/-}$ male mouse tails according to the previously published protocols [89].

qPCR analysis

To determine the expression pattern of *Rdhe2* and *Rdhe2s* genes, two male WT mice fed VAD diet for 10 weeks were sacrificed with CO_2; tissues were collected and stored at -80°C until RNA extraction. TRIZOL reagent (Ambion, Cat No. 15596018) was used for extraction of RNA from all tissues except skin, for which AurumTM total RNA Fatty and Fibrous Tissue Pack (Bio-Rad, Cat No: 732-6870) was employed. Three µg of RNA per tissue was used for reverse transcription; cDNA was purified with QIAquick Spin columns (QIAGEN Cat No.1018215). QPCR was performed with 25 ng of cDNA

per reaction. *Rdhe2* and *Rdhe2s* expression was normalized to *Gapdh* and presented as a relative expression of fold difference to the expression level in the stomach for each gene, which was set to one.

For analysis of gene expression in skin, ~75 mg of skin tissue was homogenized and RNA was extracted with Aurum^{TM} total RNA Fatty and Fibrous Tissue Pack (Bio-Rad, Cat No: 732-6870). The concentration of extracted RNA was determined using Nanodrop ND-1000 spectrophotometer (Thermo Scientific). First-strand cDNA was synthesized from 3.0 µg of total RNA with Superscript III first-strand synthesis kit (Invitrogen, Carlsbad, CA) according to the manufacturer's protocol. For real-time RT-PCR reactions, the cDNA was diluted 15-fold. Sequences of the primers are available by request. Real-time PCR analysis was conducted on Roche LightCycler®480 detection system (Roche Diagnostics) with SYBR Green as probe (LightCycler®480 CYBR Green I Master, Roche, Indianapolis, IN). Relative gene expression levels were calculated using the comparative Ct method by normalization to reference genes. Unpaired t-test was used to test for statistical significance.

Hair regrowth

The diet for DKO2 heterozygote breeder dams was switched to Vitamin A deficient (VAD) diet at mid-gestation (12-14 days post-conception), and the pups were kept on VAD diet until being sacrificed at 10 weeks of age. At 8 weeks after birth, WT and DKO2 littermates' dorsal hair was clipped and depilated with Nair® Lotion. Littermates were checked daily for hair regrowth until they were sacrificed. Animals that

had abnormal hair due to excessive grooming by female breeders were not used for the analysis of hair regrowth.

Statistical Analysis

Statistical significance was determined using two-tailed unpaired t-test.

Results

Kinetic characterization of epidermal retinol dehydrogenases

To compare the catalytic properties of murine RDHE2 (SDR16C5) and RDHE2S (SDR16C6) as retinol dehydrogenases to those of frog rdhe2, we expressed each enzyme as a fusion protein with the C-terminal His6-tag in insect Sf9 cells using the baculovirus expression system. Western blot analysis showed that the recombinant SDRs were expressed at comparable protein levels in the microsomal fractions of Sf9 cells (Fig. 1 A). Therefore, the microsomal fractions containing the RDHE proteins were used for characterization of their retinoid activities. Activity assays revealed that murine RDHE2S and *Xenopus* rdhe2 both catalyzed the oxidation of all-*trans*-retinol to all-*trans*-retinaldehyde in the presence of NAD^+. The activity rates with $NADP^+$ were at the limit of detection (data not shown); hence NAD^+ was the preferred cofactor for both enzymes. RDHE2S exhibited a higher apparent K_m value and a lower apparent V_{max} value for the oxidation of all-*trans*-retinol than *Xenopus* rdhe2 (Table 1). Thus, *Xenopus* rdhe2 exhibited a higher catalytic efficiency (V_{max}/K_m) than murine RDHE2S. Both enzymes also catalyzed the reduction of all-*trans*-retinaldehyde to all-*trans*-retinol in the presence of NADH, but their catalytic efficiencies in the reductive direction were lower than in the

oxidative direction (Table 1). In addition to all-*trans*-retinol, both RDHE2S and *Xenopus* rdhe2 recognized 11-*cis*-retinol as substrate (Table 1).

Unexpectedly, no activity towards all-*trans*-retinol was detected using the microsomal preparation of recombinant murine RDHE2 protein (Table 1). Some SDRs show dual subcellular distribution between microsomal and mitochondrial fractions [21]; therefore, we tested whether the mitochondria isolated from Sf9 cells expressing RDHE2 or RDHE2S exhibited a retinol dehydrogenase activity. No activity was detected using RDHE2-containing mitochondria, whereas 10 μg of mitochondria from RDHE2S-expressing Sf9 cells exhibited a much lower activity (0.03 nmol·min-1·mg-1) than RDHE2S microsomes under the same assay conditions (10 μM retinol and 1 mM NAD^+) (Table 1), suggesting that RDHE2S is localized primarily in the microsomal membranes.

Retinol dehydrogenase activities of murine RDHE2 and RDHE2S in intact cells

The finding that RDHE2 was inactive when assayed using either the microsomal or mitochondrial fractions of Sf9 cells prompted us to examine whether RDHE2 was catalytically active in the context of intact living cells. HEK293 cells were transiently transfected with pCS105 expression vectors encoding RDHE2 with a C-terminal FLAG tag. RDHE2S, which was previously shown to oxidize retinol in living cells [18], was also cloned into pCS105 expression vector in frame with FLAG tag and used as a positive control. The two enzymes were co-expressed with RALDH1 to enhance the relatively low endogenous retinaldehyde dehydrogenase activity of HEK293 cells (Fig. 1 B), which caused accumulation of unprocessed retinaldehyde in the cells under the conditions of this experiment. Remarkably, when expressed in intact cells, RDHE2 was

found to exhibit a retinol dehydrogenase activity, increasing the production of retinaldehyde from retinol (Fig. 1 C). This activity of RDHE2 resulted in a 3-fold increase in RA biosynthesis relative to mock-transfected cells (Fig. 1 D). In comparison, expression of RDHE2S at similar protein levels, as judged based on comparable staining intensity for FLAG tag (Fig. 1 B), resulted in a 15-fold increase in RA production (Fig. 1 D). These experiments confirmed that RDHE2S is a more active enzyme than RDHE2, but most importantly, they revealed that, although inactive towards retinol in isolated microsomes, RDHE2 was able to function as a retinol dehydrogenase in intact cells, confirming that RDHE2 is a catalytically active enzyme.

Expression patterns of murine RDHE2 and RDHE2S

To identify the tissues where RDHE2 and RDHE2S contribution could be essential for RA biosynthesis, we carried out analysis of their gene expression patterns. Tissue distribution of *Rdhe2* and *Rdhe2s* transcripts in adult mice was analyzed by qPCR. The two transcripts exhibited a largely overlapping expression pattern with the highest expression levels in skin, followed by tongue, intestine, and esophagus (Fig. 2 A). In addition, we examined the distribution of the PCR-amplified full-length mRNA corresponding to *Rdhe2* and *Rdhe2s* genes. This analysis largely confirmed the pattern determined by qPCR, with the highest expression levels observed in skin, esophagus, stomach, tongue, and trace amounts of transcripts detected in adipose tissue, intestine, colon, and possibly, testis (Fig. 2 A, inset).

To determine whether *Rdhe2* and *Rdhe2s* are expressed during embryogenesis, we employed semi-quantitative PCR. RNA was isolated from wild-type C57BL/6J embryos

between stages E9.5 to E14.5 in one day increments and utilized for the synthesis of cDNA, which then served as a template for PCR amplification using gene-specific primers (Fig. 2 B). PCR products encoding *Rdhe2* were observed starting at E12.5, increasing in abundance through E14.5. Products encoding *Rdhe2s* were detected earlier in development at E10.5 and persisted through E14.5. Thus, both *Rdhe2* and *Rdhe2s* were expressed from middle to late gestation.

Generation of RDHE2 and RDHE2S gene knockout mouse models

The ultimate proof that RDHE2 and RDHE2S are essential for RA biosynthesis would have to come from gene knockout studies. Since RDHE2S exhibited a several-fold higher catalytic activity as a retinol dehydrogenase than RDHE2 in *in vitro* assays, we decided to begin the *in vivo* functional analysis of these enzymes by focusing on RDHE2S. A RDHE2S-null mouse line was generated that carries a lacZ reporter element under the control of the native *Rdhe2s* promoter (Fig. S1 A). Upon Cre and Flp excision, exon 4 in the *Rdhe2s* was deleted and a frameshift mutation was introduced, which created a stop codon prior to catalytic residues (Fig. S1 B). Mice were genotyped using allele-specific primers, with expected product size of 570 bp for wild-type (WT) mice and a 248-bp product for *Rdhe2s*$^{-/-}$ mice (Fig. S1 C). Importantly, *Rdhe2s*$^{-/-}$ mice were obtained at Mendelian frequencies (28 out of 100 genotyped), were fertile and displayed no distinguishable phenotype, at least when maintained on a regular laboratory chow diet that contains 24.2 IU of vitamin A per gram. QPCR analysis of gene expression in skin of *Rdhe2s*$^{-/-}$ mice versus WT littermates did not reveal any significant differences (Fig. S2).

Since *Rdhe2* and *Rdhe2s* transcripts showed an overlapping expression pattern during development and adulthood, we reasoned that the lack of obvious phenotype in RDHE2S-null mice could be due to functional redundancy with RDHE2. To test this hypothesis, we generated two independent strains of *Rdhe2*$^{-/-}$;*Rdhe2s*$^{-/-}$ double knockout mice (DKO) lacking both RDHE2 and RDHE2S using CRISPR-mediated gene editing (Fig. 3). The first strain, DKO1, lacks exons 5-7 of *Rdhe2* and exons 1-5 of *Rdhe2s*. The second strain, DKO2, lacks exon 5 in *Rdhe2*, and has an 8-bp deletion in exon 2 of *Rdhe2s*, causing a frameshift (Fig. 3 A). The exact sequences resulting from these excisions are shown in Fig. S3. The absence of RDHE2 and RDHE2S proteins was confirmed by immunoblotting of microsomal fractions from skin of DKO mice with commercially available antibodies against murine RDHE2S (Fig. 3 B, upper), and antibodies against *Xenopus* rdhe2 (Fig. 3 B, lower), which recognize both murine RDHE2 and RDHE2S proteins.

The DKO mice have been backcrossed for six generations to WT C57BL/6 mice to resolve any potential off-target mutations. Both strains of mice are fertile and produce homozygous and heterozygous offspring at the expected Mendelian ratio. Interestingly, DKO mice can be readily distinguished from WT littermates by the appearance of their eyes, which have puffy eyelids and almond like shape, compared with the round eyes in a similarly aged control animal (Fig. 3 C).

Skin phenotype of DKO mouse models

The highest expression level of *Rdhe2* and *Rdhe2s* was observed in skin. Therefore, we began the investigation of functional role of RDHE2 and RDHE2S by

analyzing the retinol dehydrogenase activities of membrane fractions isolated from skin of DKO mice. Compared with WT mice, the retinol dehydrogenase activity of the microsomal fractions from DKO skin was reduced by ~10-fold ($p=0.001$) while the mitochondrial activity was reduced by ~6-fold ($p=0.02$) (Fig. 4 A).

Such a dramatic reduction in skin retinol dehydrogenase activity would be expected to have a major impact on RA biosynthesis and expression of RA target genes in DKO skin, possibly resulting in abnormal skin appearance. However, upon visual inspection there were no discernable differences in the appearance of skin or hair between DKO and WT littermates. We reasoned that the differences in RA signaling between WT and DKO mice might be exacerbated under the conditions of vitamin A deficiency. To produce vitamin A deficient mice, a cohort of pregnant dams was placed on a vitamin A deficient diet at mid-gestation and the pups were maintained on vitamin A deficient diet until sacrificed. The vitamin A deficient status was confirmed by analyzing the hepatic levels of retinyl esters (0.45 ± 0.28 nmol/mg) and retinol (0.026 ± 0.022 nmol/mg). Dorsal skin samples collected from these mice were examined for expression levels of RA-regulated and retinoid metabolic genes by qPCR. Surprisingly, the expression patterns of these genes in skin of DKO mice appeared to be only partially consistent with reduced RA signaling (Fig. 4 B). For example, the RA-inducible *Cyp26b1* was downregulated, but the expression levels of several other genes known to be regulated by RA (*Dhrs3, Rarβ*) did not change or were significantly increased (*Lrat, Stra6, Rbp1, Raldh2, Dhrs9*) [22-25].

Skin is a highly heterogeneous tissue composed of keratinocytes, hair follicles, sebaceous glands, fibroblasts, etc. The differentiation and growth of many of these cell

types is affected by RA levels [4]. To determine the exact localization of RDHE2 and RDHE2S in skin, we carried out immunohistological analysis of skin sections using custom made antibodies against *Xenopus* rdhe2 that recognize both murine proteins [18]. This analysis showed that RDHE2 and RDHE2S proteins are abundant in sebaceous gland and in epidermis (Fig. 4 C). This pattern was confirmed at the level of gene expression based on the activity of *Rdhe2s* gene promoter, which was detected by β-galactosidase staining assays in developing vibrissae and nasal pits of E14.5 *Rdhe2s*$^{+/-}$ embryos (Fig. 4 D) and also in sebaceous glands of adult *Rdhe2s*$^{+/-}$ mice (Fig. 4 E). Likewise, *Rdhe2* transcripts were detected in sebaceous glands and epidermis of adult wild-type C57BL/J6 mice by *in situ* hybridization (Fig. 4 F).

To determine whether the absence of RDHE2 and RDHE2S affected the structure of skin, we sectioned DKO and wild-type dorsal skin samples from mice on VAD diet and analyzed skin histology. The most obvious difference between DKO and WT skin from littermates was the larger size of sebaceous glands and a longer hair shaft in DKO skin (Fig. 4 G). This observation suggested that the hair follicles in skin of DKO mice were in the growth phase (anagen) whereas in WT skin they were in resting (telogen) phase. Furthermore, while the WT mice had characteristic telogen features at P50, such as a condensed dermal papilla and lack of an inner root sheath, the DKO littermate dorsal skin was in anagen, demonstrated by the enlarged dermal papilla and thickening of the keratinocyte strand between the dermal papilla and club hair (Fig. 4 H). To obtain independent and quantitative evidence that hair follicles were in anagen phase in skin of DKO mice, we carried out qPCR analysis of genes expressed in the pilosebaceous unit

[26]. Out of 18 genes tested, three were downregulated (*Cd34*, *Krt15*, and *Lgr6*) while most of the others were upregulated (Fig. 5).

The elevated expression of hair follicle growth and differentiation marker genes in DKO skin relative to littermate WT skin suggested that the hair follicles of DKO mice enter anagen sooner than in WT skin. We tested this hypothesis by shaving the backs of male and female mice and monitoring their hair regrowth. As shown in Fig. 6, both sexes displayed an accelerated hair regrowth. However, in males, this was noticeable only during the second synchronized hair cycle at the age of 60-62 days, whereas in females the difference was obvious already in the first cycle at day P29. Importantly, the difference in the hair regrowth was observed not only on VAD diet (Fig. 6 A) but also on chow diet (Fig. 6 B). The daily progression of hair growth in the 2 strains versus matched WT littermates on VAD diet is shown in Fig. S4.

Some members of the SDR superfamily exhibit broad substrate specificity [27]. Specifically, SDR9C family members, which include mouse RDH1 and human RoDH4, exhibit higher activity towards hydroxysteroids than retinol [28, 29]. Previously, we examined the activity of human RDHE2 towards a panel of hydroxysteroids but found no activity [20]. To determine whether murine orthologs exhibit activity towards steroid substrates, we compared the activity of microsomal fractions from RDHE2/E2S DKO mice and WT mice towards various functional groups in androgens, progestins, corticosteroid and estradiol: androsterone (3α-OH oxidation with NAD; 17-keto reduction with NADH), dihydrotestosterone/NAD (17β-OH oxidation), 3α-hydroxy-5α-pregnan-20-one (3α-OH oxidation with NAD; 20-keto reduction with NADH); Δ4-pregnene-3,20-dione (3 and 20-one reduction with NADH), androst-5-en-3β-ol-17-one

(3β-OH oxidation with NAD); estradiol (3β-OH and 17β-OH oxidation with NAD; corticosterone (11β-OH and 21-OH oxidation with NAD; 3-keto reduction with NADH). In contrast to retinol as substrate, where we saw a ~80% drop in activity of DKO microsomes, no decrease was observed in the activity of the same microsomes towards any of the substrates tested relative to WT microsomes (Fig. S5). In fact, there was a slight increase in the activity of DKO microsomes towards some of the steroid substrates, which could be related to the differences in hair follicle growth phase in DKO mice versus WT mice. The lack of a decrease in steroid dehydrogenase activity further strengthens our conclusion that RDHE/E2S function as retinol dehydrogenases.

Eye phenotype of DKO mouse models

To determine the underlying cause of the almond-shaped appearance of eyes in DKO mice, their eyes were dissected and compared to littermate controls. No difference in either size or weight of eyeballs was observed. However, histological analysis revealed that both the upper and lower eyelids in DKO mice were significantly thicker and longer compared to WT animals (Fig. 7 A), which explains why the eyes appeared partially closed. The expansion of eyelids appeared to be due to the larger size of meibomian glands in DKO mice. To determine the localization of RDHE2 and RDHE2S, sections of eyelids from WT mice were immunostained with custom-made antibodies against murine RDHE2S (Fig. 7 B) and commercially available antibodies against RDHE2 (Fig. 7 C). Both antibodies detected the corresponding proteins in WT meibomian glands, whereas DKO eyelids showed little or no staining. Thus, the lack of expression of RDHE2 and RDHE2S resulted in enlargement of meibomian glands of DKO animals.

Discussion

Several members of the SDR superfamily of proteins can oxidize retinol to retinaldehyde *in vitro*, however, with the exception of RDH10, their physiological relevance for RA biosynthesis remains unclear. This study provides convincing evidence that mammalian RDHE2 and RDHE2S function as physiologically relevant retinol dehydrogenases. The results of this study are important because they highlight the existence of tissue-specific retinol dehydrogenases that are essential for RA biosynthesis in specific cell types while not being critical for survival, as in the case with RDH10 during midgestation [11-15]. In fact, since RDH10-null embryos can be rescued by supplementation with retinaldehyde [11], the precursor for RA, our findings suggest that other retinol dehydrogenases, e.g., RDHE2 and RDHE2S, may be as important for postnatal development and maintenance of specific adult tissues as RDH10.

Analysis of substrate and cofactor specificity carried out in this study shows that, in agreement with their functions as oxidative enzymes, epidermal retinol dehydrogenases prefer NAD(H) as cofactors and are more catalytically efficient in the oxidative direction with all-*trans*-retinol than in the reductive direction with all-*trans*-retinaldehyde as substrate. Interestingly, like human RDH10 [30], RDHE2S recognizes 11-*cis*-retinol as substrate in addition to all-*trans*-retinol. A recent study provided evidence that RDH10 contributes to the oxidation of 11-*cis*-retinol in mouse retina, but mice deficient in both RDH10 and RDH5 still convert 11-*cis*-retinol to 11-*cis*-retinaldehyde in the visual cycle [31]. The identities of the remaining 11-*cis*-retinol dehydrogenases are currently unknown. If RDHE2S is expressed in mouse retina, this enzyme could complement RDH10 and RDH5 in oxidizing 11-*cis*-retinol.

A surprising finding of this study is that the retinol dehydrogenase activity of murine RDHE2 is undetectable in the isolated microsomal or mitochondrial fractions of RDHE2-expressing Sf9 cells. However, RDHE2 is fully functional as a retinol dehydrogenase when expressed in mammalian living cells. This observation suggests that murine RDHE2 requires additional cellular factors to exhibit its full enzymatic potential. As shown in our previous study, a member of the SDR16C family, human DHRS3 (SDR16C1) requires the presence of human RDH10 (SDR16C4) to display a measurable retinaldehyde reductase activity, and in turn, activates RDH10 [32]. However, co-expression of murine RDHE2 or RDHE2S with human DHRS3, which is 97.7% identical to murine DHRS3 in HEK293 cells had no activating effect on DHRS3 [33], indicating that RDHE2 and RDHE2S do not interact with DHRS3. Like murine RDHE2, human RDHE2 (SDR16C5) also displays a rather low activity [34]. Future affinity purification assays may be warranted in order to identify possible partners of RDHE2.

It is also interesting that while RDHE2S exhibits a higher retinol dehydrogenase activity than RDHE2, a single *Rdhe2s* gene knockout does not display the same phenotype as the DKO mice. *Rdhe2s*$^{-/-}$ mice have normal eyelids and regular hair growth (data not shown). This observation indicates that first, despite its lower enzymatic activity, RDHE2 is essential for RA biosynthesis in mice; and second, the functions of these two enzymes may be redundant because of the overlapping expression pattern. The reason for such an overlap is unclear at this time. It should be noted that in humans only *RDHE2* represents a functional gene encoding a stable protein with enzymatic activity, whereas human RDHE2S (SDR16C6) appears to have lost its function and is classified as pseudogene [34]. It is possible that in humans, *RDHE2*, which exhibits a wider tissue

distribution pattern (https://www.ncbi.nlm.nih.gov/gene/195814#gene-expression) than either murine *Rdhe2* (https://www.ncbi.nlm.nih.gov/gene/242285) or *Rdhe2s* (https://www.ncbi.nlm.nih.gov/gene/?term=Mus+musculus+Sdr16c6) fulfills the mission of both enzymes.

This study shows that in mice, RDHE2 and RDHE2S together account for up to 80% of the total membrane-associated retinol dehydrogenase activity in skin. Thus, while present in skin, RDH10 is not the major retinol dehydrogenase in this tissue. The absence of RDHE2 and RDHE2S results in significant changes in the hair cycle of mice. Hair cycle occurs in three phases: anagen (growth), catagen (regression), and telogen (resting) [35-47]. Typically, development of dorsal hair follicles continues until postnatal day 16, when the first catagen occurs on days 17-20. Telogen spans days 21-25, and anagen lasts from day 28 to day 42. This is followed by the second cycle during which hair follicles continue to cycle in a nearly synchronized manner. Anagen phase is characterized by thickening of the dermal and epidermal layers of the skin, increased size of hair follicles, extension of follicles deep into the dermal adipose tissue, and initiation of melanin synthesis. All of these features were observed in the dermis and epidermis of DKO skin but not in skin of WT littermates. Consistent with histological assessment, DKO skin showed increased expression of several markers of anagen phase [26]. For example, a strong indication of the anagen phase is the induction of the hedgehog signaling pathway. In DKO skin, both *Gli1* and *Gli2* transcriptional regulators in the hedgehog pathway were upregulated. Hair cycles are fueled by HF stem cells that reside in the “bulge” niche located at the base of the telogen phase HF [48]. In addition to *Gli1*, which is expressed in the hair bulge and germ [49, 50], several other markers of the bulge stem cell

compartment were upregulated in DKO skin. Among these the most notable are SRY(sex determining regionY)-box9(SOX-9), which is indispensable for hair homeostasis [51, 52]; T-box 1 (*Tbx1*), which is highly enriched in the bulge of developing and cycling HFs [53]; and leucine-rich repeat-containing G-protein coupled receptor 5 (*Lgr5*), a marker of hair follicle stem cells [54].

The enlargement of sebaceous glands was confirmed by several-fold higher expression of melanocortin-5 receptor (*Mc5r*), a marker of sebocyte differentiation [55]; *Prdm1* gene, which encodes BLIMP1, believed to be a marker of terminally differentiated sebocytes [56] (2010) and/or a sebocyte progenitor marker [57]; peroxisome proliferator activated receptor γ (*Pparγ*), which plays an important role in sebaceous gland development; stearyl CoA desaturase 1 (*Scd1*) and perilipin 2 (*Plin2*), which are necessary for sebocyte differentiation and sebum production in sebocytes [reviewed in 58].

One of the most upregulated genes in both males (DKO2 strain) and females (DKO1 strain) was *Lef1* gene in the Wnt signaling pathway. It is well known that the regulation of the hair follicle cycle involves cross-talk of the Wnt/β-catenin, Hedgehog, and Notch signaling pathways [59-64]. However, nonprotein factors, and in particular vitamin A [65, reviewed in 66], are also critical for maintenance of skin health. In this respect, there is evidence for mutual antagonism between Wnt/β-catenin signaling and RA signaling [67]. β-Catenin positively regulates CYP26A1, which degrades RA, and conversely, β-catenin undergoes retinoid-dependent interaction with RAR, resulting in competitive inhibition of TCF binding sites [67, 68]. Inhibition of Wnt/β-catenin signaling leads to upregulation of RA-inducible cellular RA binding protein type 2

(CRABP2), suggesting increased RA signaling [69]. It is noteworthy, however, that while RA signaling is clearly essential for epidermal differentiation, the mechanisms by which it acts are largely unexplored. This study and the generation of RDHE2 and RDHE2S DKO mouse models should facilitate the investigation of the role RA plays in the regulation of hair follicle growth and differentiation, and in general maintenance of epidermis.

Interestingly, 13-*cis*-retinoic acid (isotretinoin) is clinically used for acne treatment and believed to inhibit sebocyte differentiation and lipid synthesis [70, 71] by isomerizing to all-*trans*-retinoic acid [58]. The enlarged sebaceous glands observed in DKO mice are consistent with the decreased levels of RA biosynthesis in skin. We have also observed enlarged meibomian glands in DKO eyelids. Meibomian glands are modified sebaceous glands that secrete meibum, a lipid-rich fluid that forms a superficial oily layer on the tear film to prevent the film from evaporating. Of note, severe bilateral lower eyelid retraction and dry eye symptoms were observed in patients with the long-term use of topical retinoids for cosmetic purposes [72-74]. Thus, reduced RA biosynthesis in eyelids of DKO mice appears to be consistent with the observed enlargement of their meibomian glands. Previous studies have also noted that systemic use of retinoids for acne treatment or skin rejuvenation was associated with histopathological changes in the eyelids and degenerative changes in the meibomian gland acini [73, 74].

It is worth pointing out that, while the *in vivo* phenotype is clearly consistent with the reduced RA signaling in DKO skin as a result of the 80% reduction in retinol dehydrogenase activity, qPCR analysis of endogenous RA-regulated genes produced a

very mixed picture, with some RA-inducible genes being downregulated while others unchanged or even upregulated. Histological analysis of skin sections revealed the cause of this seemingly puzzling outcome. Since the reduced RA signaling led to enlargement of sebaceous glands, which express several RA-sensitive genes (*Dhrs9, Lrat, Stra6*), the transcript levels of these genes were likely increased as a result of an expanded number of sebocytes. Thus, measurement of total levels of RA in skin could be misleading, because it would not reflect the localized differences in cell type-specific RA levels in tissue as heterogeneous as skin.

Overall, the results of this study establish RDHE2 and RDHE2S as physiologically relevant retinol dehydrogenases in mammals, which despite their importance for RA biosynthesis are not critical for survival during embryogenesis. In view of these findings, the physiological impact of mutations in these genes or changes in their expression can be better appreciated considering their role in RA biosynthesis. As discussed previously [34], genome-wide association studies have linked the chromosomal region harboring *RDHE2* (SDR16C5) and seven other genes to stature and growth in cattle, humans, and pigs [35-82], and beak deformity in chickens [83]. *RDHE2* was also identified as the important candidate gene in pig growth trait by an integrative genomic approach [84]. Interestingly, expression of *SDR16C5* was reported to be 4-fold higher than *RDH10* in human lung (pooled RNA from five individuals) [85]. Altered SDR16C5 expression is frequently noted in various pathophysiological conditions. For example, *SDR16C5* was decreased in triple-negative breast cancer patient samples [86]. Evidence provided by this study that mammalian RDHE2/E2S function as physiologically relevant

retinol dehydrogenases implicates the decrease in RA biosynthesis as at least one of the causes leading to these pathophysiological outcomes.

Acknowledgements

The content is solely the responsibility of the authors and does not necessarily represent the official views of the National Institutes of Health. Human HA-tagged RALDH1 expression construct in pcDNA3.1-neo (CMV promoter) was a generous gift of Dr. Sylvie Mader in the Department of Biochemistry, University of Montreal, Canada. HA-epitope antibodies were received as a gift from Dr. Hengbin Wang, Department of Biochemistry and Molecular Genetics, University of Alabama at Birmingham School of Medicine. We are grateful to Dr. Anil K. Challa, University of Alabama at Birmingham, for his help with performing CRISPR-mediated gene mutations. Services provided in this publication through the University of Alabama at Birmingham Transgenic & Genetically Engineered Models facility (RAK) are supported by National Institutes of Health Grants P30 CA13148, P30 AR048311, P30 DK074038, P30 DK05336, and P60 DK079626.

Conflicts of Interest

The authors declare that they have no conflicts of interest with the contents of this article.

Author Contributions

Lizhi Wu, Olga V. Belyaeva, Alla V. Klyuyeva, Mark K. Adams, Kelli R. Goggans, and Seung-Ah Lee designed, performed experiments, analyzed the data, and

wrote the manuscript. Robert Kesterson contributed to generation of gene knockout mouse models, provided scientific advice and edited the manuscript. Kirill Popov provided scientific advice and edited the manuscript. Natalia Kedishvili planned the project, designed experiments, and wrote the manuscript.

References

1. Al Tanoury, Z., Piskunov, A., and Rochette-Egly, C. (2013) Vitamin A and retinoid signaling: genomic and nongenomic effects. J. Lipid Res. 54, 1761-1775.

2. Shannon, S. R., Moise, A. R., and Trainor, P. A. (2017) New insights and changing paradigms in the regulation of vitamin A metabolism in development. Wiley Interdiscip Rev Dev Biol. 6, doi: 10.1002/wdev.264.

3. Metzler, M. A., and Sandell, L. L. (2016) Enzymatic Metabolism of Vitamin A in Developing Vertebrate Embryos. Nutrients 8, pii: E812.

4. Everts, H. B. (2012) Endogenous Retinoids In The Hair Follicle And Sebaceous Gland. Biochim. Biophys. Acta 1821, 222-229.

5. Balmer, J. E, and Blomhoff, R. (2002) Gene expression regulation by retinoic acid. J. Lipid Res., 43, 1773-1808.

6. Benbrook, D. M., Chambon, P., Rochette-Egly, C., and Asson-Batres, M. A. (2014) History of retinoic acid receptors. Subcell. Biochem. 70, 1-20.

7. Wei, L. N. (2016) Cellular Retinoic Acid Binding Proteins: Genomic and Non-genomic Functions and their Regulation. Subcell. Biochem. 81, 163-178.

8. Iskakova, M., Karbyshev, M., Piskunov, A., and Rochette-Egly, C. (2015) Nuclear and extranuclear effects of vitamin A. Can. J. Physiol. Pharmacol. 93, 1065-1075.

9. Kedishvili, N. Y. (2013) Enzymology of retinoic acid biosynthesis and degradation. J. Lipid Res. 54, 1744-1760.

10. Napoli, J. L. (1986) Retinol metabolism in UC-PKI cells. Characterization of retinoic acid synthesis by an established mammalian cell line. J. Biol. Chem. 261, 13592-13597.

11. Rhinn, M., Schuhbaur, B., Niederreither, K., and Dollé, P. (2011) Involvement of retinol dehydrogenase 10 in embryonic patterning and rescue of its loss of function by maternal retinaldehyde treatment. Proc. Natl. Acad. Sci. USA 108, 16687-16692.

12. Sandell, L. L., Sanderson, B. W., Moiseyev, G., Johnson, T., Mushegian, A., Young, K., Rey, J.-P., Ma, J.-X., Staehling-Hampton, K. and Trainor, P.A. (2007) RDH10 is essential for synthesis of embryonic retinoic acid and is required for limb, craniofacial, and organ development. Genes Dev. 21, 1113-1124.

13. Ashique, A. M., May, S. R., Kane, M. A., Folias, A. E., Phamluong, K., Choe, Y., Napoli, J. L. and Peterson, A. S. (2012) Morphological defects in a Novel Rdh10 Mutant

that has Reduced Retinoic Acid Biosynthesis and Signaling. Genesis 50, 415-423.

14. Cunningham, T. J., Chatzi, C., Sandell, L. L., Trainor, P. A. and Duester, G. (2011) Rdh10 Mutants Deficient in Limb Field Retinoic Acid Signaling Exhibit Normal Limb Patterning but Display Interdigital Webbing. Dev. Dyn. 240, 1142-1150.

15. Sandell, L. L., Lynn, M. L., Inman, K. E., McDowell, W. and Trainor, P. A. (2012) RDH10 Oxidation of Vitamin A Is a Critical Control Step in Synthesis of Retinoic Acid during Mouse Embryogenesis. PLoS ONE 7, e30698.

16. Wu, B. X., Chen, Y., Chen, Y., Fan, J., Rohrer, B., Crouch, R. K. and Ma, J.-X. (2002) Cloning and Characterization of a Novel all-trans Retinol Short-Chain Dehydrogenase/Reductase from the RPE. Invest. Ophthalmol. Vis. Sci. 43, 3365-3372.

17. Persson, B., Bray, J. E., Bruford, E., Dellaporta, S. L., Favia, A. D., Gonzalez Duarte, R., Jörnvall, H., Kallberg, Y., Kavanagh, K. L., Kedishvili, N. *et al.* (2009) The SDR (Short-Chain Dehydrogenase/Reductase and Related Enzymes) Nomenclature Initiative. Chem. Biol. Interact. 178, 94-98.

18. Belyaeva, O. V., Lee, S.-A., Adams, M. K., Chang, C. and Kedishvili, N. Y. (2012) Short Chain Dehydrogenase/Reductase Rdhe2 Is a Novel Retinol Dehydrogenase Essential for Frog Embryonic Development. J. Biol. Chem. 287, 9061-9071.

19. Belyaeva, O. V., Chang, C., Berlett, M. C. and Kedishvili, N. Y. (2015) Evolutionary origins of retinoid active short-chain dehydrogenases/reductases of SDR16C family. Chem. Biol. Interact. 234, 135-143.

20. Lee, S.-A., Belyaeva, O. V. and Kedishvili, N. Y. (2009) Biochemical Characterization of Human Epidermal Retinol Dehydrogenase 2. Chem. Biol. Interact. 178, 182-187.

21. Labrie, F., Simard, J., Luu-The, V., Pelletier, G., Bélanger, A., Lachance, Y., Zhao, H. F., Labrie, C., Breton, N., and de Launoit, Y. (1992) Structure and tissue-specific expression of 3 beta-hydroxysteroid dehydrogenase/5-ene-4-ene isomerase genes in human and rat classical and peripheral steroidogenic tissues. J. Steroid Biochem. Mol. Biol. 41, 421-435.

22. Ross, A. C., and Zolfaghari, R. (2011) Cytochrome P450s in the regulation of cellular retinoic acid metabolism. Annu. Rev. Nutr. 21, 65-87.

23. O'Byrne, S. M., and Blaner, W. S. (2013) Retinol and retinyl esters: biochemistry and physiology. J. Lipid Res. 54, 1731-1743.

24. Lee, L. M., Leung, C. Y., Tang, W. W., Choi, H. L., Leung, Y. C., McCaffery, P. J., Wang, C. C., Woolf, A. S., and Shum, A. S. (2012) A paradoxical teratogenic

mechanism for retinoic acid. Proc. Natl. Acad. Sci. U. S. A. 109, 13668-13673.

25. Lee, S. A., Belyaeva, O. V., Wu, L., and Kedishvili, N. Y. (2011) Retinol dehydrogenase 10 but not retinol/sterol dehydrogenase(s) regulates the expression of retinoic acid-responsive genes in human transgenic skin raft culture. J. Biol. Chem. 286, 13550-13560.

26. Gonzales, K. A. U., and Fuchs, E. (2017) Skin and Its Regenerative Powers: An Alliance between Stem Cells and Their Niche. Dev. Cell. 43, 387-401.

27. Napoli, J. L. (2001) 17β-Hydroxysteroid dehydrogenase type 9 and other short-chain dehydrogenases/reductases that catalyze retinoid, 17β- and 3α-hydroxysteroid metabolism. Mol. Cell. Endocrinol. 171, 103-109.

28. Zhang, M., Chen, W., Smith S. M., and Napoli J. L. 2001. Molecular characterization of a mouse short chain dehydrogenase/reductase active with all-trans-retinol in intact cells, mRDH1. J. Biol. Chem. 276, 44083–44090.

29. Gough, W. H., VanOoteghem, S., Sint, T., and Kedishvili N. Y. (1998) cDNA cloning and characterization of a new human microsomal NAD+-dependent dehydrogenase that oxidizes all-trans retinol and 3α-hydroxysteroids. J. Biol. Chem. 273, 19778–19785.

30. Belyaeva, O. V., Johnson, M. P. and Kedishvili, N. Y. (2008) Kinetic Analysis of Human Enzyme RDH10 Defines the Characteristics of a Physiologically Relevant Retinol Dehydrogenase. J. Biol. Chem. 283, 20299-20308.

31. Sahu, B., Sun, W., Perusek, L., Parmar, V., Le, Y. Z, Griswold, M. D., Palczewski, K., and Maeda, A. (2015) Conditional Ablation of Retinol Dehydrogenase 10 in the Retinal Pigmented Epithelium Causes Delayed Dark Adaption in Mice. J. Biol. Chem. 290, 27239-27247.

32. Adams, M. K., Belyaeva, O. V., Wu, L., and Kedishvili, N. Y. (2014) The retinaldehyde reductase activity of DHRS3 is reciprocally activated by retinol dehydrogenase 10 to control retinoid homeostasis. J. Biol. Chem. 289, 14868-14880.

33. Belyaeva, O. V., Chang, C., Berlett, M. C. and Kedishvili, N. Y. (2015) Evolutionary origins of retinoid active short-chain dehydrogenases/reductases of SDR16C family. Chem. Biol. Interact. 234, 135-143.

34. Adams, M. K., Lee, S. A., Belyaeva, O. V., Wu, L., and Kedishvili, N. Y. (2017) Characterization of human short chain dehydrogenase/reductase SDR16C family members related to retinol dehydrogenase 10. Chem. Biol. Interact. 276, 88-94.

35. Myung, P., and Ito, M. (2012) Dissecting the bulge in hair regeneration. J. Clin. Invest. 122, 448-454.

36. Chase, H. B., Rauch, R., and Smith, V. W. (1951) Critical stages of hair development and pigmentation in the mouse. Physiol. Zool. 24, 1-8.

37. Plikus, M. V., Mayer, J. A., de la Cruz, D., Baker, R. E., Maini, P. K., Maxson, R., and Chuong, C. M. (2008) Cyclic dermal BMP signalling regulates stem cell activation during hair regeneration. Nature 451, 340-344.

38. Muller-Rover, S., Handjiski, B., van der Veen, C., Eichmuller, S., Foitzik, K., McKay, I. A., Stenn, K. S., and Paus, R. (2001) A comprehensive guide for the accurate classification of murine hair follicles in distinct hair cycle stages. J. Invest. Dermatol. 117, 3-15.

39. Chen, C. C., Plikus, M. V., Tang, P. C., Widelitz, R. B., and Chuong, C. M. (2016) The Modulatable Stem Cell Niche: Tissue Interactions during Hair and Feather Follicle Regeneration. J. Mol. Biol. 428, 1423-1440.

40. Hsu, Y. C., Li, L. S., and Fuchs, E. (2014) Emerging interactions between skin stem cells and their niches. Nature Medicine 20, 847-856.

41. Lay, K., Kume, T., and Fuchs, E. (2016) FOXC1 maintains the hair follicle stem cell niche and governs stem cell quiescence to preserve long-term tissue-regenerating potential. Proc. Natl. Acad. Sci. U.S.A. 113, E1506-E1515.

42. Schneider, M. R., Schmidt-Ullrich, R., and Paus, R. (2009) The Hair Follicle as a Dynamic Miniorgan. Curr. Biol. 19, R132-R142.

43. Barker, N., Tan, S., and Clevers, H. (2013) Lgr proteins in epithelial stem cell biology. Development 140, 2484-2494.

44. Goldstein, J., Horsley, V. (2012) Home sweet home: skin stem cell niches. Cell. Mol. Life Sci. 69, 2573-2582.

45. Jensen, K. B., Collins, C. A., Nascimento, E., Tan, D. W., Frye, M., Itami, S., and Watt, F. M. (2009) Lrig1 expression defines a distinct multipotent stem cell population in mammalian epidermis. Cell Stem Cell 4, 427-439.

46. Genander, M., Cook, P. J., Ramskold, D., Keyes, B. E., Mertz, A. F., Sandberg, R., and Fuchs, E. (2014) BMP Signaling and Its pSMAD1/5 Target Genes Differentially Regulate Hair Follicle Stem Cell Lineages. Cell Stem Cell 15, 619-633.

47. Ahmed, N. S., Ghatak, S., El Masry, M. S., Gnyawali, S. C., Roy, S., Amer, M., Everts, H., Sen, C. K., and Khanna, S. (2017) Epidermal E-Cadherin Dependent beta-Catenin Pathway Is Phytochemical Inducible and Accelerates Anagen Hair Cycling.

Molecular Therapy 25, 2502-2512.

48. Cotsarelis, G., Sun, T. T., and Lavker, R. M. (1090) Label-retaining cells reside in the bulge area of pilosebaceous unit: implications for follicular stem cells, hair cycle, and skin carcinogenesis. Cell 61, 1329–1337.

49. Levy, V., Lindon, C., Harfe, B. D., and Morgan, B. A. (2005) Distinct stem cell populations regenerate the follicle and interfollicular epidermis. Dev. Cell. 9, 855–861.

50. Brownell, I., Guevara, E., Bai, C. B., Loomis, C. A., and Joyner, A. L. (2011) Nerve-derived sonic hedgehog defines a niche for hair follicle stem cells capable of becoming epidermal stem cells. Cell Stem Cell 8, 552–565.

51. Nowak, J. A., Polak, L., Pasolli, H. A., and Fuchs, E. (2008) Hair follicle stem cells are specified and function in early skin morphogenesis. Cell Stem Cell. 3, 33–43.

52. Vidal, V. P., Chaboissier, M. C., Lützkendorf, S., Cotsarelis, G., Mill, P., Hui, C. C., Ortonne, N., Ortonne, J. P., and Schedl, A. (2005) Sox9 is essential for outer root sheath differentiation and the formation of the hair stem cell compartment. Curr. Biol. 15, 1340-1351.

53. Chen, T., Heller, E., Beronja, S., Oshimori, N., Stokes, N. and Fuchs, E. (2012) An RNA interference screen uncovers a new molecule in stem cell self-renewal and long-term regeneration. Nature 485, 104-108.

54. Jaks, V., Barker, N., Kasper, M., van Es, J. H., Snippert, H. J., Clevers, H., and Toftgård, R. (2008) Lgr5 marks cycling, yet long-lived, hair follicle stem cells. Nat. Genet. 40, 1291-1299.

55. Zhang, L., Li, W. H., Anthonavage, M., and Eisinger, M. (2006) Melanocortin-5 receptor: a marker of human sebocyte differentiation. Peptides 27, 413-420.

56. Sellheyer, K., and Krahl, D. (2010) Blimp-1: a marker of terminal differentiation but not of sebocytic progenitor cells. J. Cutan. Pathol. 37, 362-370.

57. Horsley, V., O'Carroll, D., Tooze, R., Ohinata, Y., Saitou, M., Obukhanych, T., Nussenzweig, M., Tarakhovsky, A., and Fuchs, E. (2006) Blimp1 defines a progenitor population that governs cellular input to the sebaceous gland. Cell 126, 597-609.

58. Zouboulis, C. C., Picardo, M., Ju, Q., Kurokaw, I., Törőcsik, D., Bíró, T., and Schneider, M. R. (2016) Beyond acne: Current aspects of sebaceous gland biology and function. Rev. Endocr. Metab. Disord. 17, 319-334.

59. Gat, U., DasGupta, R., Degenstein, L., and Fuchs, E. (1998) De novo hair follicle morphogenesis and hair tumors in mice expressing a truncated β-catenin in skin. Cell 95,

605–614.

60. Oro, A. E., and Higgins, K. (2003). Hair cycle regulation of Hedgehog signal reception. Dev. Biol. 255, 238–248.

61. Silva-Vargas, V., Lo Celso, C., Giangreco, A., Ofstad, T., Prowse, D. M., Braun, K. M., and Watt, F. M. (2005) β-catenin and Hedgehog signal strength can specify number and location of hair follicles in adult epidermis without recruitment of bulge stem cells. Dev. Cell. 9, 121–131.

62. Vauclair, S., Nicolas, M., Barrandon, Y., and Radtke, F. (2005) Notch1 is essential for postnatal hair follicle development and homeostasis. Dev. Biol. 284, 184–193.

63. Estrach, S., Cordes, R., Hozumi, K., Gossler, A., and Watt, F.M. (2008) Role of the Notch ligand Delta1 in embryonic and adult mouse epidermis. J. Invest. Dermatol. 128, 825–832.

64. Blanpain, C., Lowry, W.E., Pasolli, H.A., and Fuchs, E. (2006) Canonical notch signaling functions as a commitment switch in the epidermal lineage. Genes Dev. 20, 3022–3035.

65. Wolbach, S. B., and Howe, P. R. (1978) Nutrition Classics. The Journal of Experimental Medicine 42: 753–77, 1925. Tissue changes following deprivation of fat-soluble A vitamin. S. Burt Wolbach and Percy R. Howe. Nutr. Rev. 36, 16–9.

66. Chambon, P. (1996) A decade of molecular biology of retinoic acid receptors. FASEB J. 10, 940–954.

67. Mongan, N. P., and Gudas, L. J. (2007) Diverse actions of retinoid receptors in cancer prevention and treatment. Differentiation 75, 853–870.

68. Easwaran, V., Pishvaian, M., Salimuddin, and Byers, S. (1999) Cross-regulation of β-catenin-LEF/TCF and retinoid signalling pathways. Curr. Biol. 9, 1415–1418.

69. Collins, C. A., and Watt, F. M. (2008) Dynamic regulation of retinoic acid-binding proteins in developing, adult and neoplastic skin reveals roles for beta-catenin and Notch signalling. Dev. Biol. 324, 55-67.

70. Clarke, S. B., Nelson, A. M., George, R. E., and Thiboutot, D. M. (2007) Pharmacologic modulation of sebaceous gland activity: mechanisms and clinical applications. Dermatol. Clin. 25, 137-146.

71. Pan, J., Wang, Q., and Tu, P. (2017) A Topical Medication of All-Trans Retinoic Acid Reduces Sebum Excretion Rate in Patients With Forehead Acne. Am. J. Ther. 24,

e207-e212.

72. Winkler, K. P., Evan, H., Black, E. H., and Servat, J. (2017) Lower Eyelid Retraction Associated With Topical Retinol Use. Ophthal. Plast. Reconstr. Surg. 33, 483.

73. Kremer, I., Gaton, D. D., David, M., Gaton, E., and Shapiro, A. (1994) Toxic effects of systemic retinoids on meibomian glands. Ophthalmic Res. 26, 124-128.

74. Ding, J., Kam, W. R., Dieckow, J., and Sullivan, D. A. (2013) The influence of 13-cis retinoic acid on human meibomian gland epithelial cells. Invest. Ophthalmol. Vis. Sci. 54, 4341-4350.

75. Pryce, J. E., Hayes, B. J., Bolormaa, S., and Goddard, M. E. (2011) Polymorphic Regions Affecting Human Height Also Control Stature in Cattle. Genetics 187, 981–984.

76. Nishimura, S., Mizoshita, K., Tatsuda, K., Fujita, T., Watanabe, N., and Sugimoto, Y. (2012) Genome-wide association study identified three major QTL for carcass weight including the PLAG1-CHCHD7 QTN for stature in Japanese Black cattle. BMC Genet. 13, 40.

77. Gudbjartsson, D. F., Walters, G. B., Thorleifsson, G., Stefansson, H., Halldorsson, B. V., Zusmanovich, P., Sulem, P., Thorlacius, S., Gylfason, A., Steinberg, S., *et al.* (2008) Many sequence variants affecting diversity of adult human height. Nat. Genet. 40, 609–615.

78. Weedon, M. N., Lango, H., Lindgren, C. M., Wallace, C., Evans, D. M., Mangino, M., Freathy, R. M., Perry, J. R. B., Stevens, S., Hall, A. S., *et al.* (2008) Genome-wide association analysis identifies 20 loci that influence adult height. Nat. Gen. 40, 575–583.

79. Lettre, G., Jackson, A. U., Gieger, C., Schumacher, F. R., Berndt, S. I., Sanna, S., Eyheramendy, S., Voight, B. F., Butler, J. L., Guiducci, C., *et al.* (2008) Identification of ten loci associated with height highlights new biological pathways in human growth. Nat. Genet. 40, 584–591.

80. Karim, L., Takeda, H., Lin, L., Druet, T., Arias, J. A. C., Baurain, D., Cambisano, N., Davis, S. R., Farnir, F., Grisart, B., *et al.* (2011) Variants modulating the expression of a chromosome domain encompassing PLAG1 influence bovine stature. Nat. Genet. 43, 405–413.

81. Littlejohn, M., Grala, T., Sanders, K., Walker, C., Waghorn, G., Macdonald, K., Coppieters, W., Georges, M., Spelman, R., Hillerton, E., *et al.* (2012) Genetic variation in PLAG1 associates with early life body weight and peripubertal weight and growth in Bos Taurus. Anim. Genet. 43, 591–594.

82. Jiao, S., Maltecca, C., Gray, K. A., and Cassady, J. P. (2014) Feed intake, average daily gain, feed efficiency, and real-time ultrasound traits in Duroc pigs: II. Genomewide association. J. Anim. Sci. 92, 2846–2860.

83. Bai, H., Zhu, J., Sun, Y., Liu, R., Liu, N., Li, D., Wen, J., and Chen, J. (2014) Identification of Genes Related to Beak Deformity of Chickens Using Digital Gene Expression Profiling. PLoS ONE. 9, e107050.

84. Xiong, X., Yang, H., Yang, B., Chen, C., and Huang, L. (2015) Identification of quantitative trait transcripts for growth traits in the large scales of liver and muscle samples. Physiol. Genomics. 47, 274–280.

85. Ashmore, J. H., Luo, S., Watson, C. J. W., and Lazarus, P. (2018) Carbonyl reduction of NNK by recombinant human lung enzymes: identification of HSD17β12 as the reductase important in (R)-NNAL formation in human lung. Carcinogenesis 39, 1079–1088.

86. Qi, F., Qin, W.-X., and Zang, Y.-S. (2019) Molecular mechanism of triple-negative breast cancer-associated BRCA1 and the identification of signaling pathways. Oncol. Lett. 17, 2905–2914.

87. Belyaeva, O. V., Stetsenko, A. V., Nelson, P. and Kedishvili, N. Y. (2003) Properties of Short-Chain Dehydrogenase/Reductase RalR1: Characterization of Purified Enzyme, Its Orientation in the Microsomal Membrane, and Distribution in Human Tissues and Cell Lines. Biochemistry-US. 42, 14838-14845.

88. Challa, A. K., Boitet, E. R., Turner, A. N., Johnson, L. W., Kennedy, D., Downs, E. R., Hymel, K. M., Gross, A. K., and Kesterson, R. A. (2016) Novel Hypomorphic Alleles of the Mouse Tyrosinase Gene Induced by CRISPR-Cas9 Nucleases Cause Non-Albino Pigmentation Phenotypes. PLoS One 11. e0155812.

89. Nagy A., Gertsenstein M., Vintersten K., and Behringer R. (2003) Manipulating the Mouse Embryo: A Laboratory Manual. Cold Spring Harbor Laboratory Press, Cold Spring Harbor, New York.

90. Chetyrkin, S. V., Hu, J., Gough, W. H., Dumaual, N., and Kedishvili, N. Y. Further characterization of human microsomal 3alpha-hydroxysteroid dehydrogenase. (2001) Arch. Biochem. Biophys. 386, 1-10.

91. Schneider C. A., Rasband, W. S., and Eliceiri, K. W. (2012) NIH Image to ImageJ: 25 years of image analysis. Nat. Methods 9, 671-675.

SDR	Substrate/Cofactor	Apparent K*m* μM	Apparent V*max* nmol·min-1·mg-1	V*max*/K*m*
Xenopus rdhe2	all-*trans*-retinol	0.6 ± 0.1	19.5 ± 0.6	32.5
	NAD^+	108 ± 27	21 ± 1	
	all-*trans*-retinaldehyde	0.6 ± 0.1	3.6 ± 0.1	6
	NADH	8.4 ± 1.7	4.1 ± 0.2	
	11-*cis*-retinol	3.3 ± 0.4	3.9 ± 0.2	1.8
RDHE2 (SDR16C5)	all-*trans*-retinol	UD	UD	
	all-*trans*-retinaldehyde	N.D.	N.D.	
RDHE2S (SDR16C6)	all-*trans*-retinol	0.87 ± 0.21	8.7 ± 0.6	10
	NAD^+	460 ± 30	5.8 ± 0.2	
	all-*trans*-retinaldehyde	3.9 ± 0.2	5.4 ± 0.1	1.4
	NADH	11 ± 3	2.6 ± 0.1	
	11-*cis*-retinol	0.86 ± 0.14	1.34 ± 0.07	1.6
	9-*cis*-retinol	UD	UD	

Table 1. Kinetic Constants of SDR16C Enzymes. Kinetic constants for each enzyme were determined using the same preparation of microsomes containing the corresponding enzyme; therefore, the differences in the catalytic rates of each enzyme towards various substrates and cofactors reflect the properties of the enzymes rather than differences in protein expression levels. UD, undetectable under the conditions of the assay; N.D., not determined. The activity of murine RDHE2 towards 10 μM all-*trans*-retinol in the presence of 1 mM NAD^+ was not detectable with up to 10 μg of RDHE2 microsomal preparation.

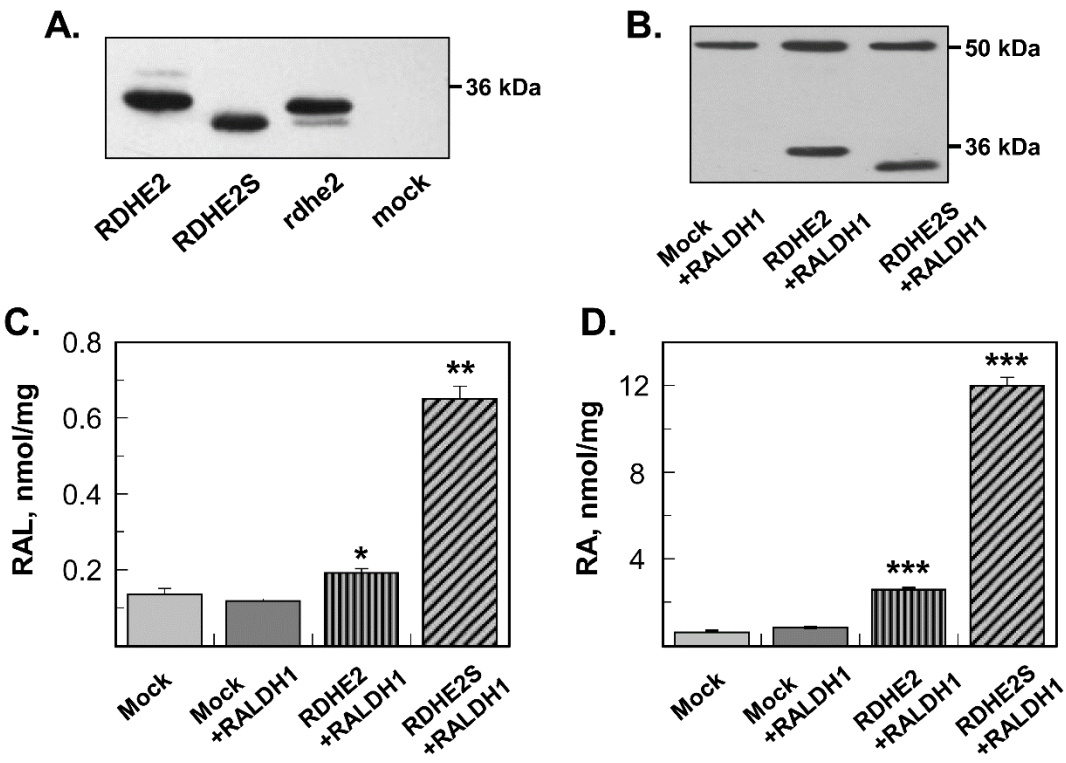

Figure 1. Expression and characterization of frog and murine RDHE2 and RDHE2S. A. Western blot analysis of microsomal fractions (5 µg) isolated from control Sf9 cells (mock) or cells expressing murine RDHE2, murine RDHE2S, or *Xenopus* rdhe2. His-tag antibodies were used at a 1:1,000 dilution. **B.** Western blot analysis of HEK293 cell lysates (20 µg) containing murine RDHE2 or RDHE2S co-expressed with human RALDH1. RDHE2 and RDHE2S were detected using Flag tag antibodies at a 1:3000 dilution. RALDH1 was detected using HA antibodies at a 1:50 dilution. **C.** HPLC analysis of all-*trans*-retinaldehyde (RAL) production from all-*trans*-retinol (10 µM). Cells were incubated for 11 hours. **D.** HPLC analysis of RA production from all-*trans*-retinol (10 µM). Samples are as indicated. Mock, cells transfected with empty vector. *p<0.01; **p<0.001; ***p<0.0001; mean ± S.D., n=3.

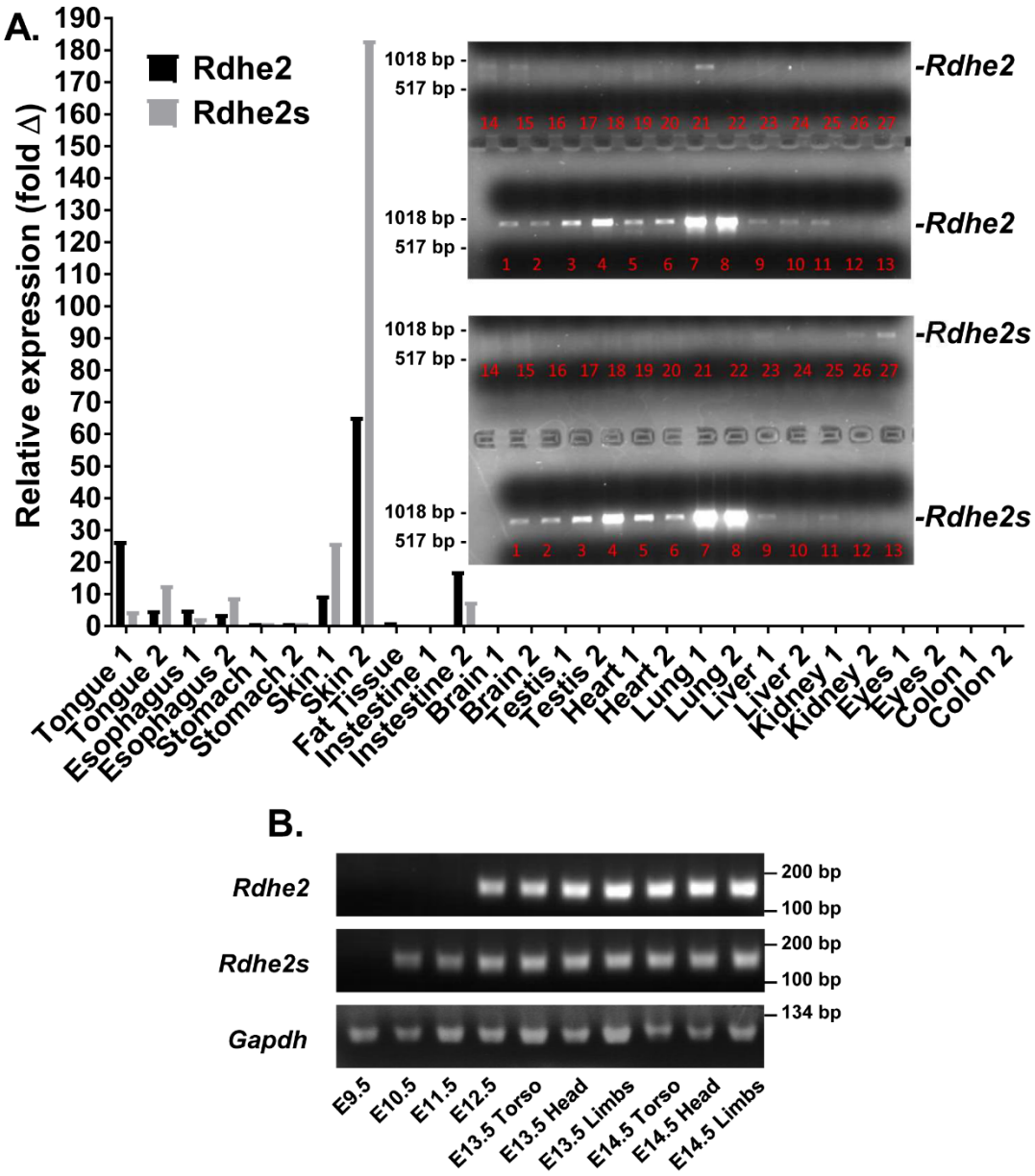

Figure 2. Expression profile of *Rdhe2* and *Rdhe2s* transcripts in mouse tissues. A. QPCR analysis of *Rdhe2* and *Rdhe2s* expression in adult tissues of two animals. Inset: PCR-amplified full length *Rdhe2* and *Rdhe2s* transcripts. Lanes are as follows: 1&2: Tongue; 3&4: Esophagus; 5&6: Stomach; 7&8: Skin; 9: Adipose tissue; 10&11: Intestine; 12&13: Brain; 14&15: Testis; 16&17: Heart; 18&19: Lung; 20&21: Liver; 22&23: Kidney; 24&25: Eyes; 26&27: Colon. **B.** Semi-quantitative PCR analysis of temporal expression patterns of *Rdhe2* and *Rdhe2s* transcript fragments in embryonic mouse tissues. C57BL/J6 embryos were collected at E9.5-E14.5 stages of development as indicated. Five micrograms of mRNA was used for reverse transcription with random hexamer primers and 1/20th of the resulting cDNA was used per reaction. *Gapdh* was used as a loading control.

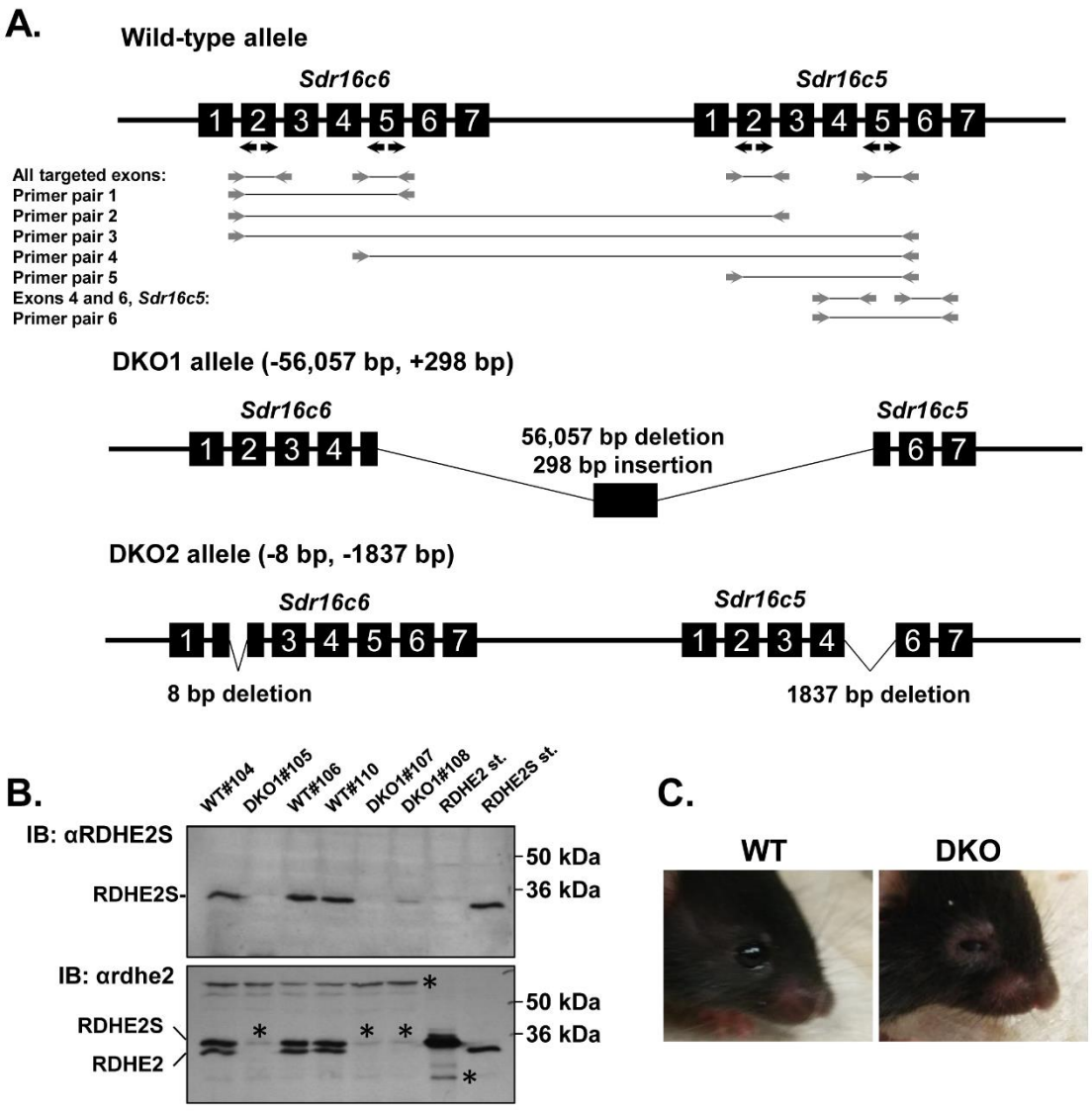

Figure 3. Generation of mice deficient in RDHE2 (SDR16C5) and RDHE2S (SDR16C6). A. CRISPR-Cas9-mediated targeting and screening strategy. Positions of guide RNA targets are indicated by black arrows. Screening PCR primers are shown as gray arrows. PCR products are shown as gray lines connecting the primers. Primer pairs 1-5 do not produce a PCR product from the wild-type allele, because the distance between the primer annealing sites is too large. Pair 4 amplifies a chimeric sequence from DKO1 allele, where rearrangement resulted in a shortening of the distance between the annealing sites. Long-range PCR with Pair 6 primers results in a 4912-bp wild-type product, and a shorter 1837-bp product from DKO2 allele. The exact positions of CRISPR-induced deletions and the sequence of the insertion in DKO1 allele is shown in Figure S3. **B.** Western blot analysis of RDHE2 and RDHE2S in skin microsomes (50 µg) of female DKO1 (n=3, #105, #107, #108) and WT (n=3, #104, #106, #110) mice using RDHE2S antibodies (upper) and *Xenopus* rdhe2 antibodies (lower), both at a 1:3,000

dilution. Note the difference in mobility of murine RDHE2 versus murine RDHE2S; * denotes a non-specific band. **C.** Eye phenotype of DKO mice. Note the puffy eyelids and partially closed eyes in DKO animal. This phenotype was observed in all mice of both sexes on chow diet as well as on vitamin A deficient diet (n>100 animals). Shown are littermates DKO1#20 and WT#18.

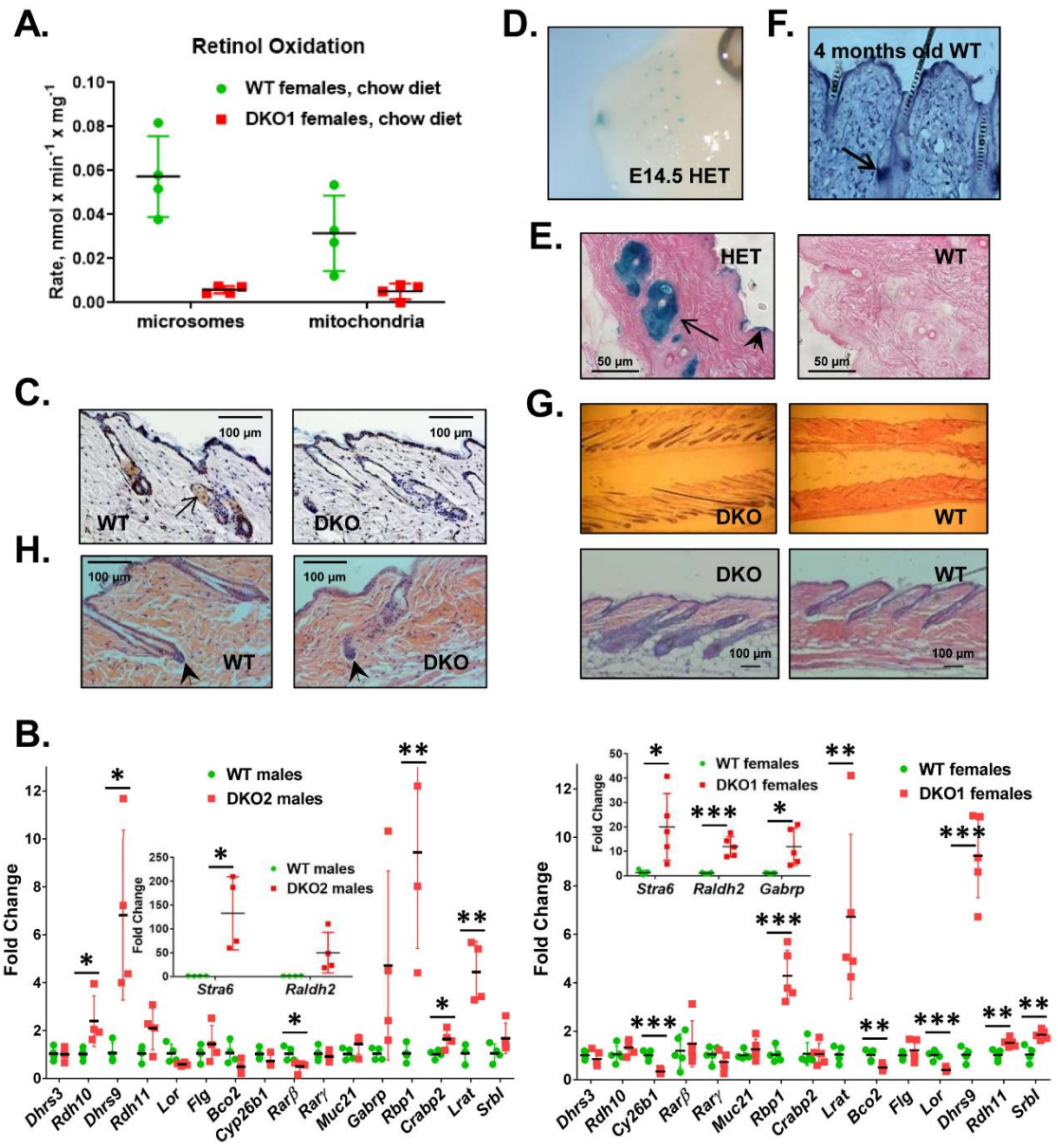

Figure 4. Skin phenotype of DKO mice. A. Analysis of retinol dehydrogenase activities. Microsomal and mitochondrial fractions (50 µg) from DKO mice and WT littermates on chow diet were incubated with 3 µM ROL and 1 mM NAD^+ for 15 min. Note the significant decrease in activity in fractions from DKO mice. **B.** QPCR analysis of RA-regulated or retinoid metabolic genes in dorsal skin of male and female mice from two different *Rdhe2*$^{-/-}$;*Rdhe2s*$^{-/-}$ strains (DKO1 (n=5) and DKO2 (n=4)). Levels of transcripts were determined by normalizing to *Gapdh*; *p<0.05; **p<0.01; ***p<0.001. **C.** Immunohistochemical detection of RDHE2 and RDHE2S in skin sections from male P60 WT and DKO2 littermates utilizing *Xenopus* rdhe2 antibodies at a 1:800 dilution. Arrow points to sebaceous gland. Images are representative of three biological replicates, with six skin sections stained from each mouse. There were four representative images with a total of 15 hair follicles captured for each mouse. Scale bar is 100 µm, 200-fold

magnification. **D.** Detection of *Rdhe2s* expression domains in E14.5 *Rdhe2s*$^{+/-}$ (HET) embryos using β-galactosidase staining. Note the strong staining in whisker pads and nasal pits. **E.** Detection of *Rdhe2s* expression domains in dorsal skin of adult *Rdhe2s*$^{+/-}$ (HET) male mice. Strong staining is observed in sebaceous glands (arrow) and epidermis (arrowhead). Scale bar is 50 μm, 400-fold magnification. **F.** *Rdhe2* detection by in situ hybridization in tail skin from wild-type C57BL/J6 male mouse. Like *Rdhe2s*, *Rdhe2* is expressed in sebaceous gland (arrow). **G.** Hematoxylin and eosin (H&E) staining of dorsal skin from WT and DKO2 male littermates at 10 weeks old. Note the enlarged hair follicles and thicker skin in DKO animals. Upper, 60-fold magnification; Lower, 100-fold magnification, scale bar is 100 μm. **H.** Hematoxylin and eosin staining of dorsal skin from WT and DKO2 male littermates at P50. The dermal papilla (arrowhead) appears to be larger in DKO skin with a thicker keratinocyte strand above, suggesting an entry into anagen phase. The images are representative of seven biological replicates with six skin sections stained from each mouse. There were three representative images with a total of 10 hair follicles captured for each mouse. Scale bar is 100 μm, 200-fold magnification.

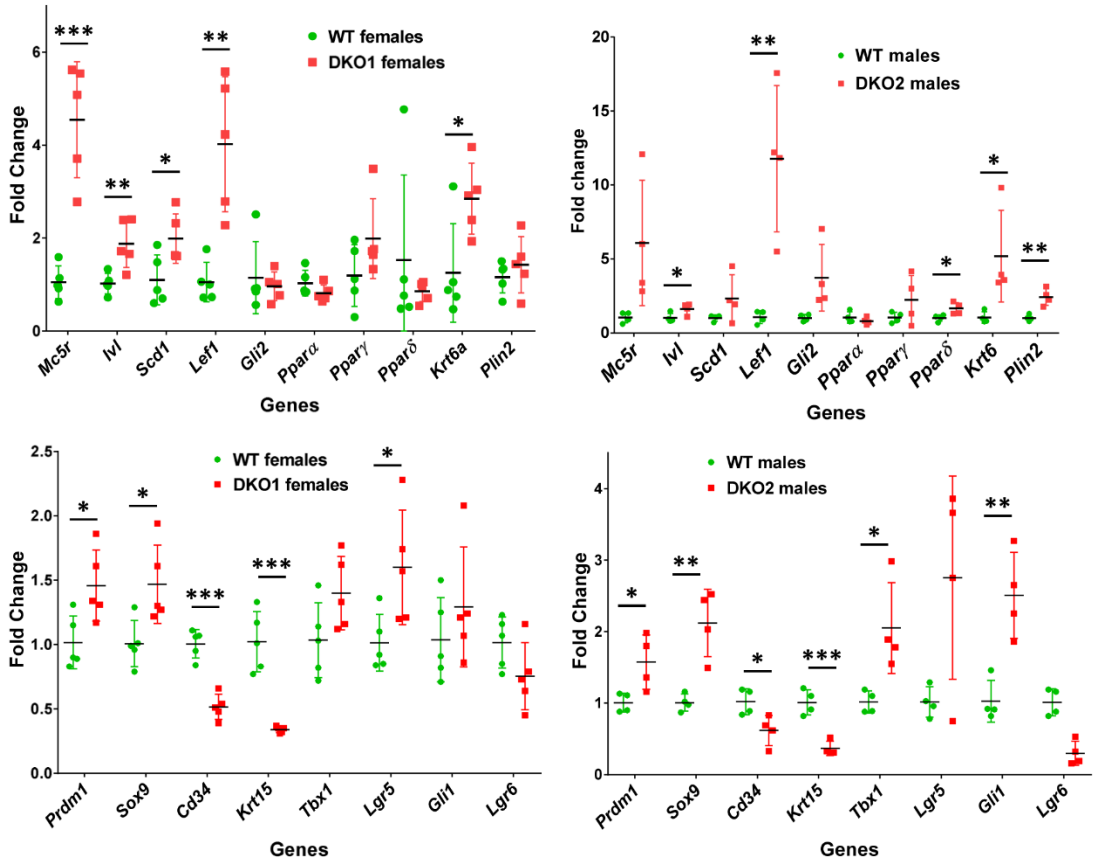

Figure 5. QPCR analysis of genes expressed in hair follicles and sebaceous glands. QPCR was performed using skin from animals (~10 weeks old) of both sexes from two independent DKO strains fed vitamin A deficient diet as described under Experimental Procedures. WT and DKO1 females, n=5; WT and DKO2 males, n=4; *p<0.05; **p<0.01; ***p<0.001.

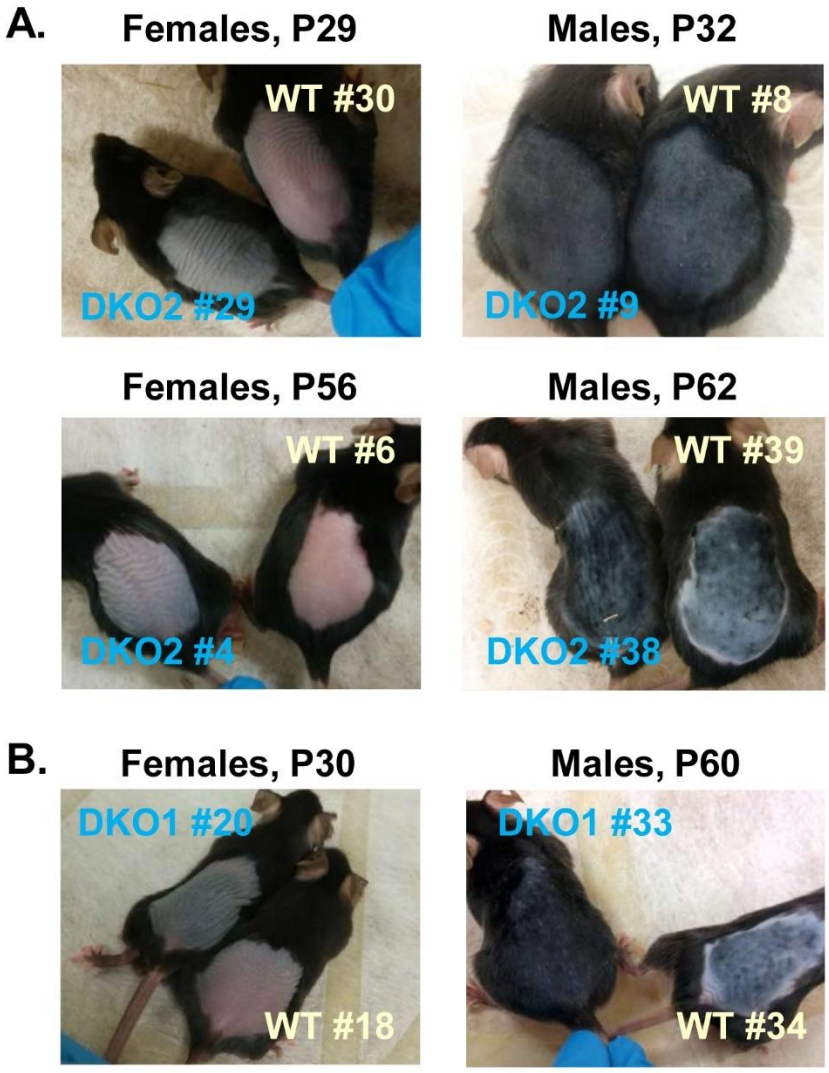

Figure 6. Hair regrowth in DKO and WT mice on vitamin A deficient diet (A) and on chow diet (B). A. DKO2 and their littermate female mice were shaved at P25 (#29) and P50 (#4) after birth and photographed at P29 (4 days of hair growth) and P56 (6 days of hair growth), respectively. Shown are representative images of 2 sets of younger females and 2 sets of older females on VAD diet. DKO2 and their littermate male mice were shaved at P25 (#9) and P49 (#38) and photographed at P32 (7 days of hair growth) and P62 (13 days of hair growth), respectively. Shown are representative images of 4 sets of younger males and 3 sets of older males on VAD diet. **B.** Female DKO1 and its WT female littermate were shaved at P25 and photographed at P30 (5 days of hair growth). Shown are representative images of 6 sets of females on chow diet. Male DKO1 and its WT male littermate were shaved at P49 and photographed at P60 (11 days of hair growth). Shown are representative images of 4 sets of males on chow diet. Images are available for additional shaved single animals from DKO1 and DKO2 strains that did not

have WT littermates. The two independent strains showed a very similar external phenotype on vitamin A deficient diet and on chow diet.

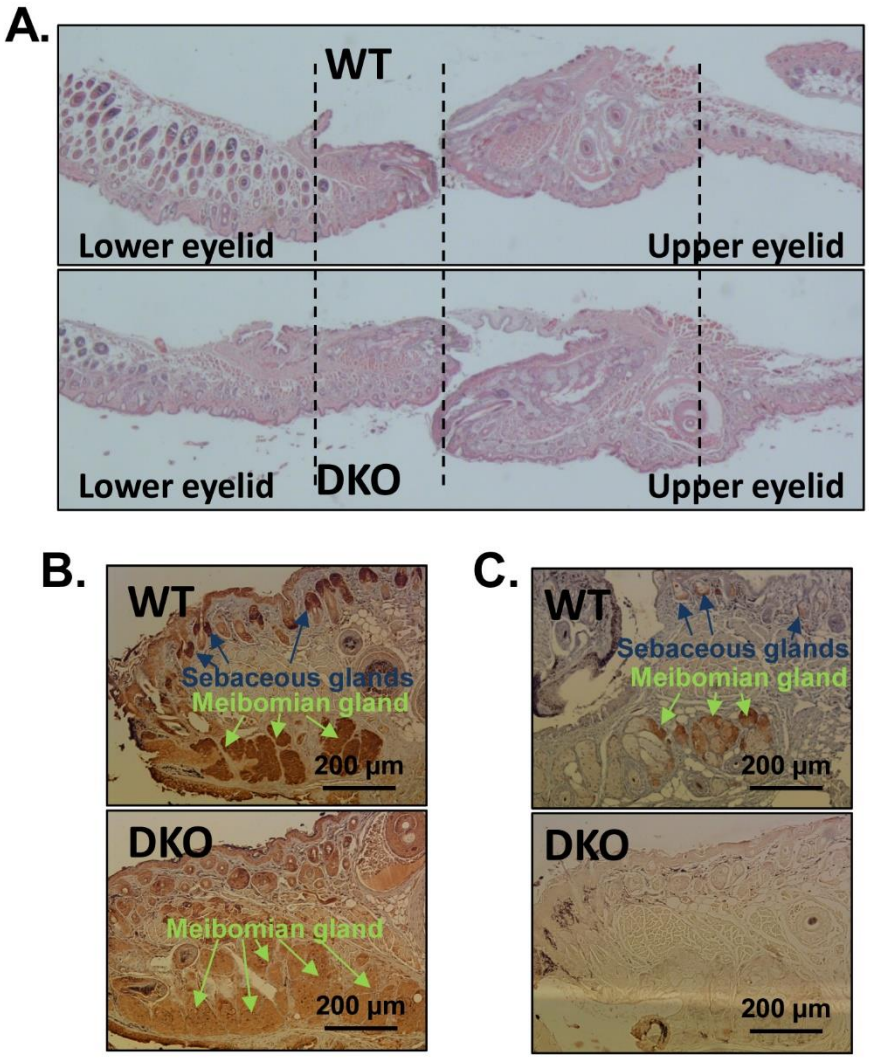

Figure 7. Eye phenotype of DKO mice. A. Histology of whole eye lids. Sixty-fold magnification. Note the longer and thicker appearance of lower and upper eyelids from DKO mice. Four biological replicas were analyzed from littermates WT#38/DKO1#37, WT#39/DKO2#40, WT#41/DKO2#38 and WT#18/DKO1#20. **B.** Immunohistology of eyelid sections using custom made RDHE2S antibodies at a 1:400 dilution. **C.** Immunohistology of eyelid sections using commercial SDR16C5 (RDHE2) antibodies (Sigma αSDR16C5 #HPA 025224, lot R11757) at a 1:200 dilution. Both RDHE2S and RDHE2 are localized in meibomian glands and sebaceous glands in eyelids. As determined by measuring a representative image of eyelid sections using image processing program ImageJ [91], the DKO meibomian glands are nearly twice the size (198%) of the WT meibomian glands. Overall, the eyelids of DKO mice are 122.5% ± 1.3% the size of WT eyelids (n=3 pairs of littermates). Scale bar is 200 µm, 100-fold magnification.

EPIDERMAL RETINOL DEHYDROGENASES FLUCTUATE ACROSS THE HAIR CYCLE AND INFLUENCE STEM CELLS

by

KELLI R. GOGGANS, OLGA V. BELYAEVA, ALLA V. KLYUYEVA, JACOB STUDDARD, HELEN B. EVERTS, NATALIA Y. KEDISHVILI

In preparation for *Cell*

Format adapted for dissertation

Summary

All-*trans*-retinoic acid (RA), the bioactive form of vitamin A, must be strictly maintained at homeostatic levels as both vitamin A deficiency and toxicity can cause disease. Retinol dehydrogenase epidermal 2 (RDHE2) and RDHE2-similar (RDHE2S; collectively referred to as RDHEs) are newly identified tissue-specific retinol dehydrogenases that perform the rate-limiting step of RA biosynthesis. RDHEs act as the primary retinol dehydrogenases in skin, and we hypothesize that RDHEs contribute to retinol dehydrogenase activity of the hair cycle in a cyclic manner and play a role in hair follicle development. This study demonstrates RDHEs' protein levels and skin retinol dehydrogenase activity fluctuate across the hair cycle, along with RA-responsive genes, in a sex-specific manner. Regardless of sex, absence of RDHEs results in an altered hair coat composition and diminished hair follicle stem cell markers. We propose that the temporal-spatial fluctuations of RA biosynthesis are essential for the development and maintenance of constantly differentiating adult tissues.

Introduction

Retinoic acid (RA), the bioactive derivative of vitamin A, is essential to the proper development and maintenance of skin (Saitou *et al.*, 1995). RA acts as an activating ligand to nuclear receptors and is capable of regulating over 530 genes (Balmer and Blomhoff, 2002). In the skin, RA is known to influence sebaceous gland size and sebum production, bacterial colonization and inflammatory response, follicular keratinization, and alopecia (hair loss) (Bazzano *et al.*, 1993; Everts, 2012; Chien, 2018). Additionally, RA derivatives are a commonly used therapeutic for skin diseases, despite a

lack of understanding of their mechanism of action and an incomplete characterization of RA biosynthesis. Recent studies highlight the diversity of the biosynthesis and regulation of RA amongst tissues, and how these mechanisms are altered in differing metabolic states (Klyuyeva *et al.*, 2021). The concept that RA levels may fluctuate is reminiscent of embryogenesis, where the proper spatio-temporal regulation of RA is required for development. The hair cycle is the perfect model to further interrogate possible physiological roles for fluctuations in RA biosynthesis and signaling, as the cells of the hair follicle undergo drastic metabolic changes through organogenesis of the hair fiber (Schneider, Schmidt-Ullrich and Paus, 2009).

The hair cycle is divided into three phases based on physiological activity, and traditionally is described beginning with anagen, the period in which hair follicle cells proliferate and differentiate to produce a hair fiber. Once the hair fiber is completed, the surrounding follicle undergoes a period of apoptosis and regression, called catagen. Following this regression, the hair follicle enters telogen, a period previously associated with quiescence because of its lack of morphological changes but which has now been shown to contribute to preparing for anagen (Müller-Röver *et al.*, 2001; Lin *et al.*, 2009). The cycle is then repeated, with the proliferation of hair follicle stem cells (HFSC) of the hair bulge initiating the telogen to anagen transition (Schneider, Schmidt-Ullrich and Paus, 2009). RA has already been implicated in having effects on the hair cycle. Exogenous application of RA to skin (Bazzano *et al.*, 1993) and increased endogenous levels of RA caused telogen to shorten and prolonged anagen (Shih *et al.*, 2009). In mouse dorsal skin, the first two hair cycles are naturally synchronized, allowing us to study populations of hair follicles at similar stages without inducing an immune response

through depilation, a common method for synchronizing the hair cycle in older mice (Müller-Röver *et al.*, 2001).

RA biosynthesis occurs at the site of action in skin (Everts, 2012), where STRA6 allows uptake of retinol (ROL) into the cell. Cellular ROL is bound to retinol binding protein 1 (RBP1) and can either be oxidized by retinol dehydrogenases (RDHs), like retinol dehydrogenase 10 (RDH10), or converted to retinyl esters (RE) by lecithin retinol transferase (LRAT) for storage in lipid droplets. The oxidation of ROL by RDHs is the first and rate-limiting step of RA biosynthesis, producing retinaldehyde (RAL) (Napoli, 1986). This reaction is also reversible by dehydrogenase reductase 3 (DHRS3). The second oxidative step is catalyzed by aldehyde dehydrogenases (ALDHs), producing RA, which binds to cellular RA binding protein 2 (CRABP2). Then RA is either transported to the nucleus to activate retinoic RA receptors (RARs) or degraded by cytochrome p450 enzymes like CYP26B1 (Fig. 2A) (Kedishvili, 2013). Many of these genes are also regulated by RA in order to fine-tune RA biosynthesis via multiple feedback mechanisms (O'Connor, Varshosaz and Moise, 2022).

Characterization of RA biosynthesis in the hair cycle has been limited to studies involving immunohistochemistry (IHC) to account for heterogeneous nature of skin (Everts *et al.*, 2007, 2021; Suo *et al.*, 2021). These studies have demonstrated proteins involved in RA biosynthesis, degradation, and signaling vary across the hair cycle in specific spatio-temporal patterns; interestingly, RA biosynthesis proteins and signaling proteins localize to the hair follicle bulge, where HFSCs reside (Everts *et al.*, 2007; Schneider, Schmidt-Ullrich and Paus, 2009). While IHC is optimal for determining protein localization in a heterogenous tissue, especially in a temporal manner from

samples at various time points, other molecular biology techniques are necessary to determine changes at the level of mRNA and protein activity. Expression of RA target genes and the activity of RDHs and ALDHs have not been characterized across the hair cycle.

In our previous work we established that RDH epidermal 2 (RDHE2) and RDHE2-similar (RDHE2S; collectively referred to as RDHEs) are localized to the hair follicle and sebaceous gland. *Rdhe2s* expression was also seen by embryonic day 14.5 (E14.5) (Wu *et al.*, 2019), when hair follicle development begins, indicating RDHEs may have developmental effects on hair follicles. Hair follicles are formed during development in three waves beginning at E14. The four hair fiber types produced by hair follicles of mouse dorsal skin are based upon which wave of development the follicle formed during. Guard hairs are produced from follicles formed during the first phase, while both awl and auchene hair fibers are produced by follicles formed during the second wave. The third and final wave produces zigzag hairs, which constitute the undercoat. These different hair types are defined by air spaces in the medulla and any bends in the hair (Sundberg and Hogan, 1994). Endogenous elevated levels of RA are known to alter the production of hair fibers, inhibiting bending of the hair fiber and reducing the percentage of zigzag hairs (Okano *et al.*, 2012).

We have demonstrated RDHEs are the primary RDHs of skin during one phase of the hair cycle (telogen) and saw an accelerated hair growth in *Rdhe2*$^{-/-}$/*Rdhe2s*$^{-/-}$ double knockout (DKO) mice, leading us to conclude that the activity of RDHEs is essential for the regulation of hair cycle progression (Wu *et al.*, 2019). We hypothesize that RDHEs and their activity vary in a cyclic manner across the hair cycle and contribute to proper

development of the hair follicle. To further characterize RDHEs and their role in the hair follicle throughout the hair cycle, we utilized whole dorsal skin of mice to further interrogate RA biosynthesis at a molecular level, while utilizing previous IHC data to guide our understanding. We also assessed DKO mice for phenotypic effects indicative of developmental problems by assessing hair types, which are determined during embryogenesis, and quantifying hair follicle stem cell markers. Additionally, while sex hormones are known to affect the hair cycle (Alonso and Rosenfield, 2003; Hu *et al.*, 2012) and are capable of interacting with RA signaling (Ross-Innes *et al.*, 2010; Rivera-Gonzalez *et al.*, 2012), this interaction in the hair cycle is only beginning to be defined (Everts *et al.*, 2021), thus we profiled both female and male mice in this study.

Methods

Mice

Rdhe2/Rdhe2s double knockout mice were generated in previous studies via CRISPR technology on a C57BL/6J background (Wu *et al.*, 2019). *Rdhe2*$^{+/-}$*;Rdhe2s*$^{+/-}$ mice were bred to obtain wild-type and *Rdhe2*$^{-/-}$*;Rdhe2s*$^{-/-}$ littermates for these studies. Genotyping for *Rdhe2/Rdhe2s* was carried out using primers Sdr16c5ex5F, 5'-CAG ACT ATT GTG CAA GTA AAT TCG C-3', and Sdr16c5ex5R, 5'-TGG GCA GAG AGT AAA TTT GAA TGC C-3', to identify the wild-type allele and Sdr16c6ex5F, 5'-ATA CTC TGT CCT CAA GGA TAA ACC-3', and Sdr16c5ex5R or Sdr16c5intr4F4, 5'-CTT GAG ATA ATC AAC TTG AAA GGA G-3', and sdr16c5intr5R2, 5'-GAA TGG GTC TGA ATG GCA TTA CG-3', to identify the DKO deletion of *Rdhe2/Rdhe2s*. Mice were housed at 23 ± 2° C with free access to water and food (standard rodent chow diet

obtained from Harlan, catalogue number 7017) in an AALAC-approved pathogen-free facility on a light cycle of 12 h light and 12 h dark. All studies were conducted with approval of the Institutional Animal Care and Use Committee of the University of Alabama at Birmingham School of Medicine.

Mice were euthanized on postnatal days (PD) 26, 30, 35, 40, 45, and 50 using CO_2. Dorsal skin was shaved and collected with a small piece fixed overnight in 10% Buffered Formalin Phosphate, transferred to 70% ethanol, processed routinely, embedded in paraffin, sectioned at 10 µm, placed on plain microscope slides, and stained with hematoxylin and eosin for histological analysis. The rest of the skin was cleaned of the underlying connective tissue and stored at -80° C for biochemical analysis. For hair fiber collection, mice were sedated with isoflurane and hair was shaved and collected from the middle back. Hair types were categorized under a dissection microscope by number of medulla cell rows and number of bends (Sundberg and Hogan, 1994; Cui *et al.*, 2010).

Isolation of Microsomal Fractions from Skin

Microsomes and mitochondria were isolated by differential centrifugation in a sucrose gradient (Wu *et al.*, 2019). Approximately 100 mg of frozen skin tissue samples were homogenized on ice by Polytron (Biospec Products, Inc., Model 985370) in 3 bursts for 10 seconds each in 1 ml of ice-cold Isolation buffer (0.25 M sucrose in PBS supplemented in 1 mM EDTA and protease inhibitors: 1 µg/ml aprotinin, 1 µg/ml leupeptin, and 1 µg/ml pepstatin A). Crude homogenates were further homogenized using 20 strokes in a glass homogenizer on ice. Samples were centrifuged at 3,000*g* for 10 min at 4° C. Supernatant was removed into pre-labeled 2 ml tubes for mitochondrial isolation;

pellets were washed with 300 µl of buffer and re-centrifuged at 3,000*g* for 5 min. The supernatant was also removed into the same pre-labeled 2 ml tube for mitochondrial isolation. The 3,000*g* supernatants were centrifuged at 10,000*g* for 10 min at 4° C. The supernatant was removed into 3 ml conical ultra-centrifuge tubes and balanced with isolation buffer before being centrifuged at 105,000*g* for 90 min at 4° C. The 10,000*g* pellet is the mitochondrial fraction and was re-suspended in 100 µl reaction buffer (90 mM K2HPO4/KH2PO4, 40 mM KCL) supplemented with 20% glycerol and 1 mM EDTA. After ultra-centrifugation, the supernatant was removed and the microsomal pellet was washed with 100 µl of isolation buffer, making sure not to disturb the pellet. The wash was discarded and the pellet re-suspended in 100 µl reaction buffer supplemented with 20% glycerol and 1 mM EDTA before being transferred to pre-labeled 1.5 ml Eppendorf tubes. All collected samples were flash frozen after re-suspension and stored at -80° C.

Western Blot Analysis

Protein concentrations were determined according to Peterson's modification with BSA as a standard. Thirty µg of microsomal fractions was loaded on SDS-PAGE using standard Laemmli system with 12% separating gel and 4.5% stacking gel (mini gel, 160 V). A PVDF membrane was pre-soaked in ethanol and gel transfer occurred for 75 min using Semi Dry transfer unit. Blots were incubated with Ponceau S solution (0.1% Ponceau, 5% acetic acid) and imaged (BIO-RAD, ChemiDoc™ MP Imaging System) for total protein quantification. Blots were blocked in 5% BSA in TBST for 1 hour.

Blots were probed overnight in a cold room with custom-made *Xenopus* rdhe2 antibodies at 1:4,000 dilution and rabbit Cytochrome P450 Reductase antibodies diluted 1:4,000 (Chemicon International, catalogue number AB1257) in 5% BSA in TBST. Secondary ECL Plex goat anti-rabbit IgG, Cy®5 (Sigma, catalogue number PA45011) was used at a 1:2,500 dilution in 5% BSA in TBST. Blots were scanned by an Amersham Typhoon to visualize fluorescent bans.

Retinol Dehydrogenase Activity in Microsomal Skin Fractions

Fifty µg of microsomal skin fractions was incubated with 3 µM all-*trans*-retinol (Toronto Research Chemicals, Toronto, Canada) solubilized with bovine serum albumin as described previously (Gallego *et al.*, 2006) and 1 mM NAD+ (Sigma-Aldrich, St. Louis, MO) in 0.5 ml of reaction buffer for 15 min at 37° C. Reactions were stopped by the addition of an equal volume of ice-cold methanol and retinoids were extracted with 2 ml of hexane. Hexane layers were dried, and dry residue was reconstituted in 0.1 ml of hexane:ethyl acetate (90:10). Retinoids were separated by normal-phase HPLC using a Spherisorb S3W column (4.6 mm×100 mm; Waters, Milford, MA) and an isocratic mobile phase consisting of hexane:ethyl acetate (90:10) at 1 ml/min and analyzed as described previously (Gallego *et al.*, 2006).

Quantification of Gene Expression in Skin Samples

Approximately 100 mg of frozen dorsal skin tissue of WT and DKO mice samples was homogenized in PURzol reagent (Bio-Rad, catalog no. 7326890) and RNA isolated via the Aurum™ Total RNA Fatty and Fibrous Tissue Pack (Bio-Rad, catalog

no. 732-6870). The concentration of isolated RNA was determined with a Nanodrop ND-1000 spectrophotometer (Thermo Scientific). ProtoScript® II First Strand cDNA Synthesis Kit (New England BioLabs, catalog no. E6560) was used for cDNA strand synthesis from 1 µg sample RNA. One WT mouse sample was used for several extra reactions simultaneously as a standard for quantification curves. All qPCR was performed with a 15X dilution of cDNA, unless otherwise noted. Curves were calculated with 3X, 9X, 27X, and 81X cDNA dilutions. Real-time PCR analysis was conducted on a Roche LightCycler®480 detection system (Roche Applied Science) with SYBR Green as the probe (LightCycler®480 CYBR Green I Master, Roche Applied Science). Gene expressions were normalized to *Gapdh* and analyzed as a relative expression of fold-difference from the expression level of WT mice at PD26 of the same sex, using the comparative Ct method. Sequences of primers are available by request.

Statistical Analysis

Males and females were analyzed separately because of their differences in hair cycle progression. Statistical significance was determined using one-way ANOVA for RDH activity and for Western blot comparison of RDHE2 and RDHE2S across the hair cycle, followed by a Tukey test post-hoc analysis. When parametric assumptions were not met, a Kruskal-Wallis was performed instead. For qPCR, a two-way ANOVA was used to determine main effects of PD and genotype (GT) and possible interactions, with a Sidak test for estimated marginal means. T-tests were used to compare WT and DKO mice pelage hair percentages.

Results

RDHEs fluctuate across the hair cycle, but RDH activity varies in a sex-specific manner

Previously we reported that the activity of RDHEs accounted for nearly 80% of RDH activity of microsomes from dorsal skin taken at postnatal (PD) 70, during telogen (Wu *et al.*, 2019). RDHs are associated with the endoplasmic reticulum and enzymes capable of oxidizing retinaldehyde, the product of RDHs, are localized in the cytoplasm; thus, isolating microsomal fractions allows for analysis of isolated RDH activity. We hypothesized that RDHEs are the primary RDH of skin throughout the hair cycle. To test this hypothesis, we examined the RDH activity in dorsal skin from WT and DKO female and male mice at various PDs across the second synchronized hair cycle (PD26, 30, 35, 40, 45). Histological analysis via hematoxylin and eosin staining was used to determine the hair cycle stage of the majority of hair follicles in the sample (Fig. 1A). Using these PDs we were able to analyze samples in various anagen stages and catagen, despite some differences in progression based on sex and genotype. Here we note that males progress faster through anagen than females, and DKO male mice progress faster than their WT counterparts (Fig. 1A).

We assessed RDH activity of WT and DKO female mice across the hair cycle (Fig 1B, left), analyzed by a two-way ANOVA, and observed a main effect of genotype, resulting in significant decreases of RDH activity in DKO mice ($p < 0.001$). Across all stages of the hair cycle, RDHEs account for approximately 80% of RDH activity. RDH activity across PDs was not significantly altered, but peaked at PD30 and decreased by 46% at PD45. Our previously reported RDH activity in PD70 skin microsomes was decreased compared to our PD45 reported here (Wu *et al.*, 2019). We hypothesized RDH

activity does vary across the hair cycle, and re-assessed the RDH activity of WT female mice from all the previous days with the addition of PD50 (telogen) skin microsomes (Fig 1B, right). A Kruskal-Wallis shows a significant difference amongst the PDs ($p = 0.037$), with PD50 significantly decreased 56% from PD30 ($p = 0.043$). In males, we assessed RDH activity in WT and DKO mice at PD30, PD40, and PD50, and a two-way ANOVA showed a main effect of genotype ($p < 0.001$), with an average decrease of approximately 80% for DKO mice (Fig. 1D, left). However, RDH activity across all PDs did not vary significantly in WT male mice (Fig. 1D, right). Thus, RDHEs are the primary RDHs of skin independent of hair cycle stage, but RDH activity only fluctuates across the hair cycle in female mice.

We anticipated the protein levels of RDHEs fluctuated in females in accordance with RDH activity levels, as the RDH activity data from Fig. 1A would indicate there are no fluctuations in the absence of RDHEs. Using a custom-made antibody for Xenopus rdhe that detects both mouse RDHE2 and mouse RDHE2S, we assessed protein levels across PD26, 30, 35, 40, and 45 and normalized by cytochrome P450 (POR), a microsome-specific protein (Fig 1C, blue). A Kruskal-Wallis test indicated that both RDHE2 ($p = 0.050$) and RDHE2S ($p = 0.042$) protein levels varied across the hair cycle, with a peak at PD30 that decreased by 64% for RDHE2 and by 84% for RDHE2S at PD40 (Fig. 1C, blue). Unfortunately, due to the introduction of PD50 as a data point later in our analysis we were unable to normalize it via POR, as the antibody had been discontinued, or re-run the complete set due to limited samples. Here we have included analysis of PD50 microsomes run alongside remaining PD45 samples and normalized via total protein amount to demonstrate that protein levels appear to remain close to those

seen in PD45 (Fig. 1C, pink). Male mouse skin microsomes were run for all PDs simultaneously and normalized by total protein. A one-way ANOVA shows RDHE2 varies between groups ($p = 0.041$) (Fig. 1E), with letters denoting significant differences between groups; RDHE2 is the less active of the RDHEs (Wu *et al.*, 2019), therefore PD variance of RDHE2 does not appear sufficient to alter RDH activity. It is important to note here that female RDHEs' protein levels and RDH activity were elevated at PD30 (mid anagen), compared to males where RDHEs' levels are elevated at PD45 (late catagen). These differences do not correlate with sex-specific shifts in hair cycle (Fig. 1A), and thus highlight sex-related differences of RA biosynthesis in the hair cycle. We also examined mRNA levels anticipating similar variances as seen at the protein level; however, only *Rdhe2* mRNA expression varied across PDs in males, correlating with changes in protein level (Fig. 1F). *Rdhe2s* does not cycle in males, and neither transcript cycles significantly in females.

Absence of RDHEs alters RA biosynthesis and gene expression patterns during the hair cycle

To further characterize RA biosynthesis and signaling through the hair cycle and the contribution of RDHEs, we performed qPCR of various genes involved in RA biosynthesis and regulated by RA signaling (Fig. 2A). Our analysis of RA associated genes not only revealed differences in the absence of RDHEs, but demonstrated genes involved in RA biosynthesis fluctuate across the hair cycle as suggested by previous IHC data (Everts *et al.*, 2007; Suo *et al.*, 2021).

Our findings show that, in WT female mice, *Lrat* ($p < 0.001$), *Cyp26b1* ($p = 0.003$), *Crabp2* ($p < 0.001$), and *Rdh10* ($p < 0.001$) fluctuate across the hair cycle (Fig. 2B). *Stra6* exhibits an interaction with PD and genotype (GT) ($p < 0.001$) and varies across PD only in WT female mice ($p < 0.001$). *Aldh1a2* also has an interaction of PD and GT ($p = 0.010$), but expression of *Aldh1a2* across PD various only in DKO female mice ($p < 0.001$). *Aldh1a2* is upregulated in DKO female mice at PD35 ($p = 0.018$), PD40 ($p < 0.001$), and PD45 ($p = 0.041$). *Rbp1* does not fluctuate across the hair cycle but is upregulated in DKO female mice ($p < 0.001$). Other genes upregulated in DKO female mice include *Crabp2* ($p = 0.004$) and *Rdh10* ($p = 0.027$). DKO female mice have downregulated expression of *Lrat* ($p = 0.013$), *Cyp26b1* ($p < 0.001$), and *Dhrs3* ($p < 0.001$).

In male mice, we observe alterations to RA associated genes across the hair cycle and in DKO male mice; however, many of the genes have significant interactions of PD and GT. *Lrat* has an interaction ($p < 0.001$) where both GTs cycle, but have different patterns of expression, with highly significant differences at PD26 and PD40 ($p < 0.001$). Similar to female mice, *Stra6* has an interaction ($p = 0.001$) where only WT mice vary across PD ($p < 0.001$). Some interactions appear to be small alterations to expression patterns, as in *Cyp26b1* ($p = 0.023$) and *Dhrs3* ($p = 0.027$). However, in interactions of PD and GT for *Rbp1* ($p < 0.001$) and *Rdh10* ($p = 0.003$) DKO male mice show upregulated expression patterns. A highly significant interaction between PD and GT in both *Crabp2* and *Aldh1a2* ($p < 0.001$) results in variance across PD only in DKO male mice ($p < 0.001$) and significant upregulation in DKO male mice at PD35, PD40, PD45 ($p < 0.001$).

Rbp1, Crabp2, Aldh1a2, and *Rdh10* were upregulated in DKO mice of both sexes indicating transcription for genes involved in RA biosynthesis are upregulated in the absence of RDHEs. Genes regulated by RA (*Stra6, Lrat, Dhrs3, and Cyp26b1*) exhibited dysregulated expression patterns, though there were no distinct conclusions across both sexes, except for the downregulation of *Lrat*.

Awl hairs are increased in the absence of RDHEs

The hair of DKO mice had a noticeably rougher appearance than that of WT littermates (Fig. 3A, B), though we previously noted there were no histological abnormalities in the hair follicle (Wu *et al.*, 2019). Studies demonstrate increased RA levels can affect development of the hair follicle, inhibiting bending of hair fibers and decreasing the percentage of zigzag hairs (Okano *et al.*, 2012). We hypothesized, based on the long hairs observed in our DKO mice (Fig. 3A, B) that DKO mice have increased guard hairs, the longest hair fiber type. Over 100 hairs from the middle back were categorized into the four main hair types of mouse dorsal hair (guard, awl, auchene, and zigzag) per mouse, to assess hair fiber composition (Sundberg and Hogan, 1994; Cui *et al.*, 2010). We noted that there was a significant increase in the percentage of awl hairs for DKO mice, without a corresponding decrease in any other hair fiber type. Awl hairs are the second longest hair and thickest hair type, alongside auchene hairs, though little is known about their physiological function (Duverger and Morasso, 2009).

Expression of hair follicle stem cell markers are diminished in the absence of RDHEs

We hypothesized that DKO mice may exhibit alterations to HFSC markers since our qPCR data suggests DKO mice have lower RA levels, in agreement with the lack of a phenotype of zigzag hairs as seen in elevated RA levels (Okano *et al.*, 2012). Elevated levels of RA increased *Sox9* expression, a transcription factor responsible for mediating the effects of RA (Gudas and Wagner, 2011); *Sox9* is also known for its role in maintenance of HFSCs in the hair follicle bulge (Nowak *et al.*, 2008). Therefore, we performed qPCR for prominent HFSC markers with known expression in the bulge region: *Sox9*, *CD34*, *Krt15*, and *Lgr5*. (Trempus *et al.*, 2003; Morris *et al.*, 2004; Vidal *et al.*, 2005; Jaks *et al.*, 2008; Nowak *et al.*, 2008; Schneider, Schmidt-Ullrich and Paus, 2009; Gudas and Wagner, 2011; Bose *et al.*, 2013; Joost *et al.*, 2020).

Our data demonstrate that all of these HFSC markers fluctuate across the hair cycle in WT mice, independent of sex, though expression patterns do differ from each other (Fig. 4). In females, all four genes are significantly decreased in DKO mice (*Cd34*, *Sox9*, *Krt15* $p < 0.001$; *Lgr5* $p = 0.002$), demonstrating lower mRNA levels across all stages of the hair cycle. An interaction of GT and PDs in *Lgr5* ($p = 0.012$) shows a complete loss of PD variance in DKO mice (Fig. 4A). In male mice, we observe an interaction of GT and PD for *Cd34* ($p = 0.018$) and *Krt15* ($p < 0.001$), as DKO mice do not exhibit the same increases at PD45 and PD50 that are present in WT mice. *Sox9* has an interaction of PD and GT ($p = 0.024$), with a unique pattern for WT and DKO mice that does not correlate with the slight differences in hair cycle progression but do both decrease significantly for PD50. *Lgr5* does vary across PD ($p < 0.001$), but there's an absence of a peak at PD35 in DKO mice. In both sexes, *Cd34* and *Krt15* demonstrate similar expression patterns, with increases in mRNA levels at late catagen/telogen, while

Sox9 and *Lgr5* appear to be more highly expressed in anagen. In agreement with our data, *Krt15* and *Cd34* are more prominently expressed in telogen bulge cells (Liu *et al.*, 2003; Trempus *et al.*, 2003).

Discussion

In this study we've demonstrated that RDHEs are the primary RDH in skin across the hair cycle, and that RDHEs are important for regulation of genes involved in RA biosynthesis across the hair cycle. RDHEs also contribute to hair follicle development, and mice lacking RDHEs have altered hair coat composition and expression of HFSC markers. Current literature highlights an important relationship between RA and the skin and hair. Retinoids, bioactive derivatives of vitamin A including RA, have been utilized in dermatotherapies since the 1960s, when they were discovered to alter skin keratinization (Stüttgen, 1986). Biopsies from patients with alopecia exhibit an increased expression of RA biosynthesis enzymes, and mouse models with altered RA biosynthesis have phenotypes which include alopecia (Duncan *et al.*, 2013). Increased endogenous levels of RA prolonged anagen and delayed catagen in one mouse model (Shih *et al.*, 2009), while treatment of cultured hair follicles with RA induced catagen (Foitzik *et al.*, 2005). Topical application of retinoids shortened telogen by accelerating anagen progression (Bazzano *et al.*, 1993), but absence of RDHEs and decreased RA biosynthesis also allows for an accelerated anagen (Wu *et al.*, 2019). Our work focused on characterizing the roles of primary epidermal retinol dehydrogenases, RDHEs, to establish a fundamental understanding of the pattern of RA biosynthesis across the hair cycle and its impact on the hair follicle that was lacking in the field.

We were unable to capture early anagen in males due to their accelerated anagen progression compared to females. The hair follicle is still undergoing morphogenesis post birth and the hair follicle bulge is not pronounced until PD21. Additionally, mice at PD26 are small and allow for limited collection of dorsal skin that is barely sufficient for all our studies performed here. Therefore, to avoid additional complications from hair follicle development and sample collection, we decided to not collect males earlier than PD26. We feel this still gives us a substantial understanding of RA biosynthesis in the hair cycle, as most results are significant between points other than early anagen.

Our work shows that RDHEs fluctuate at the protein level across the hair cycle in a sex-specific manner and contribute to the majority of skin's RDH activity independent of hair cycle phase. However, RDH activity itself only fluctuates across the hair cycle in females. There is an increasing need to interrogate the hair cycle in both sexes, despite the complexity sex-specific hormones add to hair follicle metabolism and hair cycle progression. Androgens and estrogens are known modulators of the hair cycle (Hu *et al.*, 2012), and their dysregulation is capable of causing alopecia. Additionally, androgens and estrogens interact with retinoids. Androgens signaling is inhibited by RA in multiple tissues (Ubels *et al.*, 2002; Kelsey *et al.*, 2012; Rivera-Gonzalez *et al.*, 2012). However, estrogen has a cooperative interaction with RARα, and (Everts *et al.*, 2021) has outlined the interactions of estrogen and RA biosynthesis in the hair cycle specifically.

Estrogen receptor α (ESR1) and estrogen receptor β (ESR2) localized to the hair follicle primarily during anagen, when we see stronger RDH activity and higher RDHEs expression in females. IHC also showed females displayed elevated expression of ALDH1A2, ALDH1A3, and CRABP2, compared to males which had elevated levels of

ALDH1A1 and RARβ. Treatment of dorsal mouse skin with estrogen and estrogen inhibitors also showed sex-specific expression of *Aldh1a2*, *Crabp2*, and *RA receptors* (*RARs*) (Everts *et al.*, 2021). These data support sex-specific differences in RA biosynthesis observed in this study, demonstrating how estrogen alters RA biosynthesis in a sex-specific manner; however, highlighting estrogen regulation does not explain all sex-differences. Further detailed studies into the sex-specific effects of androgens, prolactin, and progesterone on RA biosynthesis in the hair cycle need to be done to improve our understanding (Everts *et al.*, 2021).

In either sex, variation of RDH activity or RDHEs' protein levels does not correlate directly with changes in hair follicle size. For instance, in females RDH activity is the highest at PD30 (mid-anagen) and decreases through PD50 (telogen), however, PD35 and PD40 (late anagen/catagen) is when the hair follicle reaches maximum size. In females increased levels of RA biosynthesis and signaling proteins during mid-anagen have also been shown via IHC, confirming changes are not due to growth of the follicle alone (Everts *et al.*, 2007). Males exhibit their highest RDHEs' protein levels at PD45 (late catagen), when the hair follicle is rapidly decreasing in size. This demonstrates the importance of alterations in RDH activity beyond the changes potentially caused by the morphological changes of the hair cycle.

Though we have collectively studied RDHE2 and RDHE2S throughout this paper, the enzymes do have distinct individual properties (Wu *et al.*, 2019). RDHE2S activity is sevenfold higher than that of RDHE2 in *in vitro* assays, but a single knockout of RDHE2S yielded no phenotypes, possibly from RDHE2 compensation. The expression pattern of *Rdhe2* and *Rdhe2s* is overlapping throughout the body, with the highest mRNA

and protein expression levels in skin (Wu *et al.*, 2019). Additionally, human ortholog of mouse RDHE2S is nonfunctional (Adams *et al.*, 2017) and humans, like frogs (Belyaeva *et al.*, 2012), seem to rely on a single epidermal RDH, RDHE2. Thus, our use of a *Rdhe2*$^{-/-}$/*Rdhe2s*$^{-/-}$ DKO mice provides an accurate depiction of phenotypes in the absence of functional epidermal RDHs.

Overall, genes related to retinoid metabolism and signaling display a dichotomy in their response to the absence of RDHEs. Some genes (*Rbp1, Rdh10, Aldh1a2, Crabp2*) are upregulated in DKO mice compared to WT mice, while genes known to be upregulated by RA (*Lrat, Dhrs3, Cyp26b1*) exhibit decreased expression patterns in DKO mice. This suggests, along with decreased RDH activity in DKO mice, that absence of RDHEs in the skin decreases RA levels. Our analysis of mRNA expression agrees with the data reported previously by Everts, *et al.* (Everts *et al.*, 2007) that ALDH1A2 immunoreactivity (IR) in the cycling hair follicle was seen beginning from mid to late anagen (anagen IIIc) through catagen in females. We likewise see this increase in females, even though in WT female mice it is not a significant part of the interaction, there is a 14X fold change from PD26 to PD40 in WT female mice. A similar pattern of CRABP2 IR is reported for the anagen hair follicle, with IR appearing in late anagen and peaking in anagen VI/catagen I before fading. (Everts *et al.*, 2007) We also see fluctuations in transcripts for *Stra6, Lrat, Cyp26b1*, and *Rdh10* for both sexes and *Dhrs3* and *Rbp1* for males specifically, which need to be further investigated and confirmed at the protein level.

In the studies of genetically-altered mouse models, the appearance of hair phenotypes - from alterations of hair cycle progression and alopecia to hair greying - are

often unreported. Here we observe a rough coat in DKO mice, where the back hairs do not lay smoothly like the coat of WT littermates. Further characterization of the four pelage hair types demonstrated an increased percentage of awl hairs, which are induced in the second wave of hair follicle induction at E16. Awl hairs are straight and the second longest hair type. They also are one of the thickest hair types, having up to 4 rows of medulla cells within the hair cuticle (Duverger and Morasso, 2009). Alongside awl hairs, auchene hairs contain 4 rows of medulla cells, but exhibit a characteristic bend. Auchene hairs are also induced in the second wave of hair follicle induction, and some studies group these two hair types. However, our results show no differences in auchene hair percentages, indicating RDHEs are relevant to the distinction between these two hair types during the second wave of hair induction. Elevated levels of RA restricted bending of the hair fiber and development of zigzag hairs (Okano *et al.*, 2012). Our lack of alterations to bending or zigzag hairs further supports that DKO mouse skin has decreased RA levels, and that lack of RA increases the number of hair follicles that produce awl hairs.

Analysis of transcripts for HFSC markers carried out in this study demonstrates diminished expression of HFSC markers associated with the bulge region, with a greater effect in females. These data suggest the importance of precise RA levels regulated by RDHEs in maintaining proper hair cycle progression through the modulation of HFSCs. Wnt/β-catenin and Sonic HedgeHog (Shh) signaling are important for anagen initiation, where they are activating signals that overwhelm inhibitory signals from the dermal papilla to initiate proliferation of HFSCs in the bulge, signaling the telogen to anagen transition (Gonzales and Fuchs, 2017) Wnt/β-catenin signaling was upregulated in skin

from a mouse model with endogenously elevated RA levels (Okano *et al.*, 2012). In this same model, RA-regulated genes, *Crabp2* and *Stra6*, were also upregulated, alongside *Sox9*, a transcription factor regulation by RA (Gudas and Wagner, 2011). In skin, *Sox9* is essential for maintenance of the HFSCs of the hair follicle bulge (Nowak *et al.*, 2008), and previous IHC reports show ALDH1A2 and CRABP2 immunoreactivity (IR) localizes to the hair follicle bulge (Everts *et al.*, 2007; Suo *et al.*, 2021). RA signaling also acts in a mutually antagonistic manner with Wnt/β-catenin signaling (Easwaran *et al.*, 1999; Collins and Watt, 2008). Therefore, the regulation of signaling for proliferation of HFSCs is complex and multi-layered. Our data provide a basis for utilizing the hair follicle as an easily-accessible and targetable model for interrogating the relationship between RA biosynthesis and stem cell maintenance and differentiation in adult tissues.

References

Adams, M. K. *et al.* (2017) 'Characterization of human short chain dehydrogenase/reductase SDR16C family members related to retinol dehydrogenase 10', Chemico-Biological Interactions, 276, pp. 88–94. doi: 10.1016/j.cbi.2016.10.019.

Alonso, L. C. and Rosenfield, R. L. (2003) 'Molecular genetic and endocrine mechanisms of hair growth', Hormone Research, 60(1), pp. 1–13. doi: 10.1159/000070821.

Balmer, J. E. and Blomhoff, R. (2002) 'Gene expression regulation by retinoic acid', Journal of Lipid Research, 43(11), pp. 1773–1808. doi: 10.1194/jlr.R100015-JLR200.

Bazzano, G. *et al.* (1993) Effect of Retinoids on Follicular Cells, J Invest Dermatol. Available at: https://ac.els-cdn.com/0022202X9390515J/1-s2.0-0022202X9390515J-main.pdf?_tid=57f4f437-f2d5-4f77-a638-c196b96c8ea8&acdnat=1539715465_30a9e0550726055390183f14a8fda314 (Accessed: 16 October 2018).

Belyaeva, O. V. *et al.* (2012) 'Short chain dehydrogenase/reductase Rdhe2 is a novel retinol dehydrogenase essential for frog embryonic development', Journal of Biological Chemistry, 287(12), pp. 9061–9071. doi: 10.1074/jbc.M111.336727.

Bose, A. *et al.* (2013) 'Keratin K15 as a biomarker of epidermal stem cells', International Journal of Molecular Sciences, pp. 19385–19398. doi: 10.3390/ijms141019385.

Chien, A. (2018) 'Retinoids in Acne Management: Review of Current Understanding, Future Considerations, and Focus on Topical Treatments', Journal of drugs in dermatology : JDD, 17(12), pp. s51-55. Available at: http://www.ncbi.nlm.nih.gov/pubmed/30586482.

Collins, C. A. and Watt, F. M. (2008) 'Dynamic regulation of retinoic acid-binding proteins in developing, adult and neoplastic skin reveals roles for β-catenin and Notch signalling', Developmental Biology, 324(1), pp. 55–67. doi: 10.1016/J.YDBIO.2008.08.034.

Cui, C. Y. *et al.* (2010) 'Dkk4 and eda regulate distinctive developmental mechanisms for subtypes of mouse hair', PLoS ONE, 5(4). doi: 10.1371/journal.pone.0010009.

Duncan, J. F. *et al.* (2013) 'Endogenous retinoids in the pathogenesis of alopecia areata', J. Invest Dermatology, 133(2), pp. 334–343. doi: 10.1038/jid.2012.344.

Duverger, O. and Morasso, M. I. (2009) 'Epidermal patterning and induction of different hair types during mouse embryonic development', Birth Defects Research Part C - Embryo Today: Reviews, 87(3), pp. 263–272. doi: 10.1002/bdrc.20158.

Easwaran, V. *et al.* (1999) 'Cross-regulation of β-catenin–LEF/TCF and retinoid signaling pathways', Current Biology, 9(23), pp. 1415–1419. doi: 10.1016/S0960-9822(00)80088-3.

Everts, H. B. *et al.* (2007) 'Immunolocalization of enzymes, binding proteins, and receptors sufficient for retinoic acid synthesis and signaling during the hair cycle', Journal of Investigative Dermatology, 127(7), pp. 1593–1604. doi: 10.1038/sj.jid.5700753.

Everts, H. B. (2012) 'Endogenous retinoids in the hair follicle and sebaceous gland', Biochimica et Biophysica Acta - Molecular and Cell Biology of Lipids, 1821(1), pp. 222–229. doi: 10.1016/j.bbalip.2011.08.017.

Everts, H. B. *et al.* (2021) 'Estrogen regulates the expression of retinoic acid synthesis enzymes and binding proteins in mouse skin', Nutrition Research, 94, pp. 10–24. doi: 10.1016/j.nutres.2021.08.002.

Foitzik, K. *et al.* (2005) 'Towards dissecting the pathogenesis of retinoid-induced hair loss: All-trans retinoic acid induces premature hair follicle regression (catagen) by upregulation of transforming growth factor-β2 in the dermal papilla', Journal of Investigative Dermatology, 124(6), pp. 1119–1126. doi: 10.1111/j.0022-202X.2005.23686.x.

Gallego, O. *et al.* (2006) 'Comparative functional analysis of human medium-chain dehydrogenases, short-chain dehydrogenases/reductases and aldo-keto reductases with retinoids', Biochemical Journal, 399(1), pp. 101–109. doi: 10.1042/BJ20051988.

Gonzales, K. A. U. and Fuchs, E. (2017) 'Skin and Its Regenerative Powers: An Alliance between Stem Cells and Their Niche', Developmental Cell, 43(4), pp. 387–401. doi: 10.1016/j.devcel.2017.10.001.

Gudas, L. J. and Wagner, J. A. (2011) 'Retinoids regulate stem cell differentiation', Journal of Cellular Physiology, 226(2), pp. 322–330. doi: 10.1002/jcp.22417.

Hu, H. min *et al.* (2012) 'Estrogen leads to reversible hair cycle retardation through inducing premature catagen and maintaining Telogen', PLoS ONE, 7(7). doi: 10.1371/journal.pone.0040124.

Jaks, V. *et al.* (2008) 'Lgr5 marks cycling, yet long-lived, hair follicle stem cells', Nature Genetics, 40(11), pp. 1291–1299. doi: 10.1038/ng.239.

Joost, S. *et al.* (2020) 'The Molecular Anatomy of Mouse Skin during Hair Growth and Rest', Cell Stem Cell, 26(3), pp. 441-457.e7. doi: 10.1016/j.stem.2020.01.012.

Kedishvili, N. Y. (2013) 'Enzymology of retinoic acid biosynthesis and degradation', Journal of Lipid Research, 54(7), pp. 1744–1760. doi: 10.1194/jlr.R037028.

Kelsey, L. *et al.* (2012) 'Retinoids regulate the formation and degradation of gap junctions in androgen-responsive human prostate cancer cells', PLoS ONE, 7(4). doi: 10.1371/journal.pone.0032846.

Klyuyeva, A. V. *et al.* (2021) 'Changes in retinoid metabolism and signaling associated with metabolic remodeling during fasting and in type I diabetes', Journal of Biological Chemistry, 296(29), p. 100323. doi: 10.1016/j.jbc.2021.100323.

Lin, K. K. *et al.* (2009) 'Circadian clock genes contribute to the regulation of hair follicle cycling', PLoS Genetics, 5(7). doi: 10.1371/journal.pgen.1000573.

Liu, Y. *et al.* (2003) 'Keratin 15 Promoter Targets Putative Epithelial Stem Cells in the Hair Follicle Bulge', Journal of Investigative Dermatology, 121(5), pp. 963–968. doi: 10.1046/j.1523-1747.2003.12600.x.

Morris, R. J. *et al.* (2004) 'Capturing and profiling adult hair follicle stem cells', Nature Biotechnology, 22(4), pp. 411–417. doi: 10.1038/nbt950.

Müller-Röver, S. *et al.* (2001) 'A Comprehensive Guide for the Accurate Classification of Murine Hair Follicles in Distinct Hair Cycle Stages', Journal of Investigative Dermatology, 117(1), pp. 3–15. doi: 10.1046/J.0022-202X.2001.01377.X.

Napoli, J. L. (1986) '[13] Quantification of Physiological Levels of Retinoic Acid', Methods in Enzymology, 123(C), pp. 112–124. doi: 10.1016/S0076-6879(86)23015-3.

Nowak, J. A. *et al.* (2008) 'Hair follicle stem cells are specified and function in early skin morphogenesis', Cell Stem Cell, 3(1), pp. 33–43. doi: 10.1016/j.stem.2008.05.009.

O'Connor, C., Varshosaz, P. and Moise, A. R. (2022) 'Mechanisms of Feedback Regulation of Vitamin A Metabolism', Nutrients, 14(6), p. 1312. doi: 10.3390/NU14061312.

Okano, J. *et al.* (2012) 'Cutaneous retinoic acid levels determine hair follicle development and downgrowth', Journal of Biological Chemistry, 287(47), pp. 39304–39315. doi: 10.1074/jbc.M112.397273.

Rivera-Gonzalez, G. C. *et al.* (2012) 'Retinoic acid and androgen receptors combine to achieve tissue specific control of human prostatic transglutaminase expression: A novel regulatory network with broader significance', Nucleic Acids Research, 40(11), pp. 4825–4840. doi: 10.1093/nar/gks143.

Ross-Innes, C. S. *et al.* (2010) 'Cooperative interaction between retinoic acid receptor-α and estrogen receptor in breast cancer', Genes and Development, 24(2), pp. 171–182. doi: 10.1101/gad.552910.

Saitou, M. *et al.* (1995) 'Inhibition of skin development by targeted expression of a dominant-negative retinoic acid receptor', Nature, 374, pp. 159–62. doi: 10.1038/374159a0.

Schneider, M. R., Schmidt-Ullrich, R. and Paus, R. (2009) 'The Hair Follicle as a Dynamic Miniorgan', Current Biology, 19(3), pp. R132–R142. doi: 10.1016/J.CUB.2008.12.005.

Shih, M. Y. S. *et al.* (2009) 'Retinol Esterification by DGAT1 Is Essential for Retinoid Homeostasis in Murine Skin', The Journal of biological chemistry, 284, pp. 4292–4299. doi: 10.1074/jbc.M807503200.

Stüttgen, G. (1986) 'Historical perspectives of tretinoin', Journal of the American Academy of Dermatology, 15(4), pp. 735–740. doi: 10.1016/S0190-9622(86)70228-4.

Sundberg, J. P. and Hogan, M. E. (1994) 'Hair Types and Subtypes in the Laboratory Mouse', in Handbook of Mouse Mutataions with Skin and Hair Abnormalities. 1st Editio. CRC Press, p. 12.

Suo, L. *et al.* (2021) 'Dietary Vitamin A Impacts Refractory Telogen', Frontiers in Cell and Developmental Biology, 9(February), pp. 1–11. doi: 10.3389/fcell.2021.571474.

Trempus, C. S. *et al.* (2003) 'Enrichment for living murine keratinocytes from the hair follicle bulge with the cell surface marker CD34', Journal of Investigative Dermatology, 120(4), pp. 501–511. doi: 10.1046/j.1523-1747.2003.12088.x.

Ubels, J. L. *et al.* (2002) 'Down-regulation of androgen receptor expression and inhibition of lacrimal gland cell proliferation by retinoic acid', Experimental Eye Research, 75(5), pp. 561–571. doi: 10.1006/exer.2002.2054.

Vidal, V. P. I. *et al.* (2005) 'Sox9 is essential for outer root sheath differentiation and the formation of the hair stem cell compartment', Current Biology, 15(15), pp. 1340–1351. doi: 10.1016/j.cub.2005.06.064.

Wu, L. *et al.* (2019) 'Mice lacking the epidermal retinol dehydrogenases SDR16C5 and SDR16C6 display accelerated hair growth and enlarged meibomian glands', Journal of Biological Chemistry, 294(45), pp. 17060–17074. doi: 10.1074/jbc.RA119.010835.

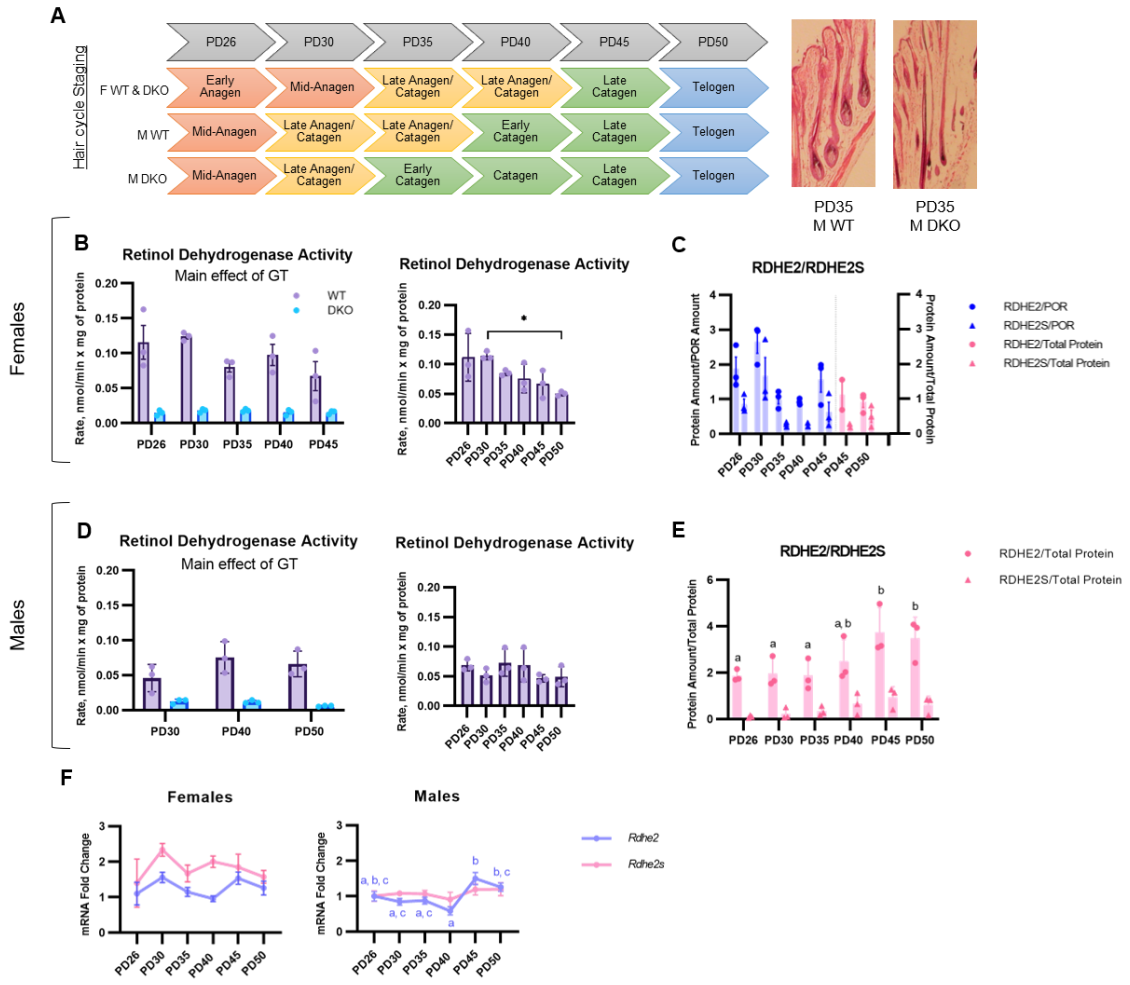

Figure 1. RDHEs fluctuates across the hair cycle, but RDH activity varies in a sex-specific manner. (A) Hair cycle staging for WT and DKO females and males at the sampled postnatal days (PD) via histological assessment, examples to the right for male differences, 4X magnification. **(B, D)** NAD^+-dependent retinol dehydrogenase activity of skin microsomal fractions isolated from dorsal skin collected at different PDs (n = 3 per PD). **(C, E)** Quantification of RDHE2 and RDHE2S protein via western blot using microsomes across PDs. **(C, blue)** RDHE2/RDHE2S protein amount was normalized by POR protein amount, a microsome-specific marker. **(C, E, pink)** Due to the discontinuation of our POR antibody and an inability to find another sufficient microsomal-specific antibody, RDHE2/RDHE2S protein amount was normalized by total protein amount. **(F)** *Rdhe2/Rdhe2s* mRNA expression across PDs as analyzed by qPCR. All data are presented as the mean, with error bars representing SEM. *, $p < 0.05$. Letters indicate significant differences by a Tukey's post-hoc, except in **(F)** where Sidak's was used for all qPCR.

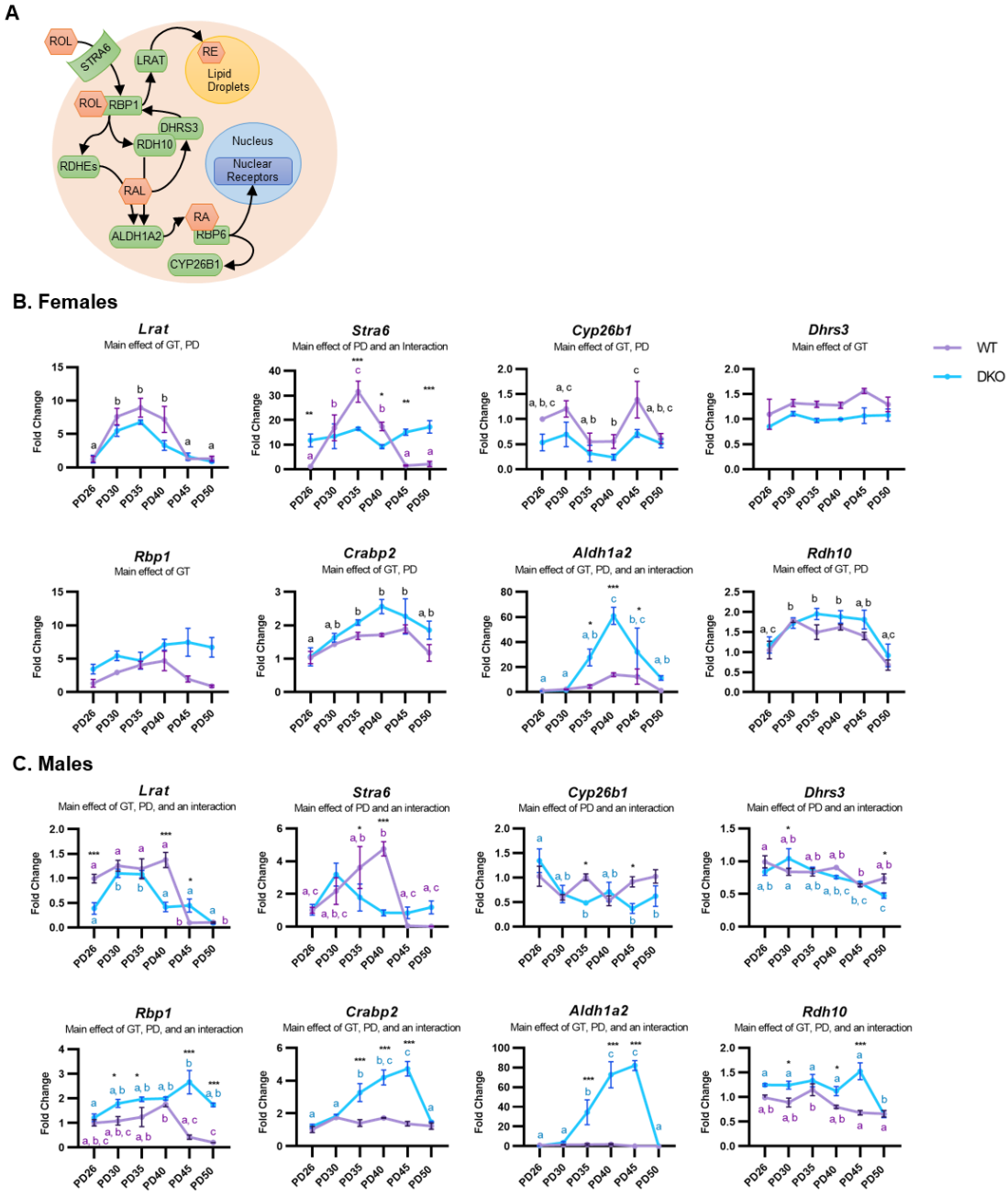

Figure 2. Absence of RDHEs alters RA biosynthesis gene expression patterns during the hair cycle. RNA was isolated from the same skin taken at PDs outlined in Fig 1. cDNA was made and qPCR was performed for genes involved in RA biosynthesis and signaling. **(A)** This diagram outlines the function of each gene examined, with the gene's protein in green and metabolites in orange hexagons. **(B)** Female and **(C)** male qPCR data for genes related to RA biosynthesis and signaling. All data are presented as the mean, with error bars representing SEM. All genes were analyzed with a two-way ANOVA and significant main effects or an interaction are listed below the graph title. GT

= genotype. PD = postnatal day. Black letters indicate significant differences by a Sidak post-hoc if there is a main effect of PD with no interaction. If there is a significant interaction, asterisk's indicate significant differences between GTs at specific PDs. *, $p < 0.05$; **, $p < 0.01$; ***, $p < 0.001$. Colored letters indicate significant differences between PDs within a GT.

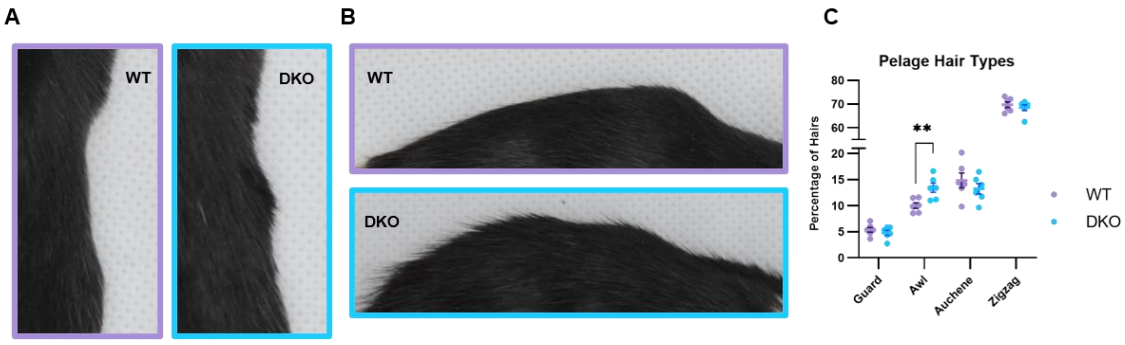

Figure 3. Awl hairs are increased in the absence of RDHEs. Images of the **(A)** side and **(B)** back of WT and DKO mice in a lightbox. (C) Quantification of pelage hair types, shaved from the middle back of mice from PD58 – PD61 (during telogen, confirmed via identification of pink skin once shaven). At least 100 hairs were counted per mouse and categorized under a dissection microscope, n = 3 males, n = 3 female. **, $p < 0.01$

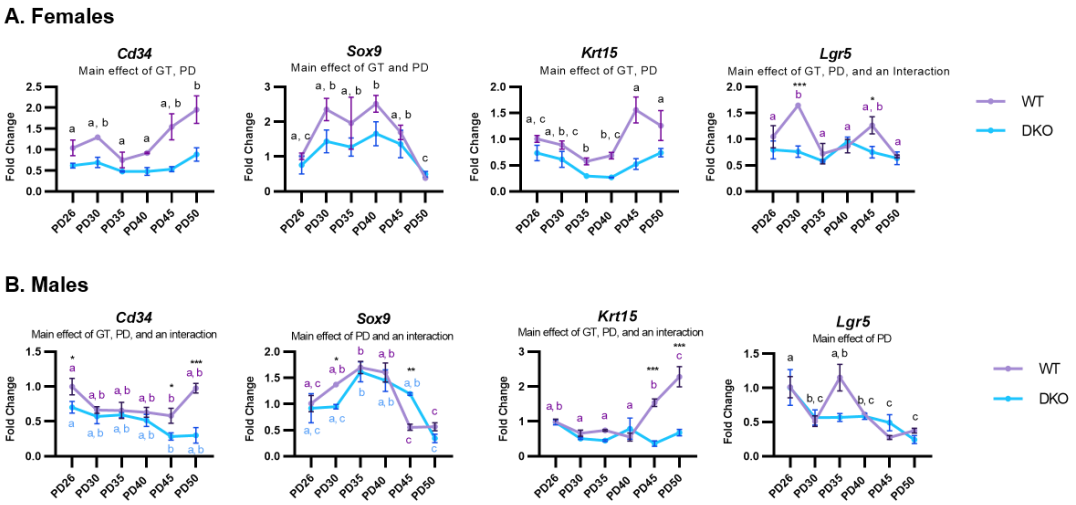

Figure 4. Expression of hair follicle stem cell markers is diminished in the absence of RDHEs. Using the same samples from Fig. 2, qPCR was performed in **(A)** females and **(B)** males for genes identified in the literature as markers of hair follicle stem cells in the bulge of the hair follicle. All data are presented as the mean, with error bars representing SEM. All genes were analyzed with a two-way ANOVA and significant main effects or an interaction are listed below the graph title. GT = genotype. PD = postnatal day. Black letters indicate significant differences by a Sidak post-hoc if there is a main effect of PD with no interaction. If there is a significant interaction, asterisk's indicate significant differences between GTs at specific PDs. *, $p < 0.05$; **, $p < 0.01$; ***, $p < 0.001$. Colored letters indicate significant differences between PDs within a GT.

ABSENCE OF EPIDERMAL RETINOL DEHYDROGENASES ALTERS BODY COMPOSITION AND METABOLISM

by

KELLI R. GOGGANS and NATALIA Y. KEDISHVILI

In preparation for *Journal of Nutritional Biochemistry*

Format adapted for dissertation

Abstract

Retinol dehydrogenases SDR16C5 and SDR16C6, also known as retinol dehydrogenase epidermal 2 (RDHE2) and RDHE2-similar (RDHE2S), function as the major retinol dehydrogenases in mouse skin, and thus are responsible for the rate-limiting step of retinoic acid (RA) biosynthesis. However, transcripts encoding these two enzymes are also detectable in several other mouse tissues. Interestingly, we have observed age-related phenotypes in the global *Rdhe2*$^{-/-}$*;Rdhe2s*$^{-/-}$ double gene knockout (DKO) mouse model. 12 month old DKO female mice had decreased body weight, fat percentage, and bone mineral density measured via dual energy x-ray absorptiometry (DXA), alongside increased dark phase locomotor activity and energy expenditure measured via indirect calorimetry. To determine whether these differences could be related to changes in the whole body vitamin A status of DKO mice, we investigated the effects of a vitamin A deficient (VAD) diet on whole body physiology in 2 month old DKO and wild-type (WT) mice using DXA and calorimetry. However, younger female mice on a VAD diet had higher bone mineral density and fat percentage, with lower locomotor activity rates but higher energy expenditure compared to age-matched mice on regular diet, suggesting the absence of RDHE2 and RDHE2S may not result in whole body VAD. Additionally, 2 month old DKO female mice on regular chow diet and on VAD diet did not phenocopy WT female mice on VAD. Surprisingly, 2 month old DKO female mice on VAD weighed less and were smaller than all other groups, had decreased energy expenditure, and exhibited an altered metabolism in which they undergo anaerobic respiration during the dark phase. These results support previous research that RDHE2 and RDHE2S are

tissue-specific retinol dehydrogenases and demonstrate how dysregulation of RA biosynthesis can have diverse whole body effects.

Keywords: vitamin A deficiency, retinol dehydrogenases, body composition, energy expenditure

Introduction

Short-chain dehydrogenases/reductases (SDRs) comprise a large family of cytoplasmic and membrane-bound enzymes that contribute to the metabolism of very diverse substrates including carbohydrates, prostaglandins, steroids, and retinoids. The products of SDR enzymatic activity play major roles in the regulation of numerous signaling pathways. In particular, recent studies from this and other laboratories identified members of the 16C family of SDRs as essential for the biosynthesis of all-*trans*-retinaldehyde, the immediate precursor of all-*trans*-retinoic acid (RA). RA is derived from vitamin A and β-carotene [1], and through interactions with nuclear transcription factors, retinoic acid receptors (RARs), RA regulates the expression of over 500 genes [2].

The production of all-*trans*-retinaldehyde, via the oxidation of all-*trans*-retinol, is the rate-limiting step of RA biosynthesis [3]. We reported that a heterooligomeric complex of two SDRs, SDR16C4 (retinol dehydrogenase 10, RDH10) and SDR16C1 (dehydrogenase/reductase 3, DHRS3) controls the flux of retinol to RA by regulating the output of retinaldehyde [4]. However, it appears that in addition to the SDR retinoid oxidoreductase complex, other SDRs may complement RA biosynthesis in a tissue-

specific manner. We have reported that murine proteins SDR16C5 (retinol dehydrogenase epidermal 2, RDHE2) and SDR16C6 (RDHE2-similar, RDHE2S) exhibit NAD^+-dependent retinol dehydrogenase activity in vitro and when transfected into cultured cells. Subsequent analysis of the *in vivo* functions of RDHE2 and RDHE2S using a double gene knockout (DKO) mouse model demonstrated that these two endoplasmic reticulum associated membrane proteins function as the major retinol dehydrogenases in skin, being responsible for nearly 80% of the total retinol dehydrogenase activity of skin microsomal fractions [5].

While the role of RDHE2 and RDHE2S in the pathway of RA biosynthesis seems to be most prominent in the skin, transcripts encoding these two enzymes are also found in esophagus, stomach, tongue, adipose tissue, intestine, and colon [5]. Whether RDHE2 and RDHE2S contribute to RA biosynthesis in these tissues is currently unknown. However, we have observed differences in the weight and size of DKO mice that were not noticeable in younger animals but developed with aging. The literature supports a role for RDHE2 in growth and body size, as RDHE2 is part of genomic areas associated with the body weight and stature of cattle [6,7], growth rate in pigs [8], human height [9–11], and beak deformity in chickens [12].

Since RDHE2 and RDHE2S are retinol dehydrogenases that facilitate the rate-limiting step of RA biosynthesis, we hypothesized these differences could be caused by a chronic deficiency in vitamin A metabolism. The effect of vitamin A deficiency (VAD) on female mouse body composition, activity, and calorimetry are also not well recorded in the literature for us to compare our observed DKO phenotypes to those of VAD. Many VAD studies begin experimental conditions after weaning, but by this time animals have

already developed liver stores of retinyl esters. Though several studies utilize serum levels of retinol as measurements of VAD, circulating levels of retinol do not necessarily reflect vitamin A stores in liver, and VAD deficiency can only be accurately quantified by analysis of liver vitamin A quantities. Our laboratory and others have shown that placing dams on VAD diet at mid-gestation deprives developing pups of free retinol in the blood stream that can be stored in then-developing livers, while not inhibiting provision of necessary RBP4 bound retinol for developmental processes.

Thus, we examined both wild-type (WT) and DKO female mice on either regular chow diet (RD) or VAD diet at 2 months old. Dams were given VAD diet beginning at mid-gestation to prevent pups from developing vitamin A stores in livers. This study was undertaken to characterize the phenotypic features of young DKO female mice and determine if they resembled phenotypes of VAD in age-matched females at the level of whole body physiology.

Experimental Procedures

Mice

A double knockout mouse strain of *Rdhe2* and *Rdhe2s* was generated in a previous study [5], and these mice along with wild-type C57Bl/6J were used for DXA and indirect calorimetry measurements. To create pups that were vitamin A deficient (VAD), dams were switched to a VAD diet mid-gestation (12 – 14 days post-conception). Pups were maintained on the VAD diet. All mice were housed with free access to water and food in an AALAC-approved pathogen-free facility at 23 ± 2° C on a 12:12 light/dark cycle. All studies were conducted with the approval of the Institutional Animal

Care and Use Committee (IACUC) of the University of Alabama at Birmingham (UAB) School of Medicine, and all animals were handled in accordance with UAB's IACUC and the National Institutes of Health guidelines.

DXA and Calorimetry Analysis

Dual-energy x-ray absorptiometry (DXA) and indirect calorimetry was performed by the University of Alabama's Small Animal Phenotyping Core on 12 and 2 month old wild-type and Rdhe2/Rdhe2s double knockout mice, bred and maintained on either regular chow diet or a VAD diet. DXA was used to measure fat and lean tissue and bone content while animals were anesthetized via isoflurane. A TSE indirect calorimetry system was used to measure oxygen consumption, carbon dioxide production, and food consumption, and utilized infra-red beams to monitor locomotor activity.

Statistical Analysis

All statistics were calculated using SPSS 28 software. Data were analyzed with independent samples t-tests, two-way ANOVAs, utilizing a co-variant when needed, and repeated measure two-way ANOVAs. Energy expenditures were adjusted via a multiple regression using fat and lean mass for the 2 month old females due to significant differences in body composition across the four groups. Significance was ascribed at $p < 0.05$. Estimated marginal means were calculated with a Sidak's test. The data that support the findings of this study are available from the corresponding author upon reasonable request.

Results

Aged Rdhe2$^{-/-}$/Rdhe2s$^{-/-}$ double knockouts have altered body composition and activity

We first observed phenotypes of altered body size in aged DKO mice compared to age-matched WT mice. We subjected mice to dual energy x-ray absorptiometry (DXA) imaging and indirect calorimetry analysis to gather preliminary data. 13 WT female mice and 12 DKO female mice 12 months old were analyzed. We also attempted to analyze males, but the WT (n = 2) and DKO (n = 9) male mice sample sizes were not sufficiently comparable.

Body weight, as assessed by DXA imaging, was significantly decreased in DKO female mice ($t = 2.621$, $p = 0.015$) (Fig. 1A), confirming our visual observations. To adjust for differences in body size, fat mass and lean mass were divided by total tissue mass to obtain respective percentages. Fat mass percentage was decreased in DKO mice ($t = 2.656$, $p = 0.014$), while lean mass percentage was significantly increased ($t = 2.643$, $p = 0.015$) (Fig. 1B). While body area and bone mineral content (BMC) were not altered significantly, bone mineral density (BMD), which is calculated by dividing BMC by body area, was significantly decreased ($t = 2.101$, $p = 0.047$) (Fig. 1C). Kilocalorie intake was not altered, even accounting for body weight differences ($F = 0.657$, $p = 0.203$).

In addition to changes in body composition, DKO female mice were more active in the dark phase than WT mice. Ambulatory activity is defined as movement across the cage, causing several beam breaks, while fine activity is recorded when the same beam is broken several times, usually representing eating or grooming activity. Ambulatory and fine activity counts were binned by the light phase and the dark phase. A repeated measures ANOVA was used to analyze for differences in time of day and genotype. As

expected, time of day was significantly different in ambulatory and fine activity across all groups (Fig. 1D). There was a significant interaction between time of day and genotype for both groups, showing DKO female mice were more active than WT female mice specifically during the dark phase for ambulatory ($p = 0.010$) and fine ($p = 0.014$) activity. Similar results were found in total energy expenditure (TEE), also categorized into light and dark phases, where DKO female mice had higher TEE in the dark phase than WT mice ($p = 0.007$). TEE was significantly different between the light and dark phases in both WT and DKO females ($p < 0.001$) (Fig. 1E).

Absence of RDHEs does not correlate to body mass changes from VAD

We examined 2 month old WT and DKO female mice on either a regular chow diet (RD) or a VAD diet to determine if phenotypes of DKOs corresponded to phenotypes of VAD, but at a lesser severity. Dams were placed on VAD diet at mid-gestation before embryonic livers were formed to ensure pups were completely VAD without causing embryonic malformities from VAD. Female pups were then maintained on a VAD diet until 2 months of age.

DXA imaging revealed a significant interaction of diet and genotype (GT) for weight ($F = 20.807$, $p < 0.001$). While VAD diet or absence of RDHEs alone do not alter weight, VAD in the absence of RDHEs significantly decreases weight ($p < 0.001$) (Fig. 2A). Area of the mouse, as viewed from above with the limbs extended in a DXA machine, also had an interaction of diet and genotype ($F = 9.968$, $p = 0.008$) (Fig. 2B). In both diets, DKO female mice exhibit decreased area (RD, $p = 0.044$; VAD, $p < 0.001$), while DKO female mice on VAD are significantly smaller than DKO female mice on RD

($p = 0.005$). To adjust for the significant differences in weight, we calculated fat and lean percentages by dividing fat or lean mass by total tissue. Fat percentage is increased on VAD ($F = 24.319$, $p < 0.001$), and lean percentage is decreased on VAD ($F = 20.742$, $p < 0.001$). These effects appear to be reduced in DKO female mice, as there is a trend towards an interaction of diet and GT for fat percentage ($p = 0.057$) and lean percentage ($p = 0.059$). While VAD on WT female mice increases fat and decreases lean percentages by 5.48% and 5.36%, respectively, VAD for DKO mice increases fat and decreases lean percentages by only 2.2% and 2.42%. Bone mineral density (BMD) shows there is a main effect of diet ($F = 12.708$, $p = 0.004$) and genotype ($F = 8.390$, $p = 0.013$), however, there is an almost significant interaction ($F = 4.653$, $p = 0.052$). While BMD of WT female mice on VAD increases 14%, BMD of DKOs on VAD only increases 4%. The absence of RDHEs seems to diminish the effects cause by VAD in alterations to fat and lean percentage along with BMD.

These alterations cannot be completely explained by energy intake, as the intake of kilocalories per day (kcal/day) was significantly decreased only by a VAD diet ($F = 14.735$, $p = 0.003$) (Fig. 2C). Weight was used as a covariant for kcal/day, but was not significant ($p = 0.663$).

VAD and absence of RDHEs decreases locomotor activity

We previously noted alterations to locomotor activity levels in 1 year old females, so we examined locomotor activity of 2 month old female mice. Locomotor activity was defined as either ambulatory of fine and binned into either the light or dark phase. A repeated measure ANOVA was used to analyze for differences in time of day, diet, and

GT. As expected, time of day was significantly different in both ambulatory and fine activity across all groups (Fig. 3A – B).

For ambulatory activity (Fig. 3A), there was an interaction of time of day with diet ($F = 5.180$, $p = 0.042$) and time of day with genotype ($F = 9.373$, $p = 0.010$). While VAD decreased the ambulatory activity of WT mice in the light phase ($p = 0.047$), there was a greater decrease in dark phase ambulatory activity ($p = 0.030$). DKO mice demonstrated similarly decreased ambulatory activity during the light and dark phases ($p = 0.004$). Fine activity (Fig. 3B) was significantly decreased on VAD diet independent of time of day ($F = 8.574$, $p = 0.013$). There was a significant interaction of time of day and genotype ($F = 6.020$, $p = 0.030$), with DKO female mice showing less fine activity during the light ($p < 0.001$) and dark phases ($p = 0.001$).

Unlike body composition differences, both VAD and absence of RDHEs result in similar phenotypes for locomotor activity, decreasing both ambulatory and fine activity without disrupting diurnal variations.

Presence or absence of RDHEs determines effect of VAD on energy expenditure, but metabolism is significantly shifted in DKOs on VAD

TEE and REE was categorized into light and dark phase and corrected for analysis by multiple regression using fat and lean mass. A repeated measures ANOVA was used to test for differences in time of day, diet, and GT. There was a significant interaction between time of day, diet, and GT for both TEE ($F = 7.907$, $p = 0.016$) and REE ($F = 12.589$, $p = 0.004$) (Fig. 4A). All groups varied significantly between light and dark phases. Both WT female mice and DKO female mice had significant differences

between RD and VAD diet for light and dark phase. VAD in WT female mice increased TEE and REE at both the light ($p = 0.036$, $p = 0.005$) and the dark phase ($p = 0.004$, $p < 0.001$). VAD in DKO female mice decreased TEE at both day ($p < 0.001$) and night ($p = 0.003$) and decreased REE during the day ($p = 0.002$) but not the night ($p = 0.348$). It is worth noting that while DKO female mice are not significantly different than WT female mice on RD, genotype determines the effect of VAD diet. On VAD, WT female mice and DKO female mice are significantly different in TEE and REE during the day ($p < 0.001$) and night ($p < 0.001$). We also conclude these differences in energy expenditure cannot be completely attributed to locomotor activity, which similarly and additively decreases with VAD and absence of RDHEs. The increased energy expenditure of VAD WT female mice is not fully explained in this dataset.

We also analyzed respiratory exchange ratio (RER), a measurement calculated from the amount of O_2 consumed and CO_2 produced (VCO_2/VO_2). A RER close to 0.7 indicates there is more metabolism of fats for energy, but a RER close to 1 indicates more metabolism of carbohydrates. When the RER exceeds 1 more CO_2 is produced than O_2 consumed, indicating anaerobic metabolism is occurring. There was a significant interaction of time of day with diet ($F = 19.9985$, $p < 0.001$) and time of day with GT ($F = 8.988$, $p = 0.011$) for RER. In RD, there is not a significant difference in light and dark phase RER ($p = 0.077$), and light phase RER is not altered by VAD ($p = 0.093$). However, dark phase RER is increased on VAD ($p < 0.001$), and on VAD there is a significant light-dark phase difference for RER ($p < 0.001$). Light phase RER is also not significantly different between WT female mice and DKO female mice ($p = 0.949$), but dark phase RER is ($p < 0.001$). WT female mice do have a significant difference between

light and dark phase RER ($p = 0.012$), but this is likely biased by the VAD WT female mice. DKO female mice have a significant light-dark phase RER difference ($p < 0.001$), but the difference is dramatically different for the mice on RD (light: 0.9097, dark: 0.9547) versus those on VAD (light: 0.8810, dark: 1.0705). Scientifically significant is that while both VAD and absence of RDHEs increases dark phase RER, the combination of DKO female mice on VAD increases night RER above 1, to $1.07 \pm .033$ (mean with SD). Thus, even though DKO female mice on VAD are moving significantly less than all groups and expending the least energy, they are undergoing anaerobic respiration during the dark phase.

Discussion

We have found alterations to RA biosynthesis, either through the absence of tissue-specific retinol dehydrogenases RDHE2 and RDHE2S or vitamin A deficiency, alter the body composition, locomotor activity, and metabolism of female mice. Our 12 month old female mice show that absence of RDHEs results in aging phenotypes, where 12 month old DKO female mice had decreased body weight and fat percentage compared to age-matched WT female mice. 12 month old DKO female mice also have increased locomotor activity and dark phase energy expenditure compared to 12 month old WT females, which could account for the decrease in weight and fat percentage. Several studies document treatment of RA decreases adipose tissue mass and improves weight loss of mice fed a high-fat diet (HFD). In these studies, RA treatment also increases dark phase energy expenditure [13], improves insulin resistance [14,15] and glucose tolerance [16], and reverses liver hepatosteatosis [13,16]. This is due to RA's ability to globally

stimulate fatty acid oxidation [17] and alter adipocyte differentiation [13]. Despite our original hypothesis that absence of RDHEs would create chronic vitamin A deficiency, our 12 month old DKO females exhibit phenotypes similar to those of treatment with RA, indicating the dysregulation of RA biosynthesis caused by the absence of RDHEs may actually produce a state of chronic vitamin A excess.

Studies of BMD support this idea and are the most consistent across literature independent of age, animal model, or other variables. Lower BMD indicates an increased risk for osteoporosis and bone fractures [18], while a higher BMD could be preventative for osteoporosis or a sign of skeletal malformations; however, even in humans, an upper limit for BMD is not yet defined [19]. Animals fed excessive levels of vitamin A have increased bone fragility, and in humans high vitamin A intake indicates an increased risk of bone fractures [18]. VAD increases bone thickness, possibly through the dysregulation of matrix molecule degradation [20]. Our data from 2 month old females on VAD is in agreement, as their BMD is significantly increased. However, the BMD of both young and old DKO females is decreased, resembling a phenotype of excess RA. Most interesting is the trend in BMD of DKO female mice on VAD, where the absence of RDHEs ameliorates most of the increase seen in WT female mice on VAD.

Changes in fat and lean percentage also support this idea of the absence of RDHEs ameliorating effects of VAD. While 2 month old DKO females on RD did not show changes in fat or lean percentage, WT females on VAD did have increased fat percentage (5.48%) and decreased lean percentages (5.36%) compared to WT females on RD. However, despite VAD significantly increasing fat percentage and decreasing lean percentage independent of GT, it is worth noting that DKO female mice on VAD

increased fat percentage and decreased lean percentage only 2.2% and 2.42%, respectively, compared to DKO female mice on RD. The trend towards an interaction for both fat and lean percentages indicates that absence of RDHEs may ameliorate the effects of VAD, like in BMD, and requires further investigation.

Literature references for how VAD alters fat mass and body weight typically begin VAD diets at weaning [21], skewing results until there is sufficient deprivation to deplete liver stores. However, significant results were noted after 5 weeks, where decreases in body mass and epididymal fat of male rats were noted [21]. This is not in agreement with our VAD WT female mice, which have increased fat percentage and no effect on overall weight, but this could be due to sex or species differences or suggest that certain post-natal development processes can change metabolic outcomes of VAD induced later in life. Studies of RA supplementation investigate older mice and specifically induce obesity through HFD, so they aren't good references for our 2 month old dataset [13–16]. This subject overall requires more research and detailed reporting of outcomes to characterize the effects of endogenous RA levels in young mice and rats.

All groups tested also exhibited phenotypes in locomotor activity, which is most well studied in the context of VAD. However, many studies of VAD which report alterations to locomotor activity and motor function do not analyze liver for vitamin A stores to prove animals are VAD [22–25]. One study from June et al [26] did administer VAD diet to dams at 2 weeks gestation, as recommended, and showed VAD rats had impaired motor function by their inability to stay on the rotarod. This is in agreement with the other studies, where VAD administered at weaning decreased locomotor activity [22–24] and impaired motor function [25], and our study where VAD decreased

locomotor activity. Therefore, locomotor activity and motor function may be more acutely affected by changes in vitamin A levels. While 12 month old DKO female mice exhibited increased locomotor activity compared to age-matched WT female mice, we cannot be sure if this is because of more severe age-related changes in WT female mice than DKO female mice or a chronic increase in DKO female mice locomotor activity over time. In 2 month old mice, it is worth noting that alongside decreases in locomotor activity from VAD, DKO female mice on RD and VAD also showed decreases in locomotor activity. This could be because tissues related to regulation of locomotor activity are either sensitive to dysregulation of RA biosynthesis in general or experience localized VAD in the absence of RDHEs, since BMD changes indicate VAD status is not applicable to the whole body.

Unexpectedly, changes in locomotor activity did not correlate with changes in energy expenditure. WT female mice on VAD displayed increased TEE and REE during both the light and dark phases; however, despite no difference between WT and DKO female mice on RD, DKO female mice on VAD displayed decreased TEE during both the light and dark phase and REE during the light phase. Thus, the effects of VAD on female mice were dependent upon genotype and do not correlate with locomotor activity, which was decreased by both diet and GT. As far as we know, literature does not describe the effects of VAD on energy expenditure, and the effects of RA supplementation are only covered in the previously mentioned HFD studies, where there is an increase in dark phase TEE [13]. RER is also not widely reported in literature for studies involving vitamin A as far as we could find, but here we report that VAD increased dark phase RER of WT female mice, causing a significant diurnal variation. This diurnal variation

was also significant in DKO female mice. Notably, the DKO female mice on VAD exceeded an RER ratio of 1 during the dark phase (1.0705 ± 0.03290), indicating they are undergoing anaerobic respiration during this time as they output more oxygen than carbon dioxide consumed. The DKO female mice on VAD are significantly smaller than any other group in weight and area, and even at this early age the difference in size could be driven by altered metabolism. Our instruments are unable to assess mice smaller than our DKO females on VAD, but VAD also shortens the lifespan of animals maintained on it significantly. Two months of age was the optimal time point for this study, but further investigation utilizing more specialized and thorough techniques and focusing on the tissue-specific phenotypes of DKO mice are required to understand this altered metabolism.

Additionally, full body composition and metabolism reports are lacking for mice given excess or restricted vitamin A/RA levels. Most reports failed to indicate if there were insignificant differences of unreported metrics, leaving us unable to determine if metrics such as area, TEE and REE, RER, lean mass weight or percentage, and locomotor activity are well-tested and assessed in the field. Without a clear understanding of how vitamin A and RA affect body composition and metabolism alone, it is unclear how to determine effects of other experimental variables or if observed phenotypes are in line with excess or diminished RA levels. Here, we report all observed metrics, many altered by VAD, and include detailed reports in the supplementary to aid the investigations of others.

References

[1] Kedishvili NY. Enzymology of retinoic acid biosynthesis and degradation. J Lipid Res 2013;54:1744–60. https://doi.org/10.1194/jlr.R037028.

[2] Balmer JE, Blomhoff R. Gene expression regulation by retinoic acid. J Lipid Res 2002;43:1773–808. https://doi.org/10.1194/jlr.R100015-JLR200.

[3] Napoli JL. [13] Quantification of Physiological Levels of Retinoic Acid. Methods Enzymol 1986;123:112–24. https://doi.org/10.1016/S0076-6879(86)23015-3.

[4] Belyaeva O V., Adams MK, Wu L, Kedishvili NY. The antagonistically bifunctional retinoid oxidoreductase complex is required for maintenance of all-trans-retinoic acid homeostasis. J Biol Chem 2017;292:5884–97. https://doi.org/10.1074/jbc.M117.776914.

[5] Wu L, Belyaeva O V., Adams MK, Klyuyeva A V., Lee SA, Goggans KR, *et al.* Mice lacking the epidermal retinol dehydrogenases SDR16C5 and SDR16C6 display accelerated hair growth and enlarged meibomian glands. J Biol Chem 2019;294:17060–74. https://doi.org/10.1074/jbc.RA119.010835.

[6] Jiao S, Maltecca C, Gray KA, Cassady JP. Feed intake, average daily gain, feed efficiency, and real-time ultrasound traits in Duroc pigs: II. genomewide association. J. Anim. Sci., vol. 92, 2014, p. 2846–60. https://doi.org/10.2527/jas.2014-7337.

[7] Edea Z, Jung KS, Shin SS, Yoo SW, Choi JW, Kim KS. Signatures of positive selection underlying beef production traits in Korean cattle breeds. J Anim Sci Technol 2020;62:293–305. https://doi.org/10.5187/JAST.2020.62.3.293.

[8] Xiong X, Yang H, Yang B, Chen C, Huang L. Identification of quantitative trait transcripts for growth traits in the large scales of liver and muscle samples. Physiol Genomics 2015;47:274–80. https://doi.org/10.1152/physiolgenomics.00005.2015.

[9] Gudbjartsson DF, Walters GB, Thorleifsson G, Stefansson H, Halldorsson B V, Zusmanovich P, *et al.* Many sequence variants affecting diversity of adult human height. Nat Genet 2008;40:609–15. https://doi.org/10.1038/ng.122.

[10] Lettre G, Jackson AU, Gieger C, Schumacher FR, Berndt SI, Sanna S, *et al.* Identification of ten loci associated with height highlights new biological pathways in human growth. Nat Genet 2008;40:584–91. https://doi.org/10.1038/ng.125.

[11] Weedon MN, Frayling TM. Reaching new heights: insights into the genetics of human stature. Trends Genet 2008;24:595–603. https://doi.org/10.1016/j.tig.2008.09.006.

[12] Bai H, Zhu J, Sun Y, Liu R, Liu N, Li D, *et al.* Identification of genes related to beak deformity of chickens using digital gene expression profiling. PLoS One 2014;9. https://doi.org/10.1371/journal.pone.0107050.

[13] Zhu S, Zhang J, Zhu D, Jiang X, Wei L, Wang W, *et al.* Adipose tissue plays a major role in retinoic acid-mediated metabolic homoeostasis. Adipocyte 2022;11:47–55. https://doi.org/10.1080/21623945.2021.2015864.

[14] Berry DC, Noy N. All- trans -Retinoic Acid Represses Obesity and Insulin Resistance by Activating both Peroxisome Proliferation-Activated Receptor β/δ and Retinoic Acid Receptor . Mol Cell Biol 2009;29:3286–96. https://doi.org/10.1128/mcb.01742-08.

[15] Saeed A, Dullaart RPF, Schreuder TCMA, Blokzijl H, Faber KN. Disturbed vitamin A metabolism in non-alcoholic fatty liver disease (NAFLD). Nutrients 2018;10:29. https://doi.org/10.3390/nu10010029.

[16] Geng C, Xu H, Zhang Y, Gao Y, Li M, Liu X, *et al.* Retinoic acid ameliorates high-fat diet-induced liver steatosis through sirt1. Sci China Life Sci 2017;60:1234–41. https://doi.org/10.1007/s11427-016-9027-6.

[17] Amengual J, García-Carrizo FJ, Arreguín A, Mušinović H, Granados N, Palou A, *et al.* Retinoic Acid Increases Fatty Acid Oxidation and Irisin Expression in Skeletal Muscle Cells and Impacts Irisin in Vivo. Cell Physiol Biochem 2018;46:187–202. https://doi.org/10.1159/000488422.

[18] Herschel Conaway H, Henning P, Lerner UH. Vitamin a metabolism, action, and role in skeletal homeostasis. Endocr Rev 2013;34:766–97. https://doi.org/10.1210/er.2012-1071.

[19] Gregson CL, Hardcastle SA, Cooper C, Tobias JH. Friend or foe: High bone mineral density on routine bone density scanning, a review of causes and management. Rheumatol (United Kingdom) 2013;52:968–85. https://doi.org/10.1093/rheumatology/ket007.

[20] Navia JM, Harris SS. Vitamin A Influence on Calcium Metabolism and Calcification. Ann N Y Acad Sci 1980;355:45–57. https://doi.org/10.1111/j.1749-6632.1980.tb21326.x.

[21] Zhang Y, Li R, Li Y, Chen W, Zhao S, Chen G. Vitamin A status affects obesity development and hepatic expression of key genes for fuel metabolism in Zucker fatty rats. Biochem Cell Biol 2012;90:548–57. https://doi.org/10.1139/o2012-012.

[22] Ponce IT, Rezza IG, Delgado SM, Navigatore LS, Bonomi MR, Golini RL, *et al.* Daily oscillation of glutathione redox cycle is dampened in the nutritional vitamin A deficiency. Biol Rhythm Res 2012;43:351–72. https://doi.org/10.1080/09291016.2011.593847.Daily.

[23] Navigatore-Fonzo LS, Delgado SM, Golini RS, Anzulovich AC. Circadian rhythms of locomotor activity and hippocampal clock genes expression are dampened in vitamin A-deficient rats. Nutr Res 2014;34:326–35. https://doi.org/10.1016/j.nutres.2014.02.002.

[24] Kitaoka K, Hattori A, Chikahisa S, Miyamoto K ichi, Nakaya Y, Sei H. Vitamin A deficiency induces a decrease in EEG delta power during sleep in mice. Brain Res 2007;1150:121–30. https://doi.org/10.1016/j.brainres.2007.02.077.

[25] Carta M, Stancampiano R, Tronci E, Collu M, Usiello A, Morelli M, *et al.* Vitamin A deficiency induces motor impairments and striatal cholinergic dysfunction in rats. Neuroscience 2006;139:1163–72. https://doi.org/10.1016/j.neuroscience.2006.01.027.

[26] June HL, Tzeng Yang ARS, Bryant JL, Jones O, Royal W. Vitamin A deficiency and behavioral and motor deficits in the human immunodeficiency virus type 1 transgenic rat. J Neurovirol 2009;15:380–9. https://doi.org/10.3109/13550280903350200.

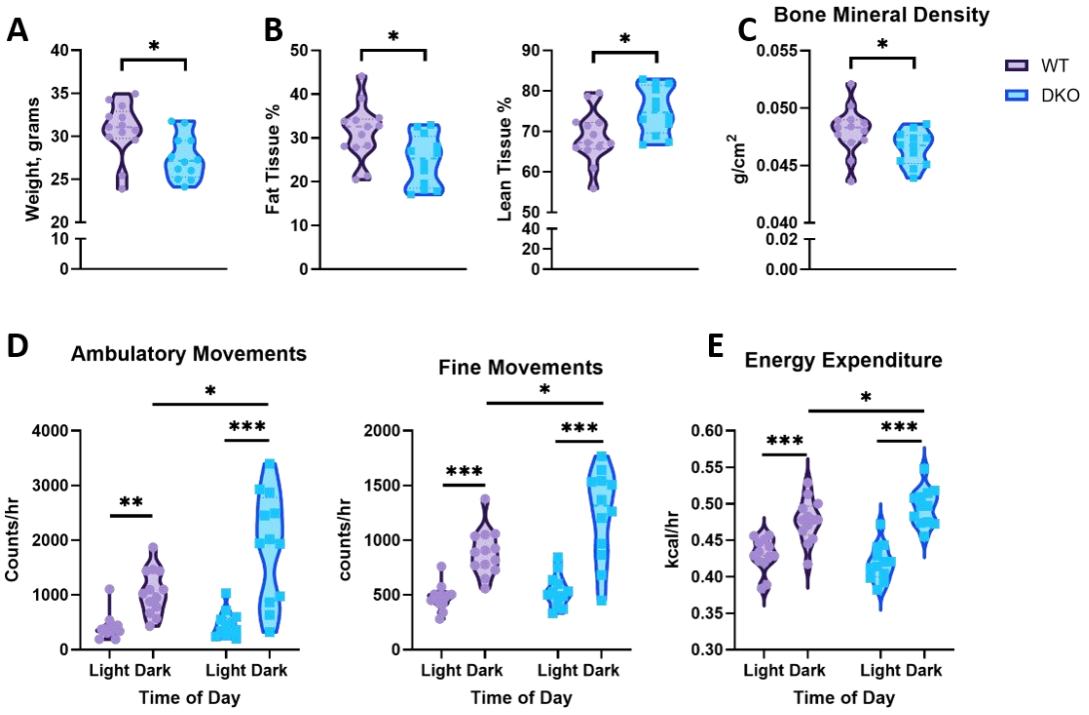

Figure 1. Aged DKO females have altered body composition, activity and energy expenditure. The **(A)** body mass and **(B – C)** composition, **(D)** locomotor activity, and **(E)** energy expenditure of WT (n = 13) and DKO (n = 12) 12 month old female mice was analyzed via DXA and indirect calorimetry. T-tests were used for A – C and RM-ANOVA was used for D – E to account for light and dark phase binning. *, $p < 0.05$; ***, $p < 0.001$.

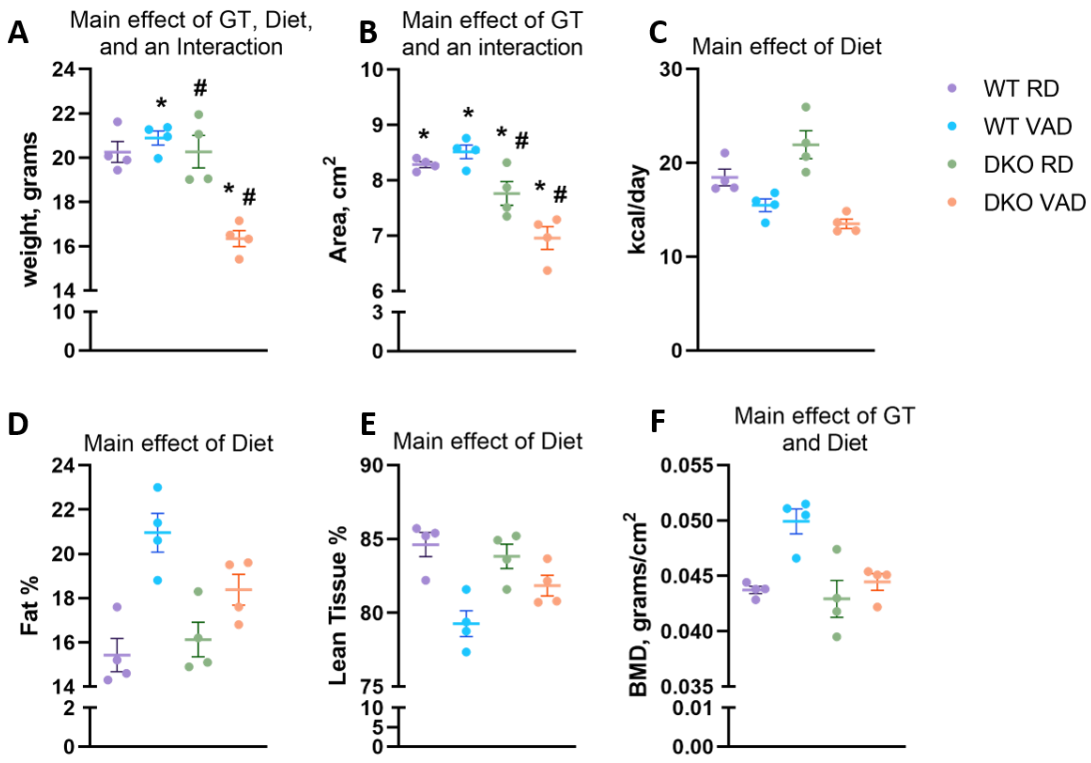

Figure 2. Absence of RDHEs does not correlate to body mass changes from VAD. A two-way ANOVA was utilized to analyze the effects of diet (RD v. VAD) and genotype (GT, WT v. DKO) for **(A)** weight, **(B)** area, **(C)** kilocalorie (kcal) intake, **(D)** fat percentage, **(E)** lean percentage, and **(F)** BMD in 2 month old females. *, Indicates a significant difference of genotype (GT) within a diet. #, indicates a significant difference of diet within a genotype.

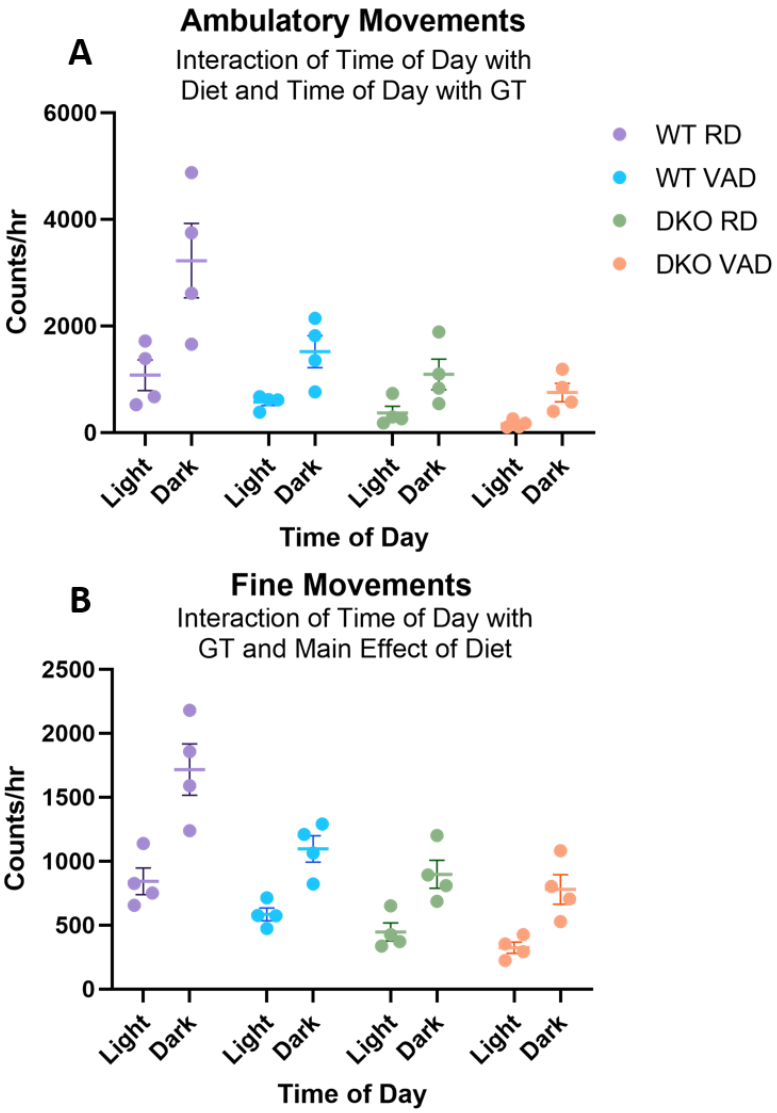

Figure 3. Both VAD and absence of RDHEs decreases locomotor activity. Locomotor activity of 2 month old females was analyzed via counts of infrared beam breaks and binned into **(A)** ambulatory or **(B)** fine movements and light or dark phase. A two-way ANOVA was utilized to analyze the effects of diet (RD v. VAD) and genotype (GT, WT v. DKO).

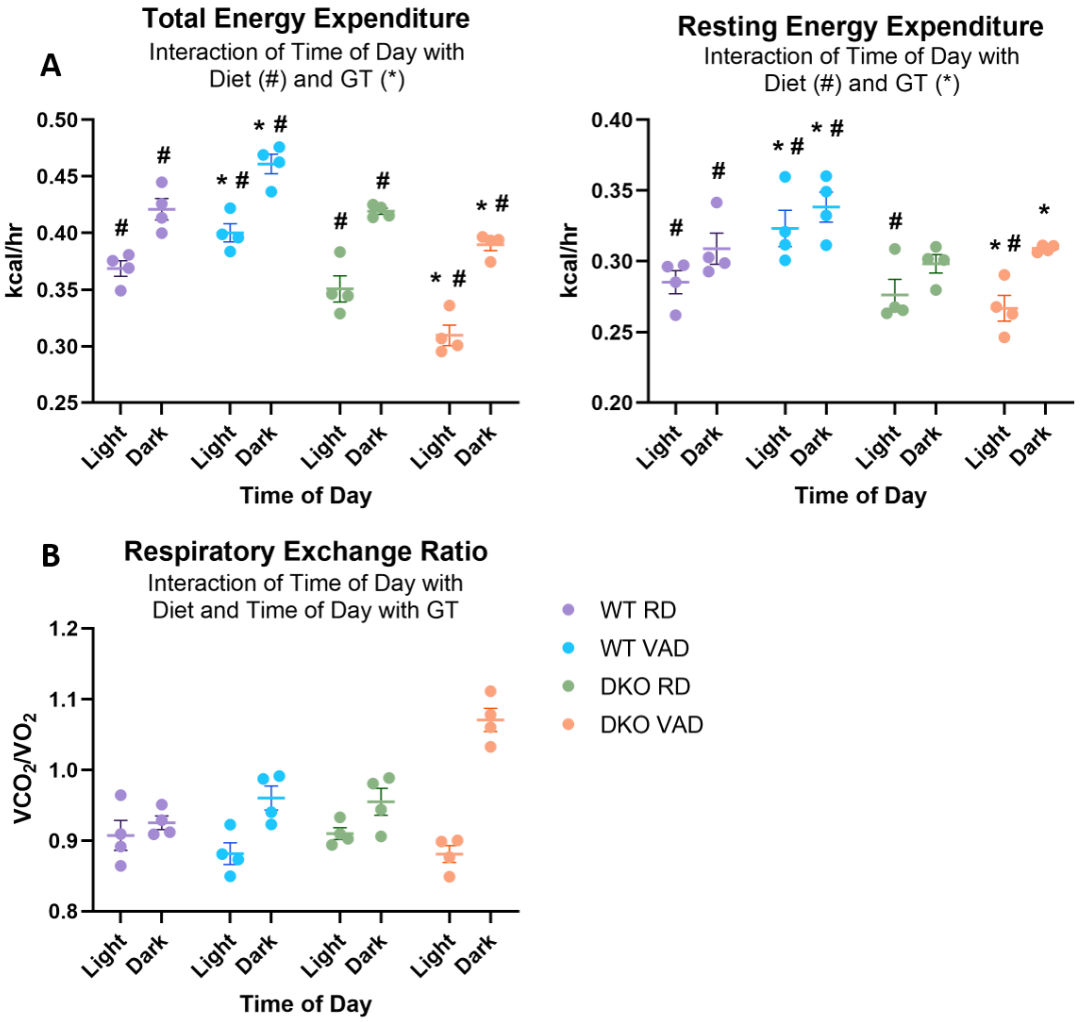

Figure 4. VAD results in opposing energy phenotypes based on presence or absence of RDHEs, while both VAD and RDHEs alter light and dark phase respiratory exchange ratios. Indirect calorimetry was utilized to examine **(A)** TEE, **(B)** REE, and **(C)** RER of 2 month old females and binned into light or dark phase. A two-way ANOVA was utilized to analyze the effects of diet (RD v. VAD) and genotype (GT, WT v. DKO). *, Indicates a significant difference of genotype (GT) within a diet. #, indicates a significant difference of diet within a genotype.

DISCUSSION

Research into RA biosynthesis and signaling has characterized many enzymes involved in RA biosynthesis that are essential for development; yet, the identification and characterizations of RA biosynthesis in adult tissues is still preliminary due to a lack of obvious phenotypes in genetically altered adult mice. However, manipulation of RA signaling through either deprivation of vitamin A or supplementation of RA via diet demonstrates roles for RA signaling involving vision, skeletal integrity, adiposity, alopecia, and cancer prevention [2,30,32,41] in adult mice and humans. Derivatives of RA are also utilized as therapeutics for human skin diseases, like acne vulgaris and psoriasis, and methods of cancer prevention [30]. Thus, RA biosynthesis and signaling has a prominent role in adult tissues that may not be essential for life but is required for health and maintenance. Retinol dehydrogenases are responsible for the rate limiting step of RA biosynthesis, the oxidation of retinol to retinaldehyde [54]. While RDH10 was the first physiologically relevant retinol dehydrogenase identified, it was embryonically lethal and rescue through retinaldehyde and RA administration produced relatively normal adult mice [9]. The persistence of RA signaling activity in RDH10-null embryos and the absence of adult phenotypes suggested the presence of other physiological retinol dehydrogenases that had yet to be identified.

RDHE2 was first identified in human psoriatic lesions [12]. Our lab determined that RDHE2 is a transmembrane protein that localized to the endoplasmic reticulum, and identified a potential paralog in mice, *Rdhe2s* [13]. Evolutionary analysis of RDHE2 and RDHE2S revealed only one homolog in *Xenopus laevis*, rdhe2, which we demonstrated was a potent retinol dehydrogenase in *X. laevis* embryos [14]. We have also characterized

the activity of human RDHE2 and RDHE2S in HEK293 cells and shown RDHE2 contributes to RA biosynthesis, while RDHE2S is unstable. This suggests that, like *Xenopus*, humans may only contain one functional RDHE [7]. Human transcripts of RDHE2 are expressed in various tissues including skin, brain, heart, digestive system tissues, lymph nodes, lungs, mammary glands, and pancreas [7]. Genome-wide association studies have linked the chromosomal region containing RDHE2 to alterations in the body weight and statue of cattle [55,56], growth rate in pigs [57], and human height [58–60]. Our research and the literature support a physiologically relevant role for RDHEs in adult physiology and disease. We hypothesized that RDHE2 and RDHE2S were physiologically relevant, tissue-specific retinol dehydrogenases of adult mice, essential for the maintenance of skin and body composition.

The first chapter of this dissertation addresses the characterization of murine RDHE2 and RDHE2S and preliminary observations of the phenotypes of mice lacking RDHEs. Enzymatic characterization of recombinant murine RDHE2 and RDHE2S in intact HEK293 cells demonstrated both enzymes had significant retinol dehydrogenase activity, though RDHE2S activity resulted in 5x higher increase in RA biosynthesis relative to RDHE2 at similar protein levels, indicating RDHE2S is the more active enzyme in mice. Transcripts of *Rdhe2* and *Rdhe2s* overlapped in expression patterns and were highly expressed in the skin of adult mice, but also found in tongue, intestine, esophagus, colon, adipose tissue, and testis. Additionally, transcripts of *Rdhe2s* and *Rdhe2* were expressed as early as embryonic day 10.5 and 12.5, respectively. Based upon these results we created an *Rdhe2s*$^{-/-}$ knockout mouse with a lacZ reporter driven by the native *Rdhe2s*$^{-/-}$ promoter. While heterozygotes from this model allowed us to visualize

Rdhe2s expression with β-galactosidase staining, specifically localizing transcripts to the developing hair follicles of mice at embryonic day 14.5, homozygous knockouts produced no observable phenotypes.

Since *Xenopus* and humans appear to only have one functioning RDHE and murine *Rdhe2* and *Rdhe2s* share overlapping expression, we theorized RDHE2 was sufficient to compensate for the loss of RDHE2S even though the catalytic activity is lower for RDHE2. We generated a double knockout mouse model of *Rdhe2* and *Rdhe2s* that is viable, unlike a knockout of the other physiologically relevant RDH, RDH10 [9], and presents phenotypes in adulthood. *Rdhe2s*$^{-/-}$*/Rdhe2*$^{-/-}$ double knockout (DKO) mice are born at mendelian ratios, display no obvious developmental defects, and are fertile. However, DKO mice are easily identifiable by their puffy eyelids, which gives their eyes an almond shape in contrast to the round eyes of their WT littermates, and a rough hair coat. We identified that the meibomian glands of DKO mice were enlarged, enlarging the entire eyelid into the physiologically visible puffy phenotype we saw. Meibomian glands are glands of the eyelids that secrete oil onto the tear film to prevent evaporation, and thus can be affected in dry eye disease. Long term use of topical retinoids is associated with symptoms of dry eye disease [61], and given the popularity of retinol in cosmetics, is an area of concern that needs to be addressed for consumer health. Similarly, in investigating the rough coat of DKO mice, we discovered that sebaceous glands of the skin were also enlarged compared to WT littermates. Sebaceous glands are similar to meibomian glands in that they are glands within the epidermis that produce oil, however, sebaceous glands are associated with hair follicles, connected to the hair shaft so the oil produced can coat the hair fiber. Alterations of meibomian glands and sebaceous glands,

including analysis of their oil compositions and differentiation processes, as well as further characterization of other similar epithelial glands in the body are currently still under investigation in our laboratory.

For this first chapter, we focused more on the characterization of RDHEs in skin, where they display the highest expression levels. Since RDHEs have previously been shown to be membrane proteins associated with the endoplasmic reticulum [13], we isolated membranous fractions from skin collected from WT and DKO mice and assessed RDH activity. Since we used dorsal skin, due to necessary protein amount requirements for experiments, the hair cycle had to be considered. The dorsal skin of mice undergoes drastic morphological and metabolic changes across the hair cycle, resulting in changes in skin thickness and mass quantities of cells undergoing proliferation or apoptosis [34,62]. We first assessed RDH activity at PD70, correlating with telogen, the stage of relative quiescence. Results showed RDHEs are the primary RDHs of the skin during telogen, accounting for 80% of the RDH activity. Via immunohistochemistry (IHC) we also demonstrated that RDHEs localize to the hair follicle, sebaceous gland, and epidermis, indicating the reduction of activity in DKO mice was likely impacting the hair cycle. We hypothesized that absence of RDHEs would thus alter hair cycle progression, as previous literature indicates abnormal RA levels can alter hair cycle progression [3,32,63,64]. We shaved WT and DKO mice during telogen, when skin is pink, and photographed them on the following days. Visibly, upon progression to anagen, the period of hair growth, the skin would darken before the appearance of hair, since melanogenesis, the production of melanin for the hair, is strictly associated with the anagen phase. DKO mice displayed an accelerated anagen progression, noted by the darkening of the skin and eventual appearance of hair, for

both sexes on regular diet (RD) and a VAD diet. We confirmed the accelerated progression from anagen to telogen via histological hair cycle staging and analysis of gene transcripts associated with anagen initiation. All data conclusively indicated DKO mice progress into anagen faster than WT mice, indicating the RDH activity of RDHEs is essential for proper hair cycle regulation.

Overall, the first chapter of this dissertation establishes that RDHEs are tissue-specific and physiologically relevant RDHs; additionally, RDHEs seem to play a more prominent role in maintenance of adult tissues than embryonic development. Unlike RDH10-null mice, DKO mice are viable and allow for more longitudinal studies of the phenotypes of the dysregulation of RA biosynthesis, The properties of the RDHE2 and RDHE2S are characterized, and despite the higher activity rate of RDHE2S, RDHE2 is sufficient for RA biosynthesis in adulthood. A review of the *Rdhe2s* reveals no minor phenotype of the eyelids, hair, or hair cycle, suggesting that RDHE2 completely compensated for RDHE2S. Since *Xenopus* and humans lack a secondary RDHE, this supports that one RDHE is sufficient for RA biosynthesis in adult tissues, and our DKO model, which completely lacks RDHEs, is a proper model for investigating the physiological role of RDHEs.

Previously we demonstrated that DKO mice had reduced RDH activity in telogen and accelerated anagen initiation; however, the role of RDHEs across the hair cycle remains unresolved. In the second manuscript, we focus on the effect of RDHEs in the skin utilizing molecular biology techniques to interrogate RDHEs in WT mice and how RA biosynthesis and signaling are affected in DKO mice. Previous data from our collaborator, Dr. Helen Everts, demonstrates that proteins involved in RA biosynthesis, including binding proteins,

enzymes, and transcription factors, vary across the hair cycle in spatio-temporal patterns [36,64]. Additionally, she highlights sex-specific differences of RA biosynthesis and signaling in the hair cycle and the effects of estrogen utilizing these same immunohistochemistry (IHC) techniques [65]. Data from our laboratory shows human RDHE2 is down-regulated by RA in human organotypic skin rafts, which replicate the differentiation of the epidermis utilizing a liquid-air interface [7]. This provides evidence that a feedback mechanism may exist in mice, where RA regulates the expression of RDHEs across the hair cycle to elicit changes in RA biosynthesis that would contribute to hair cycle progression. Additionally, disruption of hair follicle development, which continues after birth up to PD21 in a period called hair follicle morphogenesis [62], can contribute to alterations of hair cycle progression [66,67]. Increased levels of RA are shown to alter the composition of the hair coat, reducing the amount of zigzag hairs and disrupting the capability of hair follicles to create bends in hair fibers [68]. Zigzag hairs and the other pelage hair types of mice, guard, awl, and auchene, are produced from specific follicles dependent upon which wave of development the hair follicle was formed during [69]. Thus, alterations of hair fibers are indicative of disruptions during development. The second chapter of this dissertation describes how RDHEs fluctuate across the hair cycle, driving variations in RDH activity that alter RA biosynthesis, and absence of RDHEs disrupts hair follicle development, possibly contributing to alterations of hair follicle stem cells, responsible for anagen initiation.

To characterize RDHEs across the hair cycle, we collected and assessed dorsal skin from mice at various PDs to gather samples from the other two phases of the hair cycle, anagen and catagen. We eventually added in samples from the final and previously analyzed

phase, telogen, but at a PD closer to the end of catagen. We demonstrated in both male and female mice that RDHEs are the primary RDH of skin independent of hair cycle phase. When all hair cycle phases were assessed, RDH activity significantly varied across PDs in female mice, but not in male mice. In female mice, both RDHE2 and RDHE2S proteins varied across PDs, but in males only RDHE2 varied. Since RDHE2 is the less active enzyme it could not be sufficient to driven changes in RDH activity in skin; this requires further investigation from our single *Rdhe2s* knockout mouse model. In our previous paper, we described DKO mice had accelerated anagen initiation, but we also noted sex-specific differences, where male mice did not display this phenotype until the second synchronized hair cycle, whereas females displayed it in the first synchronized hair cycle. Sex-specific hormones are known to interact with both the hair cycle [70] and RA signaling [26,27], and recently co-localization of estrogen receptors (ER) and RA biosynthesis and signaling proteins has been shown in both spatial and temporal patterns of the hair cycle [65]. This same study reported not only sex-specific differences in the immunoreactivity (IR) of RA biosynthesis and signaling proteins, but sex-specific responses or RA biosynthesis and signaling proteins to treatments that alter estrogen levels, including topical application of estrogen and estrogen inhibitors. Thus, research involving the hair cycle needs to be performed on both sexes.

This study also assessed RA biosynthesis and signaling across the hair cycle at the transcript level, and utilizing our DKO mouse model, we examined how the absence of RDHEs would alter RA biosynthesis and signaling at the level of mRNA. We analyzed the expression of binding proteins (*Rbp1, Crabp2*), enzymes involved in RA biosynthesis and degradation (*Rdh10, Aldh1a2, Cyp26b1*), and RA-regulated proteins (*Stra6, Lrat, Dhrs3*).

While we showed many transcripts fluctuate across the hair cycle in WT mice of both sexes (*Lrat, Stra6, Cyp26b1, Rdh10*) some genes only varied significantly in male mice (*Dhrs3, Rbp1*). In the absence of RDHEs, variation across PDs was altered with some genes losing variation across PD (*Cyp26b1* in males, *Stra6* in males and females) while other genes gained significant variance (*Crabp2* in males, *Aldh1a2* in males and females). Transcripts that facilitate and catalyze RA biosynthesis were upregulated in DKO mice of both sexes (*Rbp1, Crabp2, Aldh1a2, Rdh10*) while *Cyp26b1*, involved in the degradation of RA and induced by RA, was downregulated in females across the hair cycle and males at PD30 and PD40. Additionally, *Lrat* and *Dhrs3*, which are upregulated by RA, were downregulated in DKO mice. Overall, this data is in agreement with the decreased RDH activity of DKO mice, indicating the skin of DKO mice has reduced levels of RA.

Since we had not seen any significant histological differences or changes in density in hair follicles, we assessed the hair fibers themselves, categorizing them into the four types of pelage hair in mice: guard, awl, auchene, and zigzag [71,72]. Previous literature demonstrates that excessive levels of RA decrease the number of zigzag hairs and inhibit bending of the hair fibers [68]. Therefore, we hypothesized that since our mice appear to have reduced RA levels and rougher, fluffier coats, they may have an increase in zigzag hairs or bending of straight hairs. However, instead we observed a significant increase in awl hairs, a straight hair, without a significant decrease in any other hair type. Thus, during development the retention of developing hair follicles that produce awl hairs is higher in DKO mice. Awl hairs are the second longest and thickest hair, also explaining the visible rough appearance of the coat of DKO mice.

Since hair follicles that produce awl hairs are defined in the second wave of hair follicle development during embryogenesis and our first chapter showed *Rdhe2s* expression in hair follicles as early as E14.5, we hypothesized the absence of RDHEs could affect hair follicle development. We tested this hypothesis by analyzing the expression of markers of the HFSCs that reside in the hair follicle bulge. The proliferation of these HFSCs marks the telogen to anagen transition, which we've previously observed is accelerated in our DKO mice. We also observed that *Sox9* expression, a transcription factor under the control of RA signaling, is downregulated in DKO female mice. *Sox9* is vital to the development and maintenance of the stem cell niche [66,67]. Similarly, in females, we found all four HFSC markers tested (*Sox9, Cd34, Krt15, Lgr5*) were downregulated; however, in males only *Cd34* and *Krt15* were significantly downregulated, though the expression patterns of *Sox9* and *Lgr5* were altered.

Overall, the second chapter provides convincing evidence that the skin of DKO mice has reduced levels of RA signaling. We cannot quantify RA levels in skin directly due to their low homeostatic levels being undetectable by HPLC. However, ongoing studies are developing techniques to attempt to quantify RA levels by mass spectrometry. Additionally, we've shown that the absence of RDHEs affects the development of hair follicles and expression patterns of HFSC markers. This indicates that RDHEs have a role in hair follicle development and may contribute to maintenance of the HFSC pool. However, we have yet to verify if these changes in transcripts are caused by downregulation in individual cells or from a decrease of HFSC cells. This will require further IHC analysis to determine. The observation that RDHEs affect HFSCs in some way does suggest a possible mechanism for how DKO mice display an accelerated anagen initiation, since these HFSCs are integral to

the telogen to anagen transition. Overall, chapter two provides substantial and convincing evidence that RDHEs are essential RDHs for hair follicles, contributing to the development and maintenance of the hair follicle throughout its progression through the hair cycle.

Previous studies in chapter one highlighted how *Rdhe2* and *Rdhe2s* are highly expressed in skin, but also present in esophagus, stomach, tongue, adipose tissue, intestine, and colon. However, in our DKO mice no obvious phenotypes were present during our hair studies, which primarily deal with mice from weaning up to 3 months maximum, except for repeated observations that DKO pups appeared smaller than WT littermates. Weight studies indicated that there were no significant differences in the weight of pups up to PD50. However, when the colony began to age, several phenotypes began to appear. We noted 12 month old DKO mice were smaller than WT littermates in the same cage, so we organized a preliminary observational study. This study accrued 13 WT female mice and 12 DKO female mice at 12 months of age; however, there were insufficient numbers of WT male mice available (n = 2) to include males in this study. For females, we assessed body composition via dual energy x-ray absorptiometry (DXA), locomotor activity via infrared beam breaks, and metabolism via indirect calorimetry. The 12 month old DKO female mice weighed significantly less and had decreased fat percentage than age-matched WT counterparts. While kilocalorie intake was similar between WT and DKO female mice, DKO female mice exhibited higher ambulatory and fine locomotor activity than WT female mice in the dark phase. Correspondingly, total energy expenditure (TEE) was also increased in DKO female mice compared to WT female mice in the dark phase. This increase in energy expenditure can reasonably explain the decreased weight, since the net calories of DKO female mice are lower than WT female mice. Interestingly, on a high-fat diet RA

supplementation is known to decrease weight and adipose tissue gain while increasing dark phase energy expenditure [41,43]. Additionally, excess RA is known to decrease BMD [52], and DKO female mice display decreased BMD compared to WT female mice. These data indicate that 12 month old DKO female mice may actually have increased RA levels in epithelial tissues. This is contrary to our working hypothesis, that DKO mice display decreased levels of RA due to the absence of two RDHs; however, since RDHEs are tissue-specific, unlike RDH10 which is ubiquitously expressed, there may be tissue-specific discrepancies in the DKO mice. For instance, we've shown convincing evidence in chapters one and two that the skin of DKO mice has decreased levels of RA.

In literature there was a lack of studies analyzing body composition and metabolism in completely vitamin A deficient (VAD) mammals. Many studies only administered a VAD diet after weaning, when pups had already accrued liver stores of vitamin A. Without sufficient treatment periods to deprive pups of these stores, the pups will not be completely VAD. Additionally, VAD can be shown through analysis of the liver stores utilizing HPLC; however, many studies failed to perform this analysis or only analyzed serum levels. Studies assessing the effects of excessive RA supplementation were also primarily done on older mice, specifically in conjunction with HFD to induce obesity [41,43]. The most sufficiently studied and conclusive area of study was BMD, which, along with studies on bone fractures and osteoporosis, firmly supports that VAD increases BMD while excess RA decreases BMD [52]. We decided to test our working hypothesis, that DKO mice would have decreased RA levels at the level of whole-body physiology, by assessing the phenotypic effects of VAD on 2 month old WT female mice alongside age-matched DKO female mice on both a regular chow diet (RD) and a VAD diet. To ensure VAD, dams were given VAD

diet at mid-gestation, before livers form, to prevent pups from accumulating vitamin A stores. At 2 months, WT and DKO female mice on both RD and VAD diet were analyzed via DXA and indirect calorimetry.

VAD results in increased fat percentage of both WT and DKO 2 month old females, with a corresponding significant decrease in lean percentage. VAD also decreased kilocalorie intake of female mice, due to keratinization of the taste buds [73], and increased the BMD of female mice. While locomotor activity was decreased for mice on VAD, WT females on VAD displayed increased energy expenditure. Further investigation is required to determine why VAD caused decreased kilocalorie intake, increased energy expenditure, and increased fat percentage, as the alterations of calorie intake and use should decrease fat percentage. The decreased locomotor activity could be the result of stress due to the lower amount of free calories, but VAD did improve the diurnal rhythms of RER in both WT and DKO female mice, indicating the source of energy changes from fats during the resting phase to more carbohydrates during the active phase. While the absence of RDHEs did not phenocopy VAD, DKO female mice on VAD did produce unique phenotypes. DKO female mice on RD displayed decreased body area, substantiating previous observations from the laboratory, DKO female mice on VAD had a significantly smaller area than caused by either VAD or absence of RDHEs alone. Additionally, weight was only decreased in DKO female mice on VAD. Thus, while DKO female mice are smaller, they don't weight less and have fat and lean mass percentages similar to WT female mice. Interestingly, BMD is significantly decreased in DKO female mice; however, this may be biased by the strongly reduced effect of VAD on the DKO female mice. Similar trends are seen in fat and lean mass percentages, where DKO female mice on VAD are not as greatly affected as WT

female mice on VAD. Locomotor activity of DKO female mice is decreased similar to VAD; however, energy expenditure is decreased in DKO female mice on VAD, in opposition to WT female mice on VAD. Despite this increase in energy expenditure, the RER of DKO female mice on VAD is significantly upregulated during the dark phase, indicating they are undergoing anaerobic respiration. This severe alteration of metabolism requires further investigation, down to tissue-specific alterations of metabolism, to understand the interaction of VAD and RDHEs.

In this third and final chapter of the dissertation, we present evidence that RDHEs do not phenocopy VAD and instead reveal novel interactions of tissue-specific dysregulation of RA biosynthesis and VAD. We demonstrate that while 12 month old DKO female mice display phenotypes similar to those of RA supplementation, suggesting that they have increased RA levels, 2 month old DKO female mice on RD only display significant decreases in body area and locomotor activity. The contribution of RDHEs to whole body physiology is still being defined, but evidence here highlights the need to focus on both whole body and tissue-specific dysregulation of RA biosynthesis. In addition to dysregulation of RA biosynthesis in tissues that express RDHEs, it is unknown how absence of RDHEs may indirectly affect tissues that lack their expression. For instance, we hypothesize that absence of RDHEs in the small intestine may affect absorption of retinol, altering biologically available levels of vitamin A. Additionally, levels of vitamin A can be influenced by inflammation, and preliminary research is ongoing on potential alterations of the immune system caused by the lack of RDHEs. This brings us back to the discovery of human RDHE2, upregulated in psoriatic skin of humans, an inflammatory dermatosis that can be therapeutically treated with derivatives of RA.

In conclusion, the studies presented in this dissertation verify that RDHEs are tissue-specific, physiologically relevant RDHs. Preliminary characterization of RDHEs demonstrated their potential to contribute to RA biosynthesis. The studies of RDHEs in the skin, hair follicle, and hair cycle revealed they have spatio-temporal physiological roles that are required for proper maintenance of at least one epithelial tissue. Additionally, RDHEs were implicated in contributing to the development of hair follicles, indicating they could be responsible for the trace amounts of RA biosynthesis and signaling seen in RDH10-null embryos [9] and thus necessary for other developmental processes. Assessments of whole body physiological alterations caused by the absence of RDHEs highlights a role for RDHEs in metabolic regulation of an organism, and DKO female mice on VAD displayed novel phenotypes not anticipated by what was assumed to be a synergetic effect of DKO and VAD. Overall, these studies reveal wide-spread and diverse effects of tissue-specific dysregulation of RA biosynthesis in adult tissues and characterize the enzymes responsible.

GENERAL LIST OF REFERENCES

[1] O'Byrne SM, Blaner WS. Retinol and retinyl esters: biochemistry and physiology. J Lipid Res 2013;54:1731–43. https://doi.org/10.1194/jlr.r037648.

[2] Kedishvili NY. Enzymology of retinoic acid biosynthesis and degradation. J Lipid Res 2013;54:1744–60. https://doi.org/10.1194/jlr.R037028.

[3] Shih MYS, Kane MA, Zhou P, Yen CLE, Streeper RS, Napoli JL, et al. Retinol Esterification by DGAT1 Is Essential for Retinoid Homeostasis in Murine Skin. J Biol Chem 2009;284:4292–9. https://doi.org/10.1074/jbc.M807503200.

[4] Naik R, Obiang-Obounou BW, Kim M, Choi Y, Lee HS, Lee K. Therapeutic Strategies for Metabolic Diseases: Small-Molecule Diacylglycerol Acyltransferase (DGAT) Inhibitors. ChemMedChem 2014;9:2410–24. https://doi.org/10.1002/cmdc.201402069.

[5] Saurat JH. Skin, sun, and vitamin A: From aging to cancer. J Dermatol 2001;28:595–8. https://doi.org/10.1111/j.1346-8138.2001.tb00040.x.

[6] Takeda A, Morinobu T, Takitani K, Kimura M, Tamai H. Measurement of Retinoids and β-Carotene 15, 15'-Dioxygenase Activity in HR-1 Hairless Mouse Skin with UV Exposure. J Nutr Sci Vitaminol 2003;49:69–72.

[7] Adams MK, Lee S-A, Belyaeva O V., Wu L, Kedishvili NY. Characterization of human short chain dehydrogenase/reductase SDR16C family members related to retinol dehydrogenase 10. Chem Biol Interact 2017;276:88–94. https://doi.org/10.1016/j.cbi.2016.10.019.

[8] Cunningham TJ, Chatzi C, Sandell LL, Trainor PA, Duester G. Rdh10 mutants deficient in limb field retinoic acid signaling exhibit normal limb patterning but display interdigital webbing. Dev Dyn 2011;240:1142–50. https://doi.org/10.1002/dvdy.22583.

[9] Rhinn M, Schuhbaur B, Niederreither K, Dolle P. Involvement of retinol dehydrogenase 10 in embryonic patterning and rescue of its loss of function by maternal retinaldehyde treatment. Proc Natl Acad Sci 2011;108:16687–92. https://doi.org/10.1073/pnas.1103877108.

[10] Belyaeva O V., Adams MK, Wu L, Kedishvili NY. The antagonistically bifunctional retinoid oxidoreductase complex is required for maintenance of all-trans-retinoic acid homeostasis. J Biol Chem 2017;292:5884–97. https://doi.org/10.1074/jbc.M117.776914.

[11] Adams MK, Belyaeva O V., Wu L, Kedishvili NY. The Retinaldehyde Reductase Activity of DHRS3 Is Reciprocally Activated by Retinol Dehydrogenase 10 to

Control Retinoid Homeostasis * □ S. J Biol Chem 2014;289:14868–80. https://doi.org/10.1074/jbc.M114.552257.

[12] Matsuzaka Y, Okamoto K, Tsuji H, Mabuchi T, Ozawa A, Tamiya G, et al. Identification of the hRDH-E2 gene, a novel member of the sdr family, and its increased expression in psoriatic lesion. Biochem Biophys Res Commun 2002;297:1171–80. https://doi.org/10.1016/S0006-291X(02)02344-6.

[13] Lee S-A, Belyaeva O V., Kedishvili NY. Biochemical Characterization of Human Epidermal Retinol Dehydrogenase 2. Chem Biol Interact 2009;178:182–7. https://doi.org/10.1016/j.cbi.2008.09.019.

[14] Belyaeva O V., Lee S-A, Adams MK, Chang C, Kedishvili NY. Short chain dehydrogenase/reductase Rdhe2 is a novel retinol dehydrogenase essential for frog embryonic development. J Biol Chem 2012;287:9061–71. https://doi.org/10.1074/jbc.M111.336727.

[15] Lin YL, Persaud SD, Nhieu J, Wei LN. Cellular retinoic acid-binding protein 1 modulates stem cell proliferation to affect learning and memory in male mice. Endocrinology 2017;158:3004–14. https://doi.org/10.1210/en.2017-00353.

[16] Evans RM, Mangelsdorf DJ. Nuclear receptors, RXR, and the big bang. Cell 2014;157:255–66. https://doi.org/10.1016/j.cell.2014.03.012.

[17] Balmer JE, Blomhoff R. Gene expression regulation by retinoic acid. J Lipid Res 2002;43:1773–808. https://doi.org/10.1194/jlr.R100015-JLR200.

[18] Gudas LJ, Wagner JA. Retinoids regulate stem cell differentiation. J Cell Physiol 2011;226:322–30. https://doi.org/10.1002/jcp.22417.

[19] Al Tanoury Z, Piskunov A, Rochette-Egly C. Vitamin A and retinoid signaling: genomic and nongenomic effects. J Lipid Res 2013;54:1761–75. https://doi.org/10.1194/jlr.R030833.

[20] Urvalek A, Laursen KB, Gudas LJ. The Biochemistry of Retinoic Acid Receptors I: Structure, Activation, and Function at the Molecular Level 2014;70:129–49. https://doi.org/10.1007/978-94-017-9050-5.

[21] Piskunov A, Rochette-Egly C. A retinoic acid receptor RARα pool present in membrane lipid rafts forms complexes with G protein αQ to activate p38MAPK. Oncogene 2012;31:3333–45. https://doi.org/10.1038/onc.2011.499.

[22] Easwaran V, Pishvaian M, Salimuddin, Byers S. Cross-regulation of β-catenin–LEF/TCF and retinoid signaling pathways. Curr Biol 1999;9:1415–9. https://doi.org/10.1016/S0960-9822(00)80088-3.

[23] Collins CA, Watt FM. Dynamic regulation of retinoic acid-binding proteins in developing, adult and neoplastic skin reveals roles for β-catenin and Notch signalling. Dev Biol 2008;324:55–67. https://doi.org/10.1016/J.YDBIO.2008.08.034.

[24] Ubels JL, Wertz JT, Ingersoll KE, Jackson RS, Aupperlee MD. Down-regulation of androgen receptor expression and inhibition of lacrimal gland cell proliferation by retinoic acid. Exp Eye Res 2002;75:561–71. https://doi.org/10.1006/exer.2002.2054.

[25] Kelsey L, Katoch P, Johnson KE, Batra SK, Mehta PP. Retinoids regulate the formation and degradation of gap junctions in androgen-responsive human prostate cancer cells. PLoS One 2012;7. https://doi.org/10.1371/journal.pone.0032846.

[26] Rivera-Gonzalez GC, Droop AP, Rippon HJ, Tiemann K, Pellacani D, Georgopoulos LJ, et al. Retinoic acid and androgen receptors combine to achieve tissue specific control of human prostatic transglutaminase expression: A novel regulatory network with broader significance. Nucleic Acids Res 2012;40:4825–40. https://doi.org/10.1093/nar/gks143.

[27] Ross-Innes CS, Stark R, Holmes KA, Schmidt D, Spyrou C, Russell R, et al. Cooperative interaction between retinoic acid receptor-α and estrogen receptor in breast cancer. Genes Dev 2010;24:171–82. https://doi.org/10.1101/gad.552910.

[28] Berry DC, Noy N. All- trans -Retinoic Acid Represses Obesity and Insulin Resistance by Activating both Peroxisome Proliferation-Activated Receptor β/δ and Retinoic Acid Receptor . Mol Cell Biol 2009;29:3286–96. https://doi.org/10.1128/mcb.01742-08.

[29] Stüttgen G. Historical perspectives of tretinoin. J Am Acad Dermatol 1986;15:735–40. https://doi.org/10.1016/S0190-9622(86)70228-4.

[30] Khalil S, Bardawil T, Stephan C, Darwiche N, Abbas O, Kibbi AG, et al. Retinoids: a journey from the molecular structures and mechanisms of action to clinical uses in dermatology and adverse effects. J Dermatolog Treat 2017;28:684–96. https://doi.org/10.1080/09546634.2017.1309349.

[31] Everts HB. Endogenous retinoids in the hair follicle and sebaceous gland. Biochim Biophys Acta - Mol Cell Biol Lipids 2012;1821:222–9. https://doi.org/10.1016/j.bbalip.2011.08.017.

[32] Duncan JF, Silva KA, Johnson C, King B, Szatkiewicz JP, Kamdar S, et al. Endogenous retinoids in the pathogenesis of alopecia areata. J Invest Dermatology 2013;133:334–43. https://doi.org/10.1038/jid.2012.344.

[33] Saitou M, Sugal S, Tanaka T, Shimouchi K, Fuchs E, Narumiya S, et al. Inhibition

of skin development by targeted expression of a dominant-negative retinoic acid receptor. Nature 1995;374:159–62. https://doi.org/10.1038/374159a0.

[34] Schneider MR, Schmidt-Ullrich R, Paus R. The Hair Follicle as a Dynamic Miniorgan. Curr Biol 2009;19:R132–42. https://doi.org/10.1016/J.CUB.2008.12.005.

[35] Lin KK, Kumar V, Geyfman M, Chudova D, Ihler AT, Smyth P, et al. Circadian clock genes contribute to the regulation of hair follicle cycling. PLoS Genet 2009;5. https://doi.org/10.1371/journal.pgen.1000573.

[36] Everts HB, Sundberg JP, King LE, Ong DE. Immunolocalization of enzymes, binding proteins, and receptors sufficient for retinoic acid synthesis and signaling during the hair cycle. J Invest Dermatol 2007;127:1593–604. https://doi.org/10.1038/sj.jid.5700753.

[37] Belyaeva O V., Wirth SE, Boeglin WE, Karki S, Goggans KR, Wendell SG, et al. Dehydrogenase reductase 9 (SDR9C4) and related homologs recognize a broad spectrum of lipid mediator oxylipins as substrates. J Biol Chem 2022;298:101527. https://doi.org/10.1016/j.jbc.2021.101527.

[38] Foitzik K, Spexard T, Nakamura M, Halsner U, Paus R. Towards dissecting the pathogenesis of retinoid-induced hair loss: All-trans retinoic acid induces premature hair follicle regression (catagen) by upregulation of transforming growth factor-β2 in the dermal papilla. J Invest Dermatol 2005;124:1119–26. https://doi.org/10.1111/j.0022-202X.2005.23686.x.

[39] Li M, Indra AK, Warot X, Brocard J, Messaddeq N, Kato S, et al. Skin abnormalities generated by temporally controlled RXRα mutations in mouse epidermis. Nature 2000;407:633–6.

[40] Li M, Chiba H, Warot X, Messaddeq N, Gerard C, Chambon P, et al. RXRα ablation in skin keratinocytes results in alopecia and epidermal alterations. Development 2001;128:675–88.

[41] Zhu S, Zhang J, Zhu D, Jiang X, Wei L, Wang W, et al. Adipose tissue plays a major role in retinoic acid-mediated metabolic homoeostasis. Adipocyte 2022;11:47–55. https://doi.org/10.1080/21623945.2021.2015864.

[42] Saeed A, Dullaart RPF, Schreuder TCMA, Blokzijl H, Faber KN. Disturbed vitamin A metabolism in non-alcoholic fatty liver disease (NAFLD). Nutrients 2018;10:29. https://doi.org/10.3390/nu10010029.

[43] Geng C, Xu H, Zhang Y, Gao Y, Li M, Liu X, et al. Retinoic acid ameliorates high-fat diet-induced liver steatosis through sirt1. Sci China Life Sci 2017;60:1234–41. https://doi.org/10.1007/s11427-016-9027-6.

[44] Amengual J, García-Carrizo FJ, Arreguín A, Mušinović H, Granados N, Palou A, et al. Retinoic Acid Increases Fatty Acid Oxidation and Irisin Expression in Skeletal Muscle Cells and Impacts Irisin in Vivo. Cell Physiol Biochem 2018;46:187–202. https://doi.org/10.1159/000488422.

[45] Zhang Y, Li R, Li Y, Chen W, Zhao S, Chen G. Vitamin A status affects obesity development and hepatic expression of key genes for fuel metabolism in Zucker fatty rats. Biochem Cell Biol 2012;90:548–57. https://doi.org/10.1139/o2012-012.

[46] Carta M, Stancampiano R, Tronci E, Collu M, Usiello A, Morelli M, et al. Vitamin A deficiency induces motor impairments and striatal cholinergic dysfunction in rats. Neuroscience 2006;139:1163–72. https://doi.org/10.1016/j.neuroscience.2006.01.027.

[47] June HL, Tzeng Yang ARS, Bryant JL, Jones O, Royal W. Vitamin A deficiency and behavioral and motor deficits in the human immunodeficiency virus type 1 transgenic rat. J Neurovirol 2009;15:380–9. https://doi.org/10.3109/13550280903350200.

[48] Ponce IT, Rezza IG, Delgado SM, Navigatore LS, Bonomi MR, Golini RL, et al. Daily oscillation of glutathione redox cycle is dampened in the nutritional vitamin A deficiency. Biol Rhythm Res 2012;43:351–72. https://doi.org/10.1080/09291016.2011.593847.Daily.

[49] Navigatore-Fonzo LS, Delgado SM, Golini RS, Anzulovich AC. Circadian rhythms of locomotor activity and hippocampal clock genes expression are dampened in vitamin A-deficient rats. Nutr Res 2014;34:326–35. https://doi.org/10.1016/j.nutres.2014.02.002.

[50] Kitaoka K, Hattori A, Chikahisa S, Miyamoto K ichi, Nakaya Y, Sei H. Vitamin A deficiency induces a decrease in EEG delta power during sleep in mice. Brain Res 2007;1150:121–30. https://doi.org/10.1016/j.brainres.2007.02.077.

[51] Whiting SJ, Lemke B. Excess retinol intake may explain the high incidence of osteoporosis in northern Europe. Nutr Rev 1999;57:192–6. https://doi.org/10.1111/j.1753-4887.1999.tb06942.x.

[52] Herschel Conaway H, Henning P, Lerner UH. Vitamin a metabolism, action, and role in skeletal homeostasis. Endocr Rev 2013;34:766–97. https://doi.org/10.1210/er.2012-1071.

[53] Navia JM, Harris SS. Vitamin A Influence on Calcium Metabolism and Calcification. Ann N Y Acad Sci 1980;355:45–57. https://doi.org/10.1111/j.1749-6632.1980.tb21326.x.

[54] Napoli JL. [13] Quantification of Physiological Levels of Retinoic Acid. Methods

Enzymol 1986;123:112–24. https://doi.org/10.1016/S0076-6879(86)23015-3.

[55] Jiao S, Maltecca C, Gray KA, Cassady JP. Feed intake, average daily gain, feed efficiency, and real-time ultrasound traits in Duroc pigs: II. genomewide association. J. Anim. Sci., vol. 92, 2014, p. 2846–60. https://doi.org/10.2527/jas.2014-7337.

[56] Edea Z, Jung KS, Shin SS, Yoo SW, Choi JW, Kim KS. Signatures of positive selection underlying beef production traits in Korean cattle breeds. J Anim Sci Technol 2020;62:293–305. https://doi.org/10.5187/JAST.2020.62.3.293.

[57] Xiong X, Yang H, Yang B, Chen C, Huang L. Identification of quantitative trait transcripts for growth traits in the large scales of liver and muscle samples. Physiol Genomics 2015;47:274–80. https://doi.org/10.1152/physiolgenomics.00005.2015.

[58] Gudbjartsson DF, Walters GB, Thorleifsson G, Stefansson H, Halldorsson B V, Zusmanovich P, et al. Many sequence variants affecting diversity of adult human height. Nat Genet 2008;40:609–15. https://doi.org/10.1038/ng.122.

[59] Lettre G, Jackson AU, Gieger C, Schumacher FR, Berndt SI, Sanna S, et al. Identification of ten loci associated with height highlights new biological pathways in human growth. Nat Genet 2008;40:584–91. https://doi.org/10.1038/ng.125.

[60] Weedon MN, Frayling TM. Reaching new heights: insights into the genetics of human stature. Trends Genet 2008;24:595–603. https://doi.org/10.1016/j.tig.2008.09.006.

[61] Moy A, McNamara NA, Lin MC. Effects of isotretinoin on meibomian glands. Optom Vis Sci 2015;92:925–30. https://doi.org/10.1097/OPX.0000000000000656.

[62] Müller-Röver S, Foitzik K, Paus R, Handjiski B, van der Veen C, Eichmüller S, et al. A Comprehensive Guide for the Accurate Classification of Murine Hair Follicles in Distinct Hair Cycle Stages. J Invest Dermatol 2001;117:3–15. https://doi.org/10.1046/J.0022-202X.2001.01377.X.

[63] Bazzano G, Terezakis N, Attia H, Bazzano A, Celleno L, Tamburro M, et al. Effect of Retinoids on Follicular Cells. vol. 101. 1993.

[64] Suo L, Vanburen C, Hovland ED, Kedishvili NY, Sundberg JP, Everts HB. Dietary Vitamin A Impacts Refractory Telogen. Front Cell Dev Biol 2021;9:1–11. https://doi.org/10.3389/fcell.2021.571474.

[65] Everts HB, Silva KA, Schmidt AN, Opalenik S, Duncan FJ, King LE, et al. Estrogen regulates the expression of retinoic acid synthesis enzymes and binding proteins in mouse skin. Nutr Res 2021;94:10–24. https://doi.org/10.1016/j.nutres.2021.08.002.

[66] Vidal VPI, Chaboissier MC, Lützkendorf S, Cotsarelis G, Mill P, Hui CC, et al. Sox9 is essential for outer root sheath differentiation and the formation of the hair stem cell compartment. Curr Biol 2005;15:1340–51. https://doi.org/10.1016/j.cub.2005.06.064.

[67] Nowak JA, Polak L, Pasolli HA, Fuchs E. Hair follicle stem cells are specified and function in early skin morphogenesis. Cell Stem Cell 2008;3:33–43. https://doi.org/10.1016/j.stem.2008.05.009.

[68] Okano J, Levy C, Lichti U, Sun HW, Yuspa SH, Sakai Y, et al. Cutaneous retinoic acid levels determine hair follicle development and downgrowth. J Biol Chem 2012;287:39304–15. https://doi.org/10.1074/jbc.M112.397273.

[69] Duverger O, Morasso MI. Epidermal patterning and induction of different hair types during mouse embryonic development. Birth Defects Res Part C - Embryo Today Rev 2009;87:263–72. https://doi.org/10.1002/bdrc.20158.

[70] Hu H min, Zhang S bing, Lei X hua, Deng Z li, Guo W xiang, Qiu Z fang, et al. Estrogen leads to reversible hair cycle retardation through inducing premature catagen and maintaining Telogen. PLoS One 2012;7. https://doi.org/10.1371/journal.pone.0040124.

[71] Sundberg JP, Hogan ME. Hair Types and Subtypes in the Laboratory Mouse. Handb. Mouse Mutataions with Ski. Hair Abnorm. 1st Editio, CRC Press; 1994, p. 12.

[72] Cui CY, Kunisada M, Piao Y, Childress V, Ko MSH, Schlessinger D. Dkk4 and eda regulate distinctive developmental mechanisms for subtypes of mouse hair. PLoS One 2010;5. https://doi.org/10.1371/journal.pone.0010009.

[73] Reifen R, Agami O, Weiser H, Biesalski H, Naim M. Impaired responses to sweet taste in vitamin A-deficient rats. Metabolism 1998;47:1–2. https://doi.org/10.1016/S0026-0495(98)90183-4.

APPENDIX

INSTITUTIONAL ANIMAL CARE AND USE COMMITTEE APPROVAL

THE UNIVERSITY OF ALABAMA AT BIRMINGHAM

MEMORANDUM

DATE: 25-Apr-2022

TO: Kedishvili, Natalia

FROM: Robert A. Kesterson, Ph.D., Chair

Institutional Animal Care and Use Committee (IACUC)

SUBJECT: **NOTICE OF APPROVAL**

The following application was approved by the University of Alabama at Birmingham Institutional Animal Care and Use Committee (IACUC) on 25-Apr-2022.

Protocol PI:	Kedishvili, Natalia
Title:	Short-Chain Dehydrogenases in Retinol/Sterol Metabolism
Sponsor:	National Institute on Alcohol Abuse and Alcoholism/NIH/DHHS
Animal Project Number (APN):	IACUC-21600

This institution has an Animal Welfare Assurance on file with the Office of Laboratory Animal Welfare (OLAW), is registered as a Research Facility with the USDA, and is accredited by the Association for Assessment and Accreditation of Laboratory Animal Care International (AAALAC).

This protocol is due for full review by 24-Apr-2025.

Institutional Animal Care and Use Committee (IACUC)